POLITECNICO DI TORINO

Master of Science degree in Mechanical Engineering

Master's Thesis

Al-foams as cores in casting technologies

Thesis supervisors:

Prof. Graziano Ubertalli

Ing. Sara Ferraris

Candidate:

Zhang Huimin

Academic year 2019/2020

Introduction

Metal foams, or metallic porous materials, are a new class of materials which have lower densities compared with their dense metallic counterparts. Many applications of metal foams have been widely developed in industries because of their advantageous properties, such as lightweight, good energy absorption ability, higher stiffness, recyclability and so on. Now, the main applications are in three fields: Architecture, Automotive and Medical.

In this thesis, the characteristics of Al-foams and the possibility to use them as cores in casting technologies are studied. For this last point, foams with different densities were inserted into the casting die and aluminum alloys were cast around the foam cores.

At first non-inserted foams were characterized in terms of porosity, skin and wall thickness and microstructure by means of optical microscopy. Foam density was evaluated through weight and volume measurements. Moreover, chemical composition and morphology of the foam surface (outer skin) and cross section was investigated by means of Scanning Electron Microscopy (SEM) equipped with Energy Dispersive Spectroscopy (EDS). Finally, thermal conductivity of foams samples was measured by the hot disk technique.

After insertion in casting optical microscopy was used to investigate the degree of foam infiltration, the eventual foam-dense metal bonding and the foam and dense metal microstructure.

Chapter 1

Metal foams typologies and properties

Porous structures have been studied by many people and the advantageous aspects over the dense materials have been tested many times. Particularly, foams made from metal possess some superior properties over other materials. Metallic foams show higher mechanical strength than polymeric ones and they have higher thermal and electrical conductivity, which allows for a lot of applications in industries [1]. Metal foams can work in some severe conditions, for example, when fire resistant property is necessary. In addition, they can be recycled, which is an important property required for advanced and new materials. Polymeric foams are widely used as impact-absorber such as helmet. Metallic foam is more impact resistant but it will have plastic deformation after impact.

The characteristics of metal foams are determined not only on the typology, but also on the porosity and the manufacturing process.

There are two types of metallic foams according to their pores structure, which are closed-cell foams and open-cell foams.

1.1 Foam typologies

1.1.1 Closed-cell foams

Closed-cell foams have separated pores without interconnection. An example of closed-cell structure is shown in Figure 1.1:

Figure 1.1: Closed-cell aluminum foam [2]

In 1926, closed-cell foam was first introduced by Meller in a French patent in which

the foaming methods of metal were illustrated. Even though the concept of metal foam and prototype were developed a lot, the commercial production began in the 1990s. Closed-cell structure is often preferable to open one because it is cheaper and easier to produce. Therefore, a lot of researches were focused on this kind of structure.

Closed-cells aluminum foam has a porosity of 80 to 98%. The main feature of metal foams is that they can have high strength and stiffness combined with low weight [3]. This material has great potential, especially for applications as means of transport in the automotive industry, the aerospace industry and shipbuilding. The weight reduction leads to fuel savings or makes it possible to increase the weight of the load to be transported.

Metals can be foamed by many different methods and some methods are nowadays in commercial production. However, each method is restricted to a certain range of materials and cell sizes. As for most closed-cell aluminum foams, gas bubbles can be generated by inert gas injection or by the introduction of a blowing agent [1].

In the foaming process, gas tend to escape from the upper surface of the molten metal since the density of gas is much lower than the one of the dense metal. Therefore, it is necessary to use some stabilizing additives to avoid this problem. The principle behind this solution is that some types of "stabilizing" particles can increase the viscosity of the mixture of molten metal and gas bubbles and impede the rise of gas. The commonly used stabilizing particles are ceramic powders and alloying elements [4]. The ceramic particles, typically of diameter 0.5–25 μm, can be zirconia, alumina, silicon carbide, or titanium diboride [5]. 1–2% of calcium metal can also be added as stabilizing particles which rapidly oxidizes and forms finely dispersed CaO and $CaAl_2O_4$ particles [5].

1.1.2 Open-cell foams

Open cell foams are also called metal sponges and they are characterized by interconnected pores, they are permeable and they do not block vapor but allows it to pass through the foam matrix. The generally more homogeneous structure of open cell foams makes their characteristics more constant. Open cell foams have a wide range of pore sizes and densities, which makes it possible to precisely adjust sound absorption, mechanical strength and other properties [6]. An example of open-cell structure is shown in Figure 1.2.
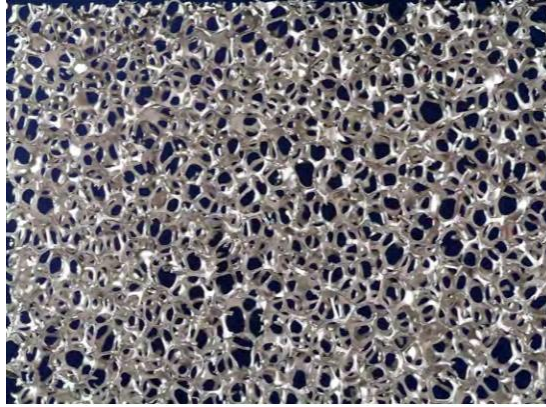
Figure 1.2: Open-cell aluminum foam [6]

The high cost of open-cell foams production imposes some restrictions on their applications. However, they are still preferable in some areas. For example, they can be used as catalyst support because of their high specific surface area (surface area per unit weight). The low thermal conductivity of cellular metals makes high material efficiency possible when used as heat insulation components.

Open-cells aluminum foams are permeable to gases and liquids. Permeability increases the use of aluminum foam. This kind of material, in fact, can be used to filter gases and liquids, to reduce the noise of pneumatic devices, as forming tools for the production of EPP/EPS (Expanded polypropylene/Expanded Polystyrene) products, for vacuum tables, for various heat exchangers, etc. [3]

Open cell metal foams can be manufactured by powder metallurgy, and almost all materials can be made into foams if powder are available.

Since the properties of closed and open-cell foams are different, their applications are different as well, which is shown in Figure 1.3:
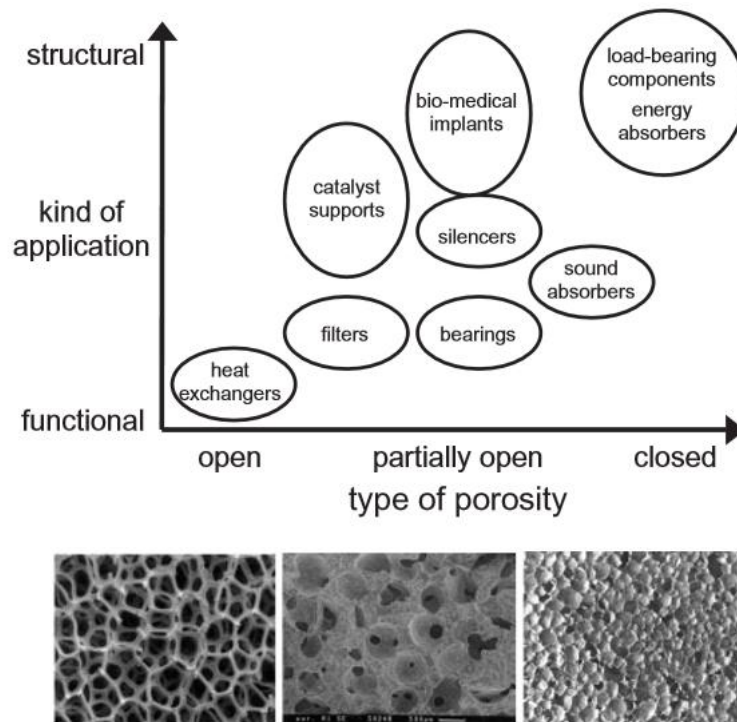
Figure 1.3: Applications of metal foams grouped according to type of porosity [1]

1.2 Production of Foams

Metallic foams can be made from metallic melts or metal powders. Nowadays, metal foams have been produced based on aluminum (Al), zinc (Zn), magnesium (Mg), copper (Cu), nickel (Ni), lead (Pb), bronze and titanium (Ti) alloys [7].

1.2.1 Foaming from melts

Melt route foaming process for closed-cell foam is one of the most attractive process because it allows to handle a great amount of material. In the foaming process, gas introduction could be the most significant step, which can be done either by gas injection or by in-situ gas generation. In the second method, a foaming agent should be dispersed homogeneously in the melt metal quickly, at least faster than its decomposition and reaction. Besides, gas escapement should be avoided, which can be done by increasing the melt viscosity. A few options can be chosen to solve this problem: a) foaming in the semi-liquid state; b) adding ceramic particles; c) oxidation [1].

• Gas injection

There are two representative gas injection foam process Cymant/Alcan and

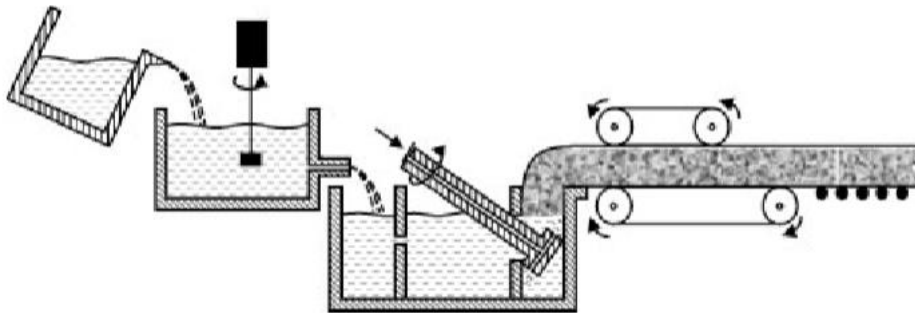Nosk/Hydro process, which were developed in 1980s and 1990s respectively [8].

Figure 1.4 Melt foaming of Cymat [8]

Figure 1.4 shows the principle of the melt-foaming route adopted by Cymat. Wrought or Cast Aluminum alloy matrix + 10-3-vol.% SiC or Alumina is the starting molten material. Air is injected into rotating impellers through nozzles and it will disperse to form bubbles. It is possible to control the bubble size by changing the gas flow rate, the rotational speed of the impeller and the number of nozzles. After the gas bubbles are formed, they tend to rise to the surface. In this case, ceramic particles are necessary to increase the melt viscosity and reduce the kinetic energy of the gas bubbles, which also decreases the danger of mechanical rupture. Then a conveyor belt will carry the liquid metal foam away, where the foam will solidify and cool. The density can be controlled by rotor speed, gas flow, the quantity of particles and the solidification condition [1].

This method is suitable for slabs production whose relative density are between 2-20% and the average cell size is between 2.5mm and 30mm [1]. The final foam does not have a continuous dense skin [1].

• In-situ gas generation

This kind of foaming process generate relatively small bubbles, which result in more irregularly shaped pore distribution. The principle of this foaming technique is to generate gas by thermal decomposition of a solid agent. There are two representative foaming process of this type: the Shinko Wire Process and the FORMGRIP process.

a)   Shinko Wire manufacturing process

Shinko Wire Company in Japan has developed the manufacturing process of the Alporas foam, which allows to make foamed aluminum with large sizes. The addition of 1.5% wt of Ca at 680℃ and further agitation will facilitate the formation of oxides: CaO, alumina and $CaAl_2O_4$, which will increase the viscosity of the molten metal.

Besides, the addition of 1.6% TiH$_2$ is needed as foaming agent, which will dissociate to generate H$_2$ bubbles in the molten metal. After that, the foamed material is solidified by cooling. The final foam product does not have a dense skin [1]. The large sized foam part can be sliced into thin plates. The manufacturing process is shown in Figure 1.5.
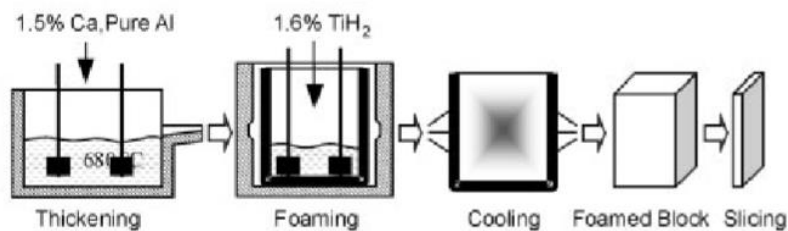

Figure 1.5 Shinko Wire manufacturing process of Alporas foam [9]

b) FORMGRIP process

The FORMGRIP (Foaming of Reinforced Metals by Gas Release in Precursors) process combines the advantages of melt-route and powder routes. It includes precursor material and foaming agents "baking" process, which is similar to the powder routes but the precursor is made from melt processing.

The precursor is prepared by the dispersion of mixed powder (AlSi12 powder and foaming agent TiH$_2$) in an Al-9Si/SiCp melt and mechanical stirring at a speed of 1200rpm. The hydrogen released is limited in this method for three reasons: hydride is introduced at low temperature; the addition of silicon carbide increases melt viscosity a lot and the oxidized foaming agent slow down the gas evolution. The pore dimension is limited by the cooling of mixed melt in the mold.

The second step is to heat the precursor above the solidus temperature and hydrogen will expands bubbles further. A scheme of the process is reported in Figure 1.6
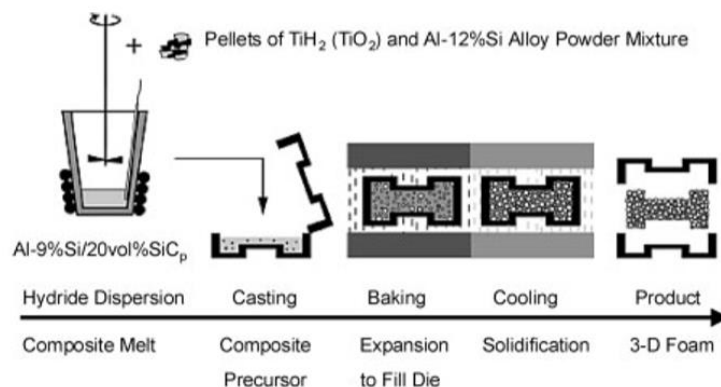
Figure 1.6 Melt-based FORMGRIP process [1]

The relation between cell size and density in Cymat and FORMGRIP foams is shown in Figure 1.7:
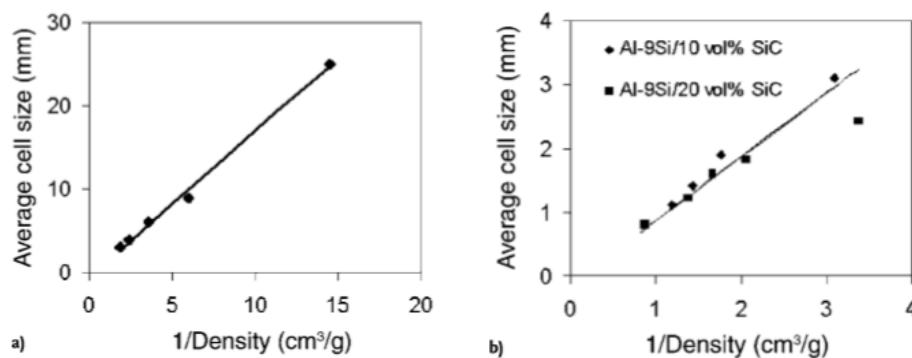

Figure 1.7 Relation between cell size and density: a) Cymat; b) FORMGRIP [1]

As is shown in Figure 1.7, the cell size is inversely proportional to the density in both type of foams, but the relative densities lie in different ranges. The final foam obtained by this process has a continuous dense skin [1].

1.2.2 Production from powder

This method has become more and more popular in the past few years and nowadays it is in the industrial implementing stage.

Foaming agents are mixed with aluminum or aluminum alloy powders before it is compacted by powder rolling, hot pressing or conform extrusion. The compacted dense product is called "foamable precursor material". In addition to be directly compacted, it can be cold compacted which is better for handing in extrusion and rolling. When the precursor is heated up to its solidus temperature, the pressure on the foaming agents get released which makes them to decompose and bubbles are formed. After cooling, a closed cell foam is obtained [1]. A schematic description of the process is shown in Figure 1.8.
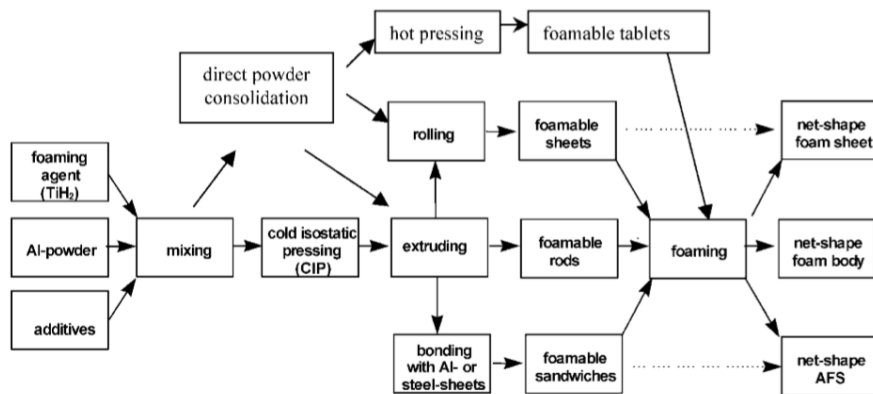
Figure 1.8 Foam production by powder compact foaming technique [1]

This route is commonly used in the production of casting alloys such as AlSi7Mg(A356) and AlSi12 because of their good foaming properties and low melting point. It is also frequently used in wrought alloys such as aluminum 2xxx,6xxx or 7xxx.

This method allows to create foam and bulk metal sandwiches without adhesives.

The pros and cons of this method is listed in Table 1.1:

Advantage	Problem	Disadvantage
Net-shape foaming possible	Uniformity of pore structure still not satisfactory	Cost of powders
Composites can be manufactured	Process control must be improved	Very large volume parts difficult to make
Parts are covered by metal skin	Permeable (holes)	Coating process requires sealing
Graded porosity can be achieved	Difficult to control	
Flexibility in alloy choice		
No stabilising particles have to be added		
Ceramics and fibers can be added		

Table 1.1 Advantages and disadvantages of powder compacting foaming technique [1]

No ceramic additives are needed to stabilize the foam, while in many other foaming processes a certain amount of silicon carbide is necessary.

There are some aspects should be concerned in the powder-compact technique.

a) Powder selection

A successful foaming depends on many factors, such as purity, alloying elements,

particle sizes and distribution and so on. These properties can be of great significance in the production. Different manufacturers may expect different foam behaviors, so they can differ in the controlling of these parameters of production and may also adopt some empirical criteria.

b) Mixing

In order to have a high-quality foam, the mixing process is significant which ensures the alloying elements and foaming agents to be distributed uniformly. Powders can be mixed in tumbling mixers or aerodynamic mixing which have been achieved by Schunk-Honsel and GmbH Austria respectively.

c) Densification

There are a variety of methods for powder consolidation. The attention should be paid to make sure that foaming agents are fully embedded in the metal matrix. Cold isostatic pressing (CIP) and subsequent extrusion can be one of the techniques to obtain foamable precursor. Firstly, CIP is adopted to consolidate the powder mix to billets with a relative density between 0.7-0.8 and the typical mass is 50 kg. Then, they can be extruded in an extrusion machine. In fact, prior consolidation of CIP is not needed sometimes but it helps to prevent the contamination of powders and powder de-mixing. Apart from this technique, foamable material can be manufactured by CONFORM process by Mepura (Ranshofen) [10], in which a rotary continuous extrusion is adopted. The powder is dragged by a rotating wheel into a consolidation chamber and the material is pulled off in radial direction as a compacted wire. A schematic description is shown in Figure 1.9.
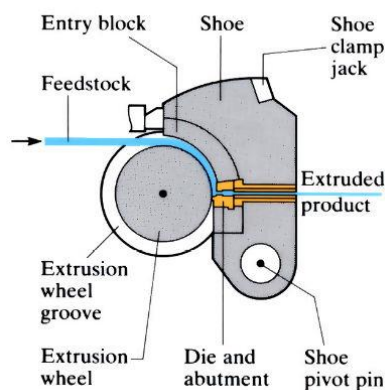
Figure 1.9 CONFORM process [2]

d) Further processing

The material after extrusion can be foamed directly or it can be further processed to other desired shapes. Conventional rolling allows for the production of sheets with thickness of around 2 mm. In addition, two sheets can be attached before rolling, which produces a metallic sandwich. By deep drawing, the sheets and sandwiches can be converted into 3D shaped sheets for other required shapes.

e) Foaming

By heating the foamable material to a temperature higher than the solidus one, foam structure can be created. Foaming agent dissociates and releases gas to form pores in the solid. The density and its distribution can be influenced by several factors, such as foaming agent content, furnace temperature and heating rate. Initially, the mold is directly heated, while the foam material receives heat from mold. As the temperature increases, the precursor become soft and gradually fill along the shape of the mold, which leads the increase of the heat transfer. Once the mold has been filled, it has to be cooled down to a temperature lower than the solidus one. An important issue in this process is that liquid foam is thermodynamically unstable and conditions change continuously.

The density of aluminum foams produced through this route is in the range 0.4-0.8 g/cm^3, and the corresponding relative density is 0.15-0.3. The final foam produced by powder compact foaming process has a continuous dense skin [1].

1.3 Properties of metal foams

Some properties of metal foams are consistent with the corresponding dense metals, for example:

• crystal structure;

• heat capacity;

• thermal expansion coefficient;

• melting temperature [1]

However, other properties, such as mechanical properties, stiffness and thermal and electrical conductivity, differ from dense metal since they depend both on the density and the structure of materials.

1.3.1 Mechanical properties

• Young's modulus

Linear elastic behavior is one of the most significant characteristic to define mechanical properties. For isotropic materials, Young modulus E and Shear modulus are often needed to describe the linear elastic response.

$$G = \frac{E}{2(1+v)} \qquad\qquad K = \frac{E}{3(1-2v)} \quad [1]$$

Where K is bulk (shear ??) modulus and v is elastic Poisson's ratio

In fact, it is not proper to define the cellular material by "modulus", instead, "stiffness" should be used. There are three main factors that can influence the moduli:

a. Foam structure

A significant difference can be found between open cell and closed cell foams. Cell walls in closed-cell structure imposes some constraints on the material, so closed-cell structure has much higher Young's modulus compared with open cell one in case of the same density. However, imperfections of cell wall also influence the stiffness. [1]

b. Foam density

The relative density (with respect to the dense metal) is the biggest influencing factor of mechanical properties.

$$E \approx (\frac{\rho}{\rho_s})^2 \text{ (open cell)}$$

$$E \approx \Phi^2(\frac{\rho}{\rho_s})^2 + (1-\Phi)\frac{\rho}{\rho_s} \text{ (closed-cell) [1]} \qquad \text{(What is the meaning of } \Phi?)$$

Where the subscript "s" indicates the solid-compact metal properties.

The relationship between (relative ??) density and Young's modulus is plotted in Figure 1.10.
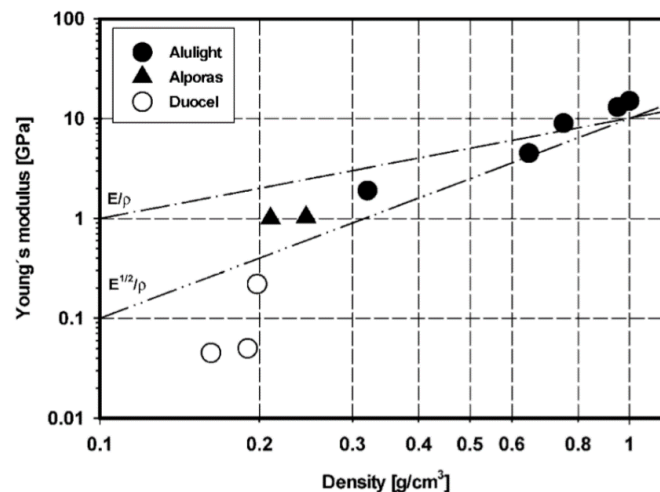
Figure 1.10 Young's modulus - Density diagram for different types of aluminum foams [1]

c. Deformation

Since buckling, stretching, bending and cracking of the cell walls changes the structure of foam, Young's modulus will change with strain. Furthermore, with increasing strain, it decreases faster in compression than in tension.

• Compression behavior

Many investigations have indicated that, in compression, cellular metals present a region where the stress remains almost constant with a large change of strain. This behavior is associated with foam ability to adsorb energy and is of interest in energy absorption applications. Normally, metallic foams are quite ductile. Compression loading at small strains lead to deformation (bending, extension or compression) of cell walls. However, if the load exceeds a certain value, known as yield stress, the deformation will not be reversed any more. Inhomogeneity of real cellular foam has the problem of early "plastification", which means that plastic deformation can happen at low strains. The compression behavior (stress-strain curve) is plotted in Figure 1.11.
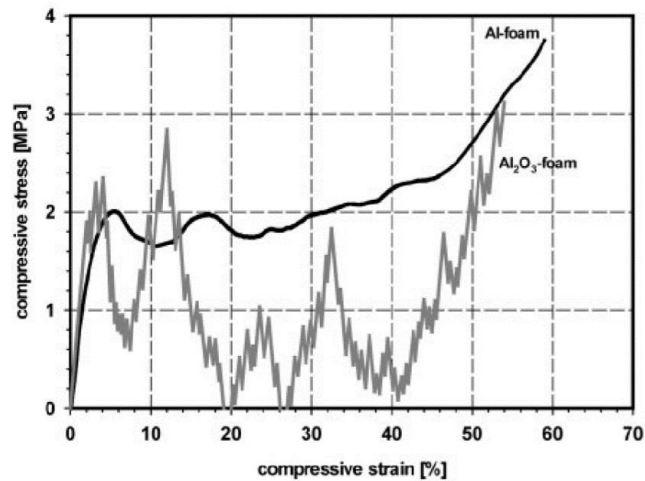
Figure 1.11 Stress – strain response of aluminum foam [1]

• Tension behavior

In the initial stage, the deformation is similar to compression, while in the post-yield phase, the deformation is much different. The deformation of foams is concentrated in weak regions and formed during the final failure. The final failure depends on the material ductility. For brittle materials, microcracking can be observed in cell walls with high stress; if it exceeds a critical value, the crack will propagate and lead to final failure. For ductile materials, like aluminum, a fracture-process zone, where the deformation is concentrated, can develop with increasing deformation. Further deformation makes a main crack propagate in weak parts of foam structures.

Some significant mechanical and thermal properties of commercially available aluminum foams are listed in Table 1.2:

Property, symbol [units]	Cymat	Alulight	Alporas	ERG	Inco
Material	Al−SiC	Al	Al	Al	Ni
Relative density, ρ/ρ_0	0.02−0.2	0.1−0.35	0.08−0.1	0.05−0.1	0.03−0.04
Structure	Closed cell	Closed cell	Closed cell	Open cell	Open cell
Young's modulus, E [GPa]	0.02−2.0	1.7−12	0.4−1.0	0.06−0.3	0.4−1.0
Poisson's ratio, ν	0.31−0.34	0.31−.34	0.31−0.34	0.31−0.34	0.31−0.34
Compressive strength, σ_{pl} [MPa]	0.04−7.0	1.9−14.0	1.3−1.7	0.9−3.0	0.6−1.1
Tensile elastic limit, σ_y [MPa]	0.04−7.0	2.0−20	1.6−1.8	0.9−2.7	0.6−1.1
Tensile strength, σ_{UTS} [MPa]	0.05−8.5	2.2−30	1.6−1.9	1.9−3.5	1.0−2.4
Endurance limit, σ_e^c [MPa]	0.02−3.6	0.95−13	0.9−1.0	0.45−1.5	0.3−0.6
Densification strain, ε_D	0.6−0.9	0.4−0.8	0.7−0.82	0.8−0.9	0.9−0.94
Tensile ductility, ε_{UTS}	0.01−0.02	0.002−0.04	0.01−0.06	0.1−0.2	0.03−0.1
Fracture toughness, K_{IC}^c [MPa.m$^{1/2}$]	0.03−0.5	0.3−1.6	0.1−0.9	0.1−0.2	0.6−1.0
Thermal conductivity, λ [W/m·K]	0.3−10	3.0−35	3.5−4.5	6.0−11	0.2−0.3
Resistivity, R [$10^{-8}\Omega\cdot$m]	90−3000	20−200	210−250	180−450	300−500

Table 1.2 Properties of commercial foams [1]

As can be seen from Table 1.2, closed-cell aluminum foams have higher relative density, tensile and compressive strength compared with open cell foams. This is the reason why, as previously cited, they are mainly used in structural applications.

1.3.2 Thermal properties

Thermal properties are of great practical significance for applications. The most important properties might include melting point, thermal conductivity, heat capacity and fire resistance. Some properties of cellular metals may remain the same as the bulk materials, while others may change a lot with the change of the porosity amount.

• Melting point

Melting point of metal foam is the same of the dense material, which mainly depends on the composition of the alloy [1]. However, some metals can be easily oxidized which

means that an oxide layer will cover the surface which may slightly increase the melting point.

• Heat capacity

Thermal capacity is defined as the energy requirement to change a unit of temperature for a unit mass of material. Heat capacity of metal foam can be calculated as the sum of heat capacity of different phases multiplied by their corresponding weight percentage. In the metal foam, oxides layer on the surface and air in the pores will decrease the specific heat, therefore, metal foams can be applied in some cases where lower thermal capacity is required, for example, rapid heating and cooling [1].

• Thermal conductivity

The thermal conductivity of metal foams is lower than the one of the corresponding dense metal due to the presence of porosity which is filled with air (lower thermal conductivity than metal). Considering the effect of porosity on thermal conductivity its value depends on the foam relative density.

The thermal conductivity of metal foams (λ_s) can be expressed in the formula:

$$\lambda_s = \lambda_0 (\frac{\rho}{\rho_0})^t \ [11]$$

Where λ_0 is the thermal conductivity of the dense structure, $\frac{\rho}{\rho_0}$ is the relative density of metal foam with respect to the dense metal and t is the critical exponent and its predicted value in 3D is   t = 2.0 [11].

Normally, thermal conductivity of alloys increases with temperature. According to the formula above, same behavior can be evidenced for metal foams.

1.3.3 Sound absorption

Metal foams are good in sound absorption since their structure make it possible to absorb many different kinds of mechanical energy. The sound absorption ability of aluminum foams is much higher than the dense metal. They can be applied to reduce the noise level by decrease reflection of sound from boundaries. Closed-cell aluminum foams are poorer than open cell foams in terms of sound absorption capacity, but it can be improved by drilling holes within the foams to allow the entry of sound.

According to the research of University of Cambridge, the experiments conducted on ALPORAS foam show that metal foams with lower relative density have better sound

absorption capacity [12]. They measured the absorption coefficient by using an impedance tube. At one end of the tube, the sinusoidal sound wave was generated through a loudspeaker in the frequency range of 10-20 kHz. The sample was placed in a holder which was clamped to the other end of the tube. A movable probe microphone was directed through a hole in the loudspeaker to measure the maximum and minimum of pressure. Then, the absorption coefficient (α) can be calculated by the formula:

$$\alpha = 1 - (\frac{p_{max}/p_{min}-1}{p_{max}/p_{min}+1})^2 \quad [12]$$

Figure 1.12 (a) shows the measured sound absorption coefficient of as-received cast foam panels of thickness 10mm for three different relative densities: 0.09, 0.13 and 0.15. As can be seen from the figure, the foam with lower density has a higher sound absorption capability.

Figure 1.12 (b) shows the measured sound absorption coefficient of as-received foams of relative density of 0.09 for 5 different thicknesses: 6mm, 10mm, 20mm, 40mm and 50mm. In the frequency range of 100-1800 HZ, there is a maximum sound absorption coefficient of about 0.6 with a thickness of 20mm.
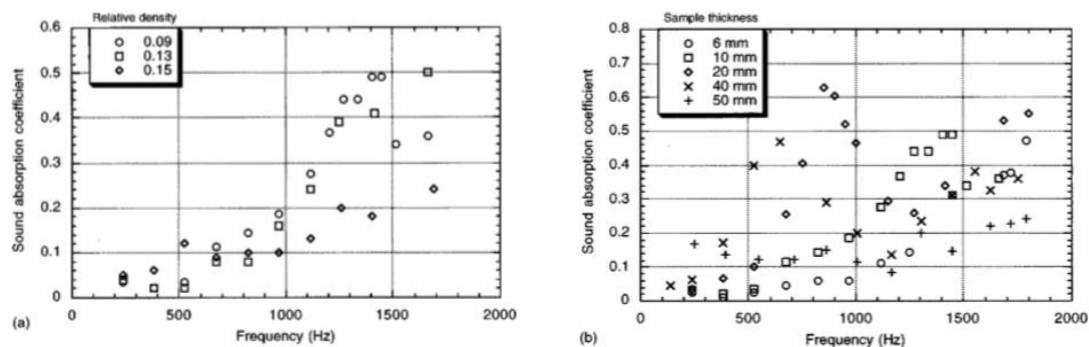
Figure 1.12 Sound absorption coefficient of foams with(a) different porosities (b)same porosity and different thicknesses [12]

1.3.4 Vibration damping in metal foams

Vibration damping capacity of metal foams depends on the porosity, cell size and shape, treatment of the sample and so on. The existence of internal friction in the material makes it possible to convert mechanical energy into heat. The friction between the surfaces of cells and the cracks result in the dissipation of vibrations, which increases with the strain amplitude. Furthermore, the resonant frequency is proportional to the square of strain amplitude. Damping capacity can be increased by

decreasing the cell wall thickness or adding structural irregularities, such as ceramic particles (SiC, graphite and so on) [7].

1.3.5 Impact energy absorption

As illustrated in 1.3.1, the special compression behavior of metal foams allows for applications for impact energy absorption, which is one of the most significant properties. The average absorption of ALPORAS in 55% deformation is 1.0 MJ/m^3 for static load and 1.51 MJ/m^3 for dynamic load [7]. The ability of absorption is related to the structure of foams (open or closed) and to the relative density. When the torque generated by compression load exceeds the plastic limit, plastic collapse will appear.

Aluminum foams are ideal materials for impact energy absorption since they have a wide range of constant stress in stress-strain curve. For this reason they are particularly interesting in automobile industry [7].

1.3.6 Recyclability

Recyclability is another required property for advanced materials since recycling is more and more important. Metals can be recycled again and again without degradation of properties. The recyclability is a superior property both from financial and environmental aspects. First of all, it requires less energy to process than adopting virgin raw materials, which saves natural resources. Secondarily, less carbon dioxide and harmful gases are emitted by recycling metals.

Scrap metal recycling provides raw material for new goods production, which involves recovery and processing of metals from end-of-life products.

Recycling process starts with collection. Metal collectors pick up scrap metals and sell to scrap yards. Then metals are sorted by magnets, sensors or by observing the colors. Metals are then shredded to increase the surface-to-volume ratio which promotes the melting process. Scrap metals are melted in a large furnace which enables them to be formed into specific shapes.

An oxidized layer will be formed on the surfaces of the cellular structure when it is heated in air. The oxidation process is very fast initially, when its thickness reaches a value close to the cell-wall thickness, about 100 μm, the oxidation will then slow down. So, the cellular aluminum is gradually converted into cellular alumina structure [1].

The cellular part tends to float on its melt because of its low density. Since the

containing air has to be replaced by melt, the cellular structure should be compressed, like packaging foils or shredder scrap before melting.

The oxides may decrease the efficiency of recycling, so oxides and other impurities should be removed by normal cleaning. Ti, remaining from the common blowing agent (TiH$_2$) is soluble below 0.12 wt% at the peritectic temperature of binary aluminum and it does not degrade the quality of the alloy. ALPORAS alloys contains about 2 wt% Ca, which will be partly oxidized, so attention should be paid not to exceed the impurity level for the secondary alloy. Anyway, the purity requirement for secondary aluminum cast alloy is not very strict, which means that the scraps of common types of cellular aluminum can be remelted [1].

After purification, the conveyor belt is used to cool and solidify the metals. In this stage, scrap metals are formed into specific shapes that can be easily used to produce various metal products.

Chapter 2

Metal foams in casting technologies

2.1 Aims and potentialities

Light-weight load bearing components are extremely interesting in automotive and aerospace applications, where weight saving is one of the most important properties. This goal can be achieved by castings with weight-saving cavities. Since the wall thickness is restricted by technology, it is not allowed to design the thickness according to the requirements. Generally, the thickness is designed by considering the maximum loading point, however, it will increase the unnecessary weight at other less loaded cross sections. Bending stiffness depends on Young's modulus and the moment of inertia of the cross section. Young's modulus is constant, so in order to increase the bending stiffness, the moment of inertia of the cross section, or the area of cross section should be increased.

There are two possible ways:

• Increase the volume. When the available thickness or the volume is restricted, this way is infeasible.

• Introduce some stiffening ribs into the cavities.

For both two ways mentioned above, there are some limitations. However, foam cores can be a superior solution to this issue. In the past, sand cores were used in casting, which aims to create cavities. After casting process is done, it remains in the casting [13] or it can be removed but requires sand decontamination before further use.

Foam cores can replace the cavities in most heavily loaded part without much overall weight or volume increasing. In this way, shell thickness can be reduced. In addition, due to good mechanical properties of metal foams, it has other benefits:

• save cost for sand cores manufacturing and removal

• absorb impact energy and damp the vibration

• can be applied when the use of sand cores is not possible (e.g. squeeze casting, thixocasting, HPDC) [13].

In the casting of aluminum with a foam core, the shell is designed to have many functions in addition to load carrying. Besides, because of the one step manufacturing process, it is economical and attractive.

There are a lot of potential applications for this type of castings, especially for higher loaded structures, such as control arms, space frame nodes, cross-members and knuckles. This method also has the potential in the production of quasi-hollow castings, where foam cores replace the salt or sand cores.

Manufacturing casting components with aluminum foam cores are of interest in automotive industry because of the advantages of sound attenuation, impact energy and vibration absorption. On the one hand, for safety reason, impact energy and vibration absorption are quite important in case of an automobile crash. The mechanical vibrations can be transferred into heat which will be dissipated into the atmosphere. On the other hand, components with good vibration damping will make it more comfortable for people driving. When an automobile is driven, the noise both from outside and itself could decrease the comfort of passengers.

2.2 Core production

For the foam core in casting, it is preferable to have foam inserts with a dense skin, because it allows to pour the molten metal around the foam core limiting the risk of infiltration with melt metal [13]. At present there are two production routes which can create a solid skin, the powder compact forming and the FORMGRIP method. These two methods have been described in detail in chapter 1. Both of them include

heating the precursor in a mold, but the precursor can be made from different ways. For aluminum foam cores used in casting, powder compact technique is more suitable.

2.3 Examples

According to the research of T. Hopler, F. Schorghuber and F. Simancik, improvements of castings with foam cores were investigated [13]. They did experiments to figure out if it was feasible to have aluminum foam as a permanent core in aluminum castings. Foams both made from cast and wrought alloys were prepared by injection moulding technique. The powdered mixture was extruded into a foamable precursor, which was then heated in a chamber to allow for foam formation. During foam formation, it was injected from the chamber into the desired cavity. The aluminum castings with foam cores were tested to be compared with hollow parts in terms of weight, compression strength, deformation work and loss factor. The results are shown in Figure 2.1.
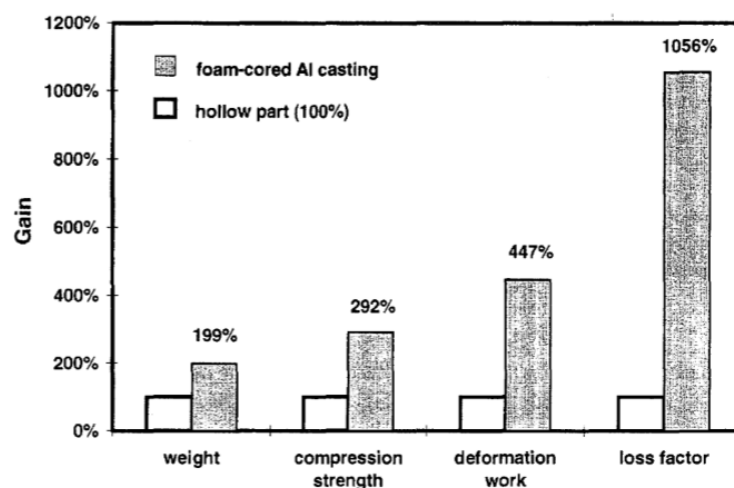
Figure 2.1 Comparison of properties between foamed-core casting and hollow part [13]

From Figure 2.1, it can be seen that the improvements are much more than the weight increase with respect to the hollow parts.

Another example can be an engine mounting bracket designed by LKR (Austria) and applied to the German car maker BMW (as shown in Figure 2.2). The starting shaped part of aluminium Metcomb or Alulight foam (indirect or direct foaming) has a dense outer skin and used as cores in low pressure die-casting. The engine mounting bracket is based on this kind of composite, which has a dense cast shell and light-weight foam core. During casting, no noticeable infiltration by the melt was evidenced [14]. The produced part is 25cm long and can be loaded with the high weight of the car engine.

The stiffness is improved and it absorbs mechanical vibrations by dissipating into heat. Because of its high fracture toughness, it increases safety in case of crash [15].
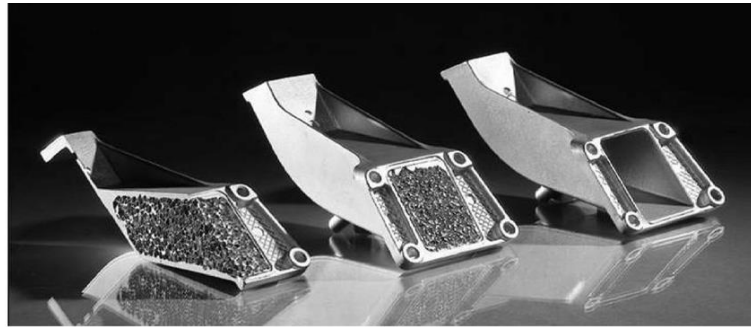
Figure 2.2 Engine mounting bracket of BMW [15]

Another example can be the application on the machine tools. Modern manufacturing technology is trying to achieve higher feed rate, which means increased acceleration and deceleration of workpieces and spindle. Traditional casting components with heavy weight impose the limit for the feed rate, while casting aluminum with foam core can be a good solution, which has the same stiffness with lower weight. In addition, the vibration produced can be attenuated, which also increases the accuracy of machine [7]. An example of the structure of a machine tool with foam core is shown in Figure 2.3:
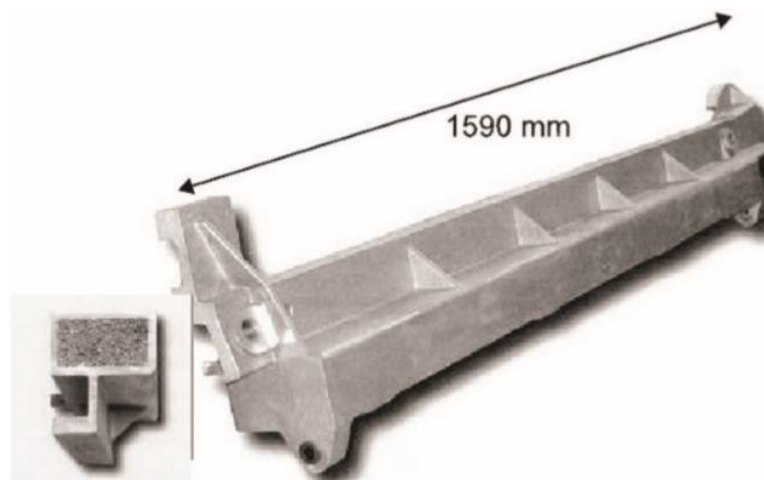
Figure 2.3 Machine tool cross beam with aluminum foam core [7]

Metal foams in casting is possible to be applied in a variety of areas.

• In transportation industry, heat and fire insulation and sound proof ability in compartments are needed.

• In architecture area, heat insulated walls, energy saving mobile house and fire insulated doors can be achieved with metal foams.

• In mechanical and aerospace engineering.

2.4 Criticism

Casting around foams cores faces some criticisms, among which infiltration and deformation of foam cores can be the most important.

• Infiltration

The prerequisite of reproducible and sound castings is to avoid infiltration, which can be achieved at first by the presence of a continuous dense skin on the foam surface and eventually by coating of the foam cores. There are two requirements for coating: it is able to be applied to complicated geometries and in proper thickness.

• Local melting

Particularly in the gate area, the hot molten metal may cause damage to the foam skin by heat and erosion [1]. The solution to this problem can be coating or by using foam core with thicker skin.

• Dwell pressure control

There are two stages in die casting: fill the die with melt as fast as possible and compress entrapped gas with high pressure to balance shrinkage and minimize porosity. High velocity of piston will result in a high pressure peak, which will cause the problem of infiltration and collapse for foam. Therefore, it is necessary to control the pressure by a real-time control machine. An example of the dwell pressure in a casting experiment is shown in Figure 2.4.
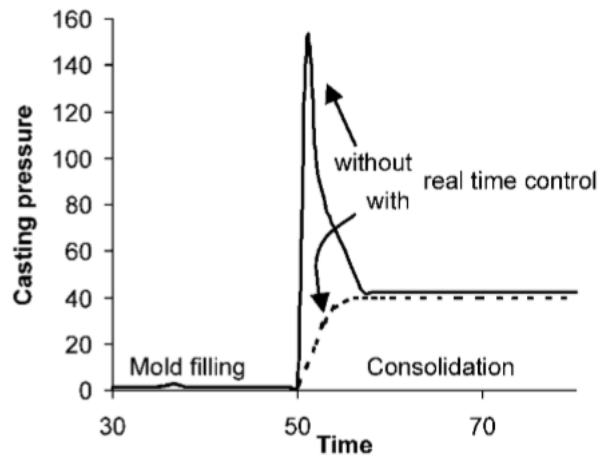
Figure 2.4 Dwell pressure in casting machine [1]

• Preheating of foam cores in gravity casting

In gravity casting, foam cores are inserted into a casting die and the alloy melt is used to cast the shell around the foam by gravity force. When the hot melt metal is poured into the die, the foam core can be heated and the gas in the pores will expand and diffuse into the melt, which causes bubble formation and porosity in the shell. The solution to this problem can be the pre-heating of the foam cores before their insertion. The test of temperature changes of the shell and the foam cores during casting process will be illustrated in the third and fourth chapters.

• Bonding between the shell and the foam

Normally, it is difficult to have bonding between the dense metal shell and the foam core because the alloy elements such as aluminum and magnesium, are easy to be oxidized and the resultant oxide layer will prevent reaction between the melt metal and foam core. Generally, bonding can be improved by mechanical and metallurgical ways. Mechanical bonding is to deliberately weaken the skin of foam, for example, by sand blasting. In this way, the specific surface of the core will increase and the bonding ability is increased (mechanical interlocking). Another method is to coat the cores with agents that allow diffusion through the oxide layer.

Sometimes bonding is not necessary, especially in the cases when structural damping is required since energy can also be dissipated at the interface of the shell and the core.

• Future work on the use of foamed-core in castings can be summarized as follows:

a) cost saving in foam manufacturing;
b) methods to improve casting quality should be developed;
c) density of foamed part should be decreased;
d) develop the manufacturing technology for reproducible foam structure

Chapter 3

Materials and methods

3.1 Samples preparation

Three types of foams (two bars for each type) were studied in the present research. The difference between these foams was the average density. Foams were characterized as received and used as cores in gravity casting experiments.

The foams are shown in Figure 3.1:

	Overview	Cross-section
SET 1		
SET 2		
SET 3		
SET 4		

	Overview	Cross-section
SET 5		
SET 6		

Figure 3.1 Foams studied in the present research

From Figure 3.1, the difference among the various foam samples is quite evident. All the specimens have thick skins but the pore sizes and densities are quite different.

These foams were used as cores in gravity casting experiments. The melt aluminum was poured into the die in the direction indicated in Figure 3.2, filling in the chamber between the mold and the foams. Finally, the casting aluminum with foam was obtained (Figure 3.3).

(a)

(b)
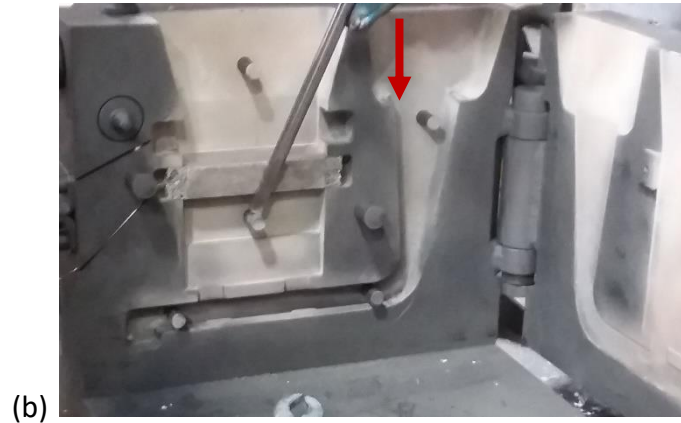
Figure 3.2 Casting mold
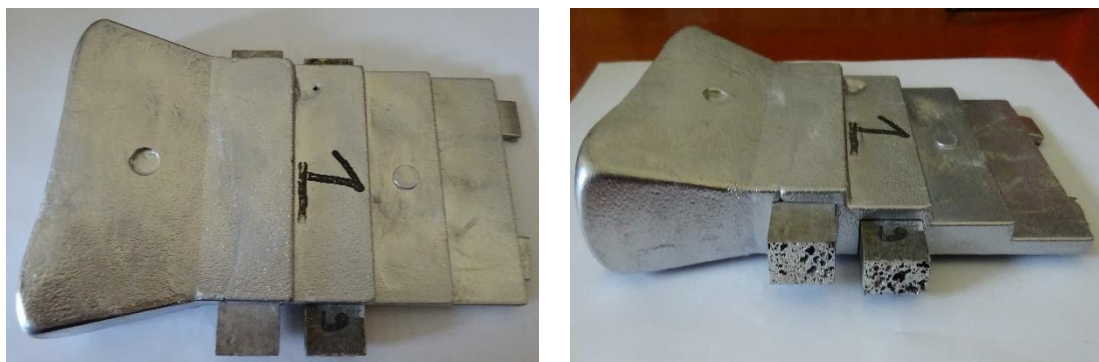
Figure 3.3 The cast samples

As shown in Figure 3.3, the part has 4 steps with different thicknesses and foam cores are inserted in the third and fourth steps. The foam core in the third step has one surface exposed to the environment, while the foam in the fourth step is completely surrounded by dense aluminum. During casting process, the melt metal firstly filled the first step which was at the bottom, then filled the second step, the third step and finally the fourth step.

The third step is required to have one surface exposed to the environment, which allows it to be extracted from the cast sample easily. Since there is a clearance between the foam skin and the moving part of the mold, the melt metal can flow into the gap and partly cover the foam skin, as shown in Figure 3.4 (left). The solution to this problem is to reduce the thickness at both ends of the foam so that the surface is able to be in contact with the mold, as shown in Figure 3.4 (right).

Figure 3.4 The initial third step of cast sample (left) and the one after thickness reduction (right)

3.2 Density measurements

In order to obtain foam densities, the mass and volume of each sample have to be measured. The mass of the samples was measured by means of a precision balance. Since the shape of the foam inserts is regular, the dimensions measurements can be easily done by a caliper and subsequently the volume calculated. The dimensions to be measured are shown in Figure 3.5:
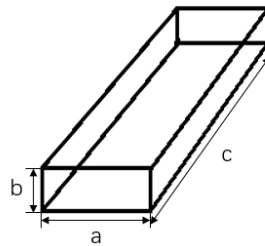
Figure 3.5 Volume measurement of foams

The density was calculated by the formula $\rho = \frac{m}{V}$ and the relative density with respect to the dense aluminum can be computed as $r = \frac{\rho}{\rho_{d.a}}$, where $\rho_{d.a}$ is the density of dense aluminum, ~2.7 g/cm³.

3.3 Optical microscopy

In order to investigate the microstructure of the dense aluminum and of the foams, they should be observed by optical microscope. Optical microscope has a system of different lenses which can magnify areas of samples with the use of visible light. The magnification and focus can be adjusted to obtain desirable images. Modern microscopes are often connected with computers which help to snap images for further analysis.

The roughness of the metal surface makes it impossible for optical microscope to focus all the points on the surface, which results in the difficulty in observation. Therefore, it is necessary to polish the surface of the samples which we want to observe.

All the samples were very small, so they were mounted in resin in order to facilitate the handling and polishing processes. The resin is a solid polymer which is the product of reaction of different solid powder and liquid monomer. The sample was inserted into a mould and surrounded by a fluid mixture of the resin components. After the reaction was completed (overnight), the sample embedded in the resin was extracted from the mold and ready for polishing.

In the polishing process, abrasive papers with different silicon carbide particle sizes were used to obtain homogenous metal surfaces, while mirror polishing was achieved by diamond and alumina suspensions. The polishing machine is shown in Figure3.6:

Figure 3.6 Polishing machine

After polishing, there may be a lot of small particles attached to the surface of samples, so it is necessary to clean the surface by distilled water in order to obtain a clear observation without impurity. Then the samples should be dried by compressed air.

There were three types of samples that were observed by optical microscope: non-inserted foams, dense metal of casting samples, and inserted foams.

Three non-inserted foams, foam 3 (0.98g/cm^3), foam 7 (1.25g/cm^3) and foam 11 (1.5g/cm^3) were polished and observed by optical microscope in a similar way to dense metal observation. The scanning images of non-inserted foam 3 and 7 are shown in Figure 3.7:
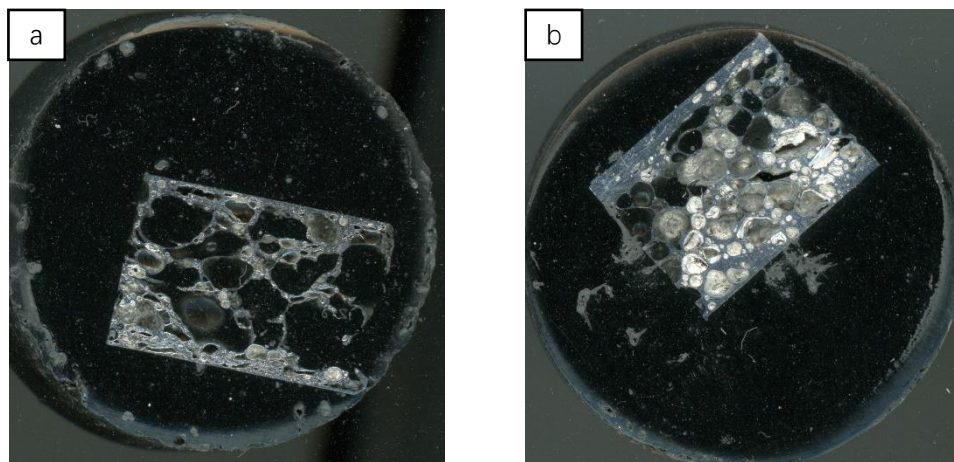
Figure 3.7 Scanning images: (a) foam 3; (b) foam 7
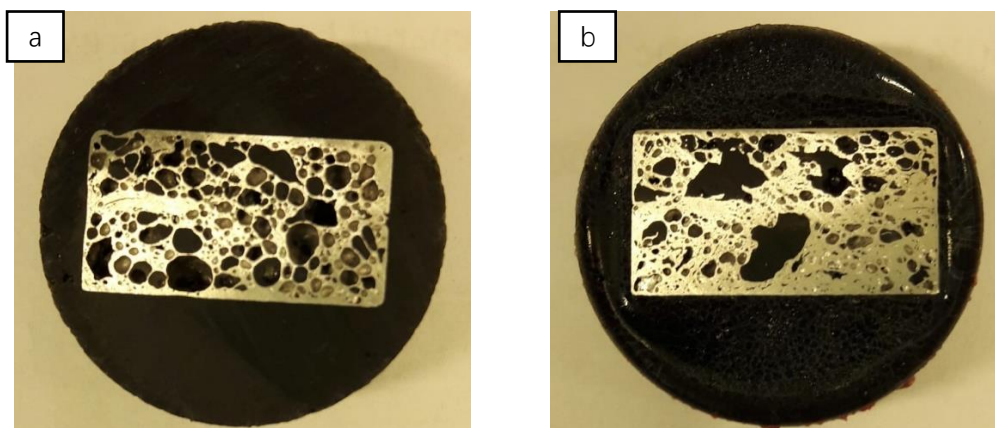
Figure 3.8 Scanning images of foam 11: (a) side 1; (b) side 2

Figure 3.8 shows the photo of two sides of foam 11. These images evidence that the foams, as widely reported, are not homogeneous and pore size and distribution can vary inside samples.

The resin used here was added with a black pigment in order to increase the contrast for the porosity evaluation, which will be illustrated in detail in Chapter 4.

The dense metal part of casting samples were polished and prepared for observation. The two dense metal samples that were cut from the first two steps of a cast object (cast 1) were named as 1-1 and 1-2, as indicated in Figure 3.9:
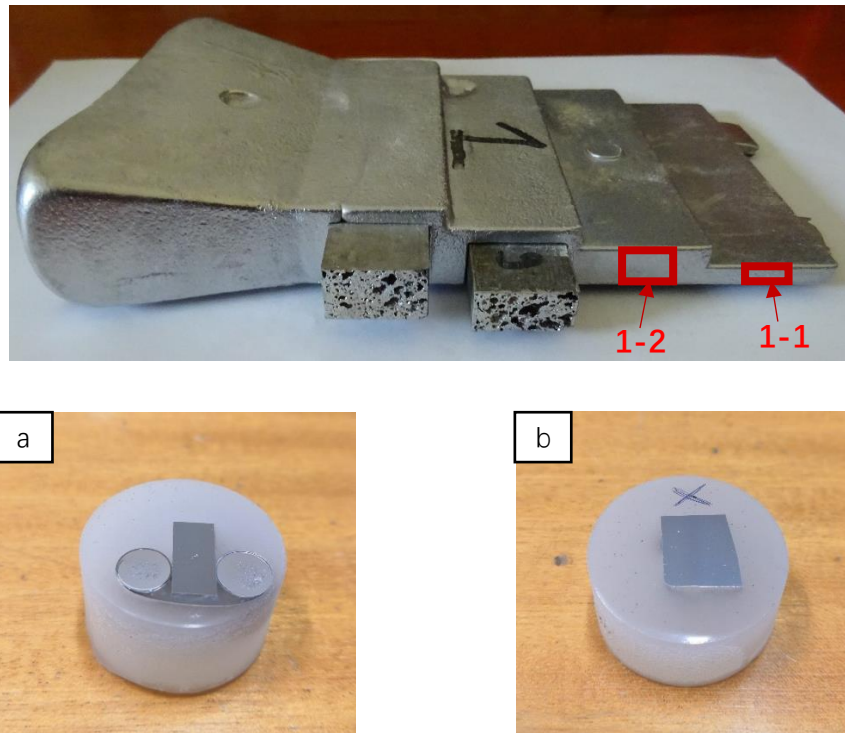
Figure 3.9 Macroscopic appearance: (a) Sample 1-1; (b) Sample 1-2

For the inserted foam observation, there were 3 samples cut from the third step. The samples were named as 1-3, 1-3 Et and 1-3 El. Sample 1-3 had 2 parts, dense metal part and foam part, which were useful to obtain some microstructure information on the boundary between the dense metal and the foam. Sample 1-3 Et was cut transversally from the end of the foam inserts that were not covered by dense metal, while sample 1-3 El was cut longitudinally. Figure 3.10 shows the way of cutting before observation. Figure 3.11 shows the observed foams embedded in resin after mirror polishing.
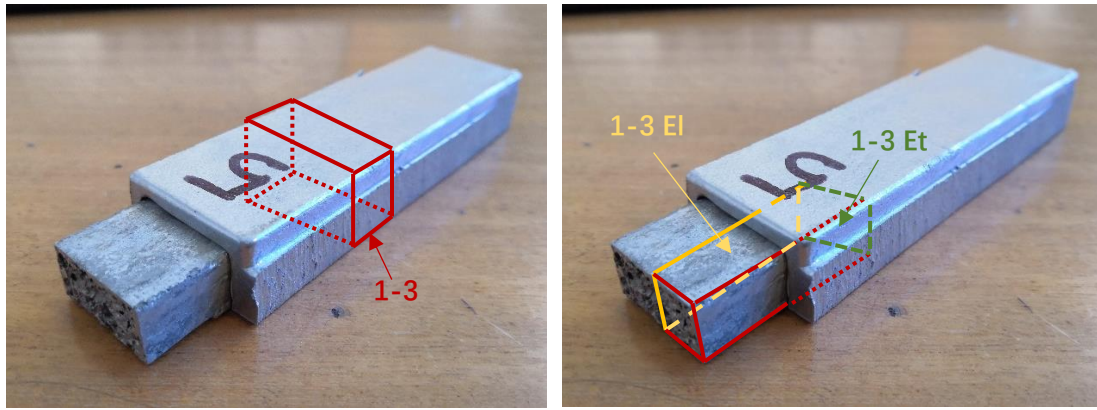
Figure 3.10 The observed surfaces of the casting sample

| *1-3* | *1-3 El* | *1-3 Et* |

Figure 3.11 The macroscopic appearances of observed samples

After the images were obtained, microstructure was analyzed and a software, called ImageJ, was used to analyze the pore dimension, wall and skin thickness of these samples. For dense metal, SDAS (secondary dendrite arm spacing) was measured for each sample.

3.3.1 SDAS measurements

SDAS (Secondary Dendrite Arm Spacing) is the distance between secondary dendrite arms which can be found in microstructures of cast metal and alloys. SDAS is a significant quantity since it is closely related to mechanical properties. Normally, smaller SDAS represents better mechanical properties. [16]

SDAS mainly depends on the cooling rate, which is determined by different casting techniques. [17] The relationship of SDAS and cooling rate is shown in the following Figure 3.11:
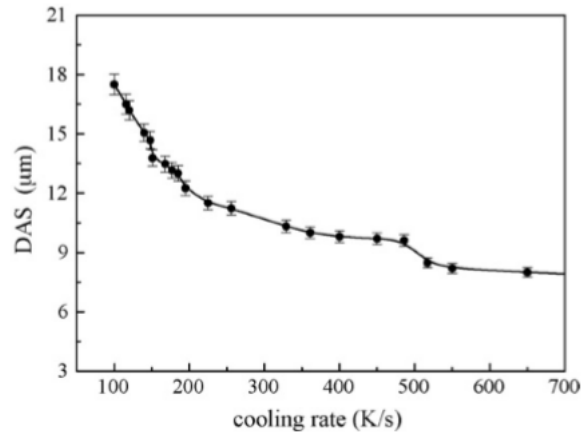
Figure 3.12 The relationship between SDAS and cooling rate [17]

The trend in Figure 3.12 indicates that SDAS decreases with increasing cooling rate.

Before starting measuring SDAS, it was necessary to set the scale to convert pixel to micrometer. 100x magnification optical images were used for these calculations. In each picture, at least five dendrites with at least five secondary arms were measured. Two examples of measuring technique are shown in Figure 3.13:
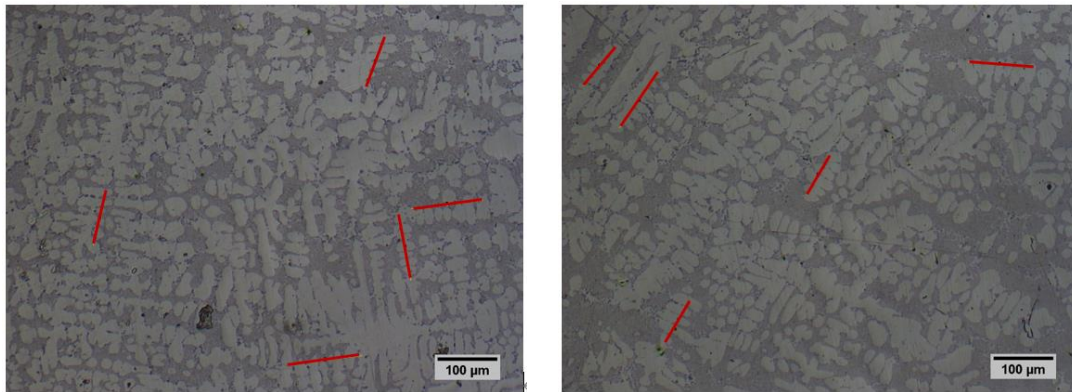
Figure 3.13 SDAS calculation by ImageJ

As shown Figure 3.13, the length of the lines and the number of the arms can be obtained. SDAS can be calculated through the formula:

$$\lambda_2 = \frac{L}{n-1} \quad [18]$$

Where L is the length of the line and n is the number of arms.

3.3.2 Pore sizes

For the pore size, the Feret's method, normally used for the measurement of the sizes of irregular shape particles, was adopted. The Feret diameter is defined as the distance between two parallel planes which restrict the movement along the direction perpendicular to the planes [19].

The measurements were done on optical images at 20x magnification (2x for the objective lens and 10x for the eyepiece lens) and at least 10 measurements for each picture. An example is shown in Figure 3.14:
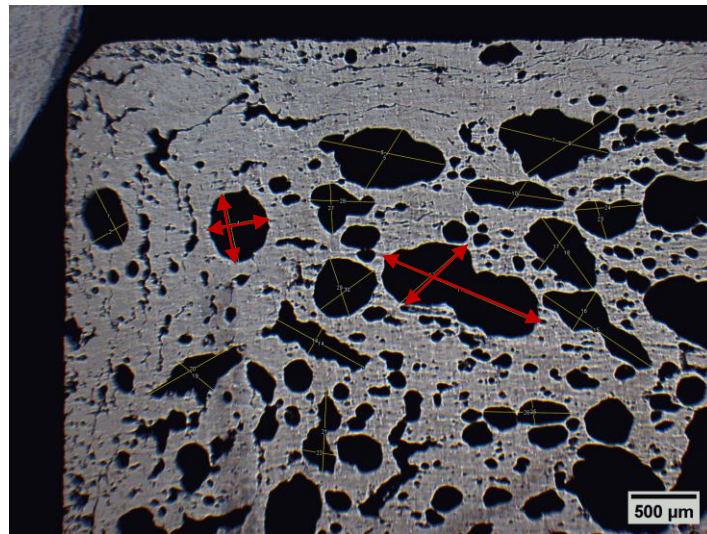
Figure 3.14 Calculation of pore sizes by ImageJ

3.3.3 Skin thickness

The skin thickness can be defined as the distance between the border and the first pore. The measurements were done on optical images at 20x magnification for each image, there were at least 5 measurements. An example is shown in Figure 3.15:
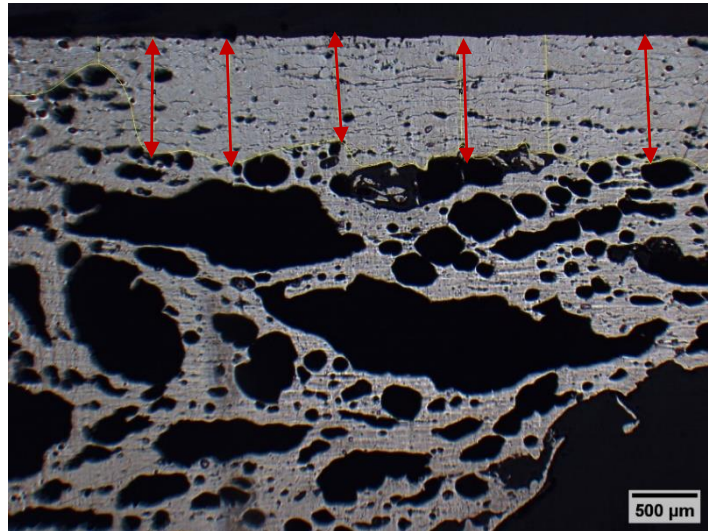
Figure 3.15 Calculation of skin thicknesses by ImageJ

In the evaluation of skin thickness, some small pores and cracks can be neglected because possibly they were defects caused by different shrinkage during foaming process.

3.3.4 Wall thickness

Wall thickness is the thickness of the cell wall (cell boundaries). The measurements were done on optical images at 20x magnification, for each image, there were at least 10 measurements. An example is shown in Figure 3.16
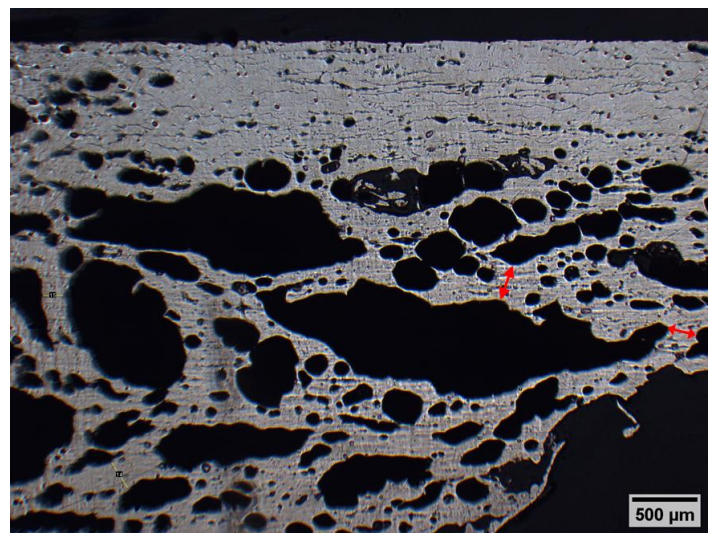
Figure 3.16 Calculation of wall thicknesses by ImageJ

3.4 Scanning Electron Microscopy (SEM) with Energy Dispersive Spectroscopy (EDS)

SEM (scanning electron microscope) is a kind of microscope that produces images of

a sample and gives information of chemical composition. The focused electron beam with high energy scans the surface of the sample and interact with the atoms, producing different signals which give information on the morphology and the chemical composition of the sample. The internal structure of SEM is shown in Figure 3.17:
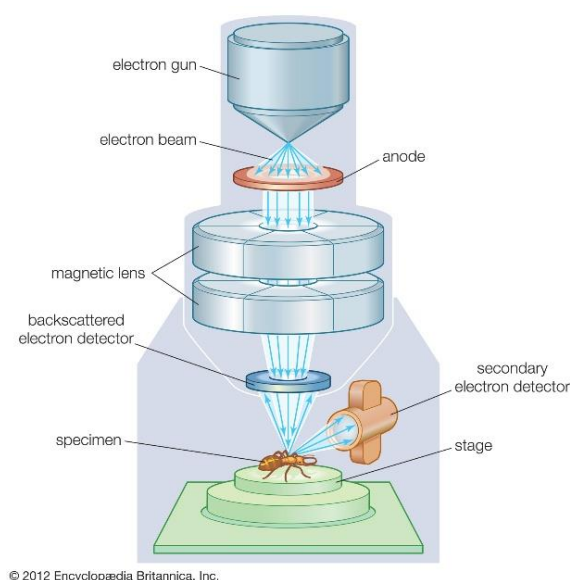
Figure 3.17 The internal structure of SEM [20]

The electron gun emits an electron beam with an energy ranging between 0.2keV and 40keV. It is then focused to a spot of diameter ranging from 0.4nm to 5 nm by condenser lenses. The scanning coils or deflectors, which are normally in the final lens, deflect the beam in x and y axes so that it scans the rectangular area of the sample surface in raster [21].

The interaction between the electrons and the sample generates secondary electrons, backscattered electrons and X rays. Detectors collect these signals and form images to be displayed on the computer. Then electron beam can penetrate the sample to a depth of a few microns, forming a teardrop-shaped volume, known as interaction volume. The penetrating depth depends on the accelerating voltage and the density of the sample. The secondary electrons and X-rays are produced by the interaction inside the sample [22]. A Scheme of the electron-sample interaction is shown in Figure 3.18:
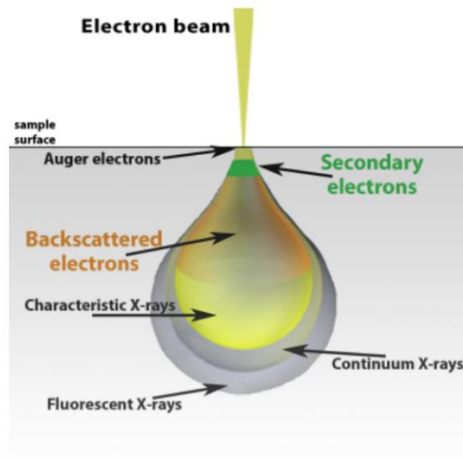
Figure 3.18 Electron-Sample interaction [22]

SEM is a powerful instrument to analyze the material. First of all, it has higher magnification than the optical microscope. Secondarily, even rough surfaces can be observed (differently from optical microscopy). In addition, most SEMs are equipped with EDS (Energy Dispersive Spectroscopy) which helps to analyze the elemental composition in the same time.

Figure 3.19 is the SEM used in the experiments, whose model is JCM 6000 Plus.

Figure 3.19 (a) JCM-6000 Plus; (b) Sample mounting

SEM can only work in vacuum condition. The reason for this is that the electron beam will interact with gases in the environment and can be deflected. So before starting the analysis, evacuation of gases in the chamber should be done in order to obtain a precise result. Generally, this process takes a few minutes.

The sample was installed into the specimen holder by the carbon tape (conductive) by which the sample can be fixed during observation.

3.5 Thermal conductivity measurements

The Transient Plane Sources (TPS) method is the most precise and convenient method to measure the thermal constants of materials, such as thermal conductivity, thermal diffusivity and specific heat per unit volume [23].

• TPS sensor

A transient plane sensor, also known as Hot Disk Thermal Constants Analyzer, is used in this method both as heat source and temperature sensor. The sensor includes an electrical conducting pattern of thin nickel foil in the shape of double spiral, which is embedded in an insulating layer of Kapton. Figure 3.19 shows the structure of the sensor:
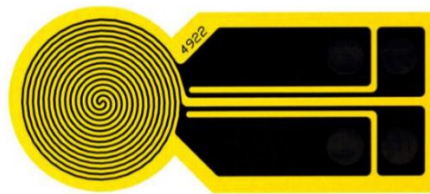
Figure 3.20 Schematic diagram of TPS sensor [23]

The nickel is chosen because of its high temperature coefficient of resistivity [23].

• Sample preparation

A basic assumption of the solution of the thermal conductivity equation is that the sensor is located in an infinite material, which means that the sample sizes should be large enough. During the experiment, the "thermal wave" or "thermal penetration depth" should not reach the sample boundaries. The probing depth, which is the proceeding depth in the experiment, is a function of the measuring time.

$$\Delta p = 2 \cdot \sqrt{k \cdot t} \ \ [23]$$

Where k is the thermal diffusivity and t is the measuring time. A conclusion can be drawn from this equation: the distance between any point of the sensor and any point on the surface of the samples must exceed Δp when the measuring time is t. Therefore, it is easier to conduct the measurement on large samples in order to have

a precise result. For flat samples, the thickness should not be less than the radius of the hot disk.

If the sample does not meet this requirement, i.e. the probing depth exceed the diameter of the hot disk, the measuring time should be controlled, theoretically between one third and one whole characteristic time τ. The characteristic time τ, is a function of the radius of the sensor a, and the thermal diffusivity k, of the sample.

$$\tau = \frac{a^2}{k} \ [23]$$

• Measuring process

The sensor is placed in between two pieces of the sample, each surface directly contacting with the sensor. Figure 3.20 shows the installment of the experiment.
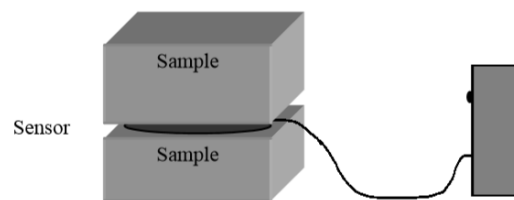
Figure 3.21 Experimental set-up for thermal conductivity measurement [24]

A constant electric power is supplied to the sensor and the temperature increase is reflected in the resistance variation. Therefore, the thermal transport properties can be evaluated by the recorded resistance.

• Samples to be measured in this thesis (Figure 3.21)

In this work two foam samples, with characteristic comparable with the ones of foam inserts previously described, but with suitable shape/dimensions for the test were used.
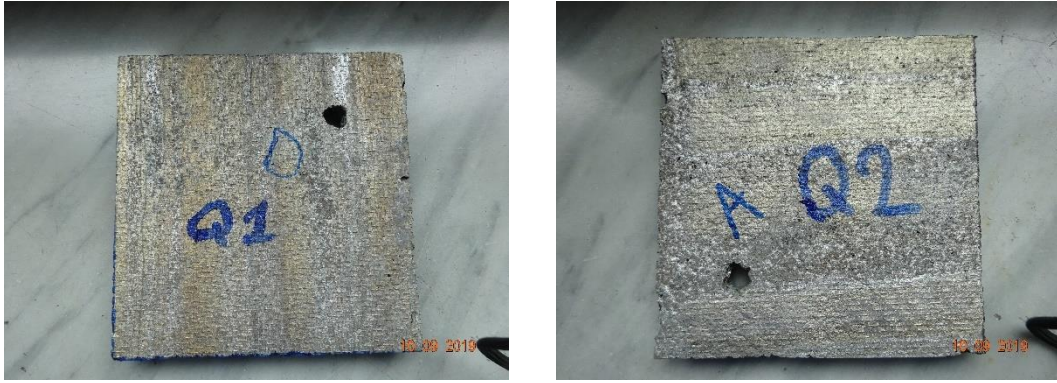
Figure 3.22 Samples for porosity conductivity measurement: Q1 (left) and Q2 (right)

Chapter 4

Results and discussion

4.1 Density measurements-results

	SET 1	SET 2	SET 3	SET 4	SET 5	SET 6
Average Density (g/cm³)	1.05	1.54	1.27	1.28	1.53	1.03
Relative Density	0.39	0.57	0.47	0.47	0.57	0.38

Table 4.1 Densities of foam inserts

The results of density measurements are reported in Table 4.1. it can be observed that effectively three types of foams are present with average densities of 1 g/cm^3 (set 1 and 6), 1.3 g/cm^3 (set 3 and 4) and 1.5 g/cm^3 (set 2 and 5).

4.2 Optical Microscopy

4.2.1 Non inserted foams

Three non-inserted foams, foam 3 (0.98 g/cm^3), foam 7 (1.25 g/cm^3) and foam 11 (1.5 g/cm^3) were observed in optical microscope. The images of microstructures of these non-inserted foams under optical microscope are shown in Figure 4.1-4.6:

• Foam 3
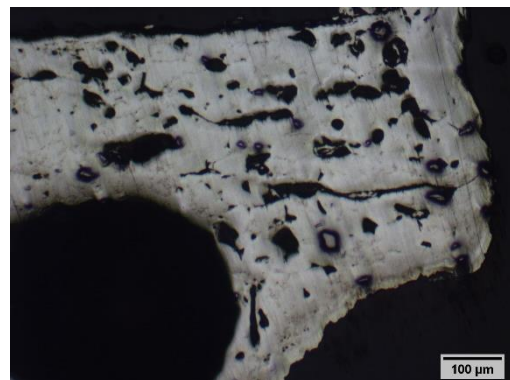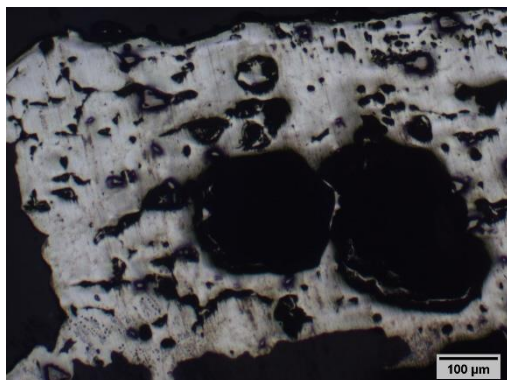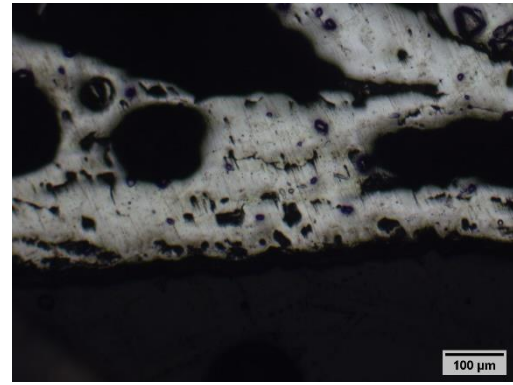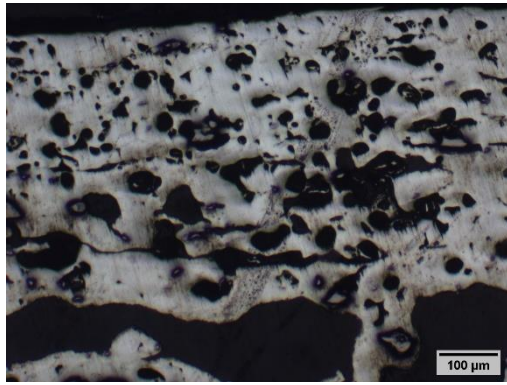
Figure 4.1 Microstructure-Optical microscopy observations (100x) – Foam 3 no etching
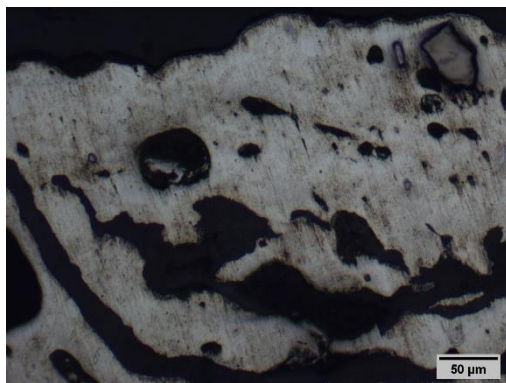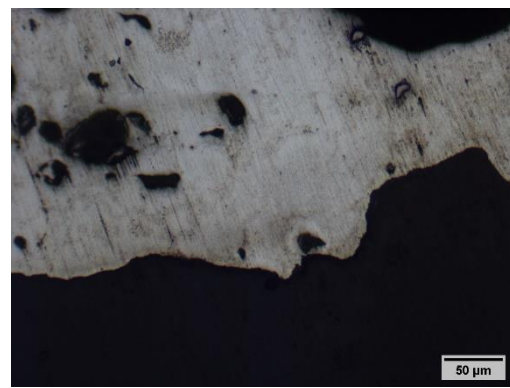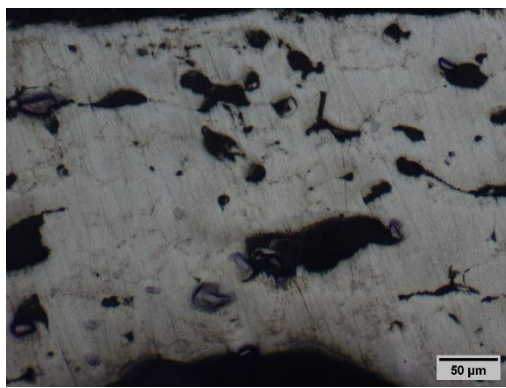
Figure 4.2 Microstructure-Optical microscopy observations (200x) - Foam 3 no etching
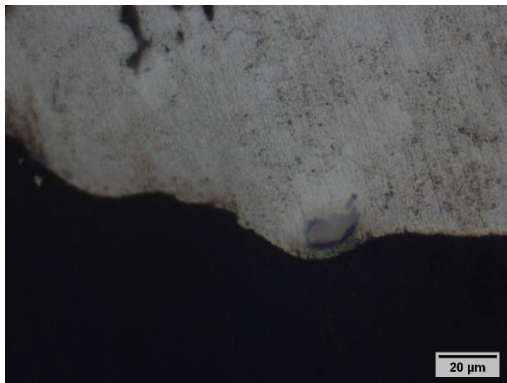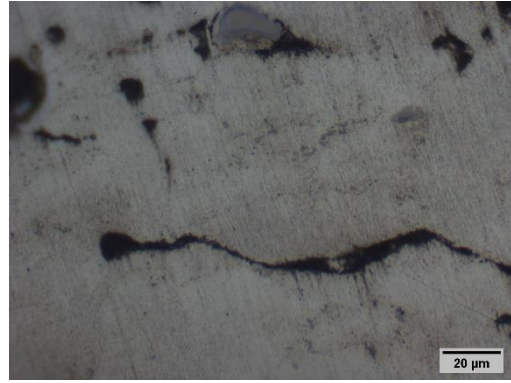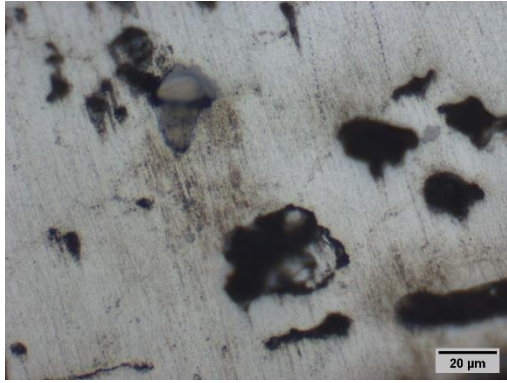
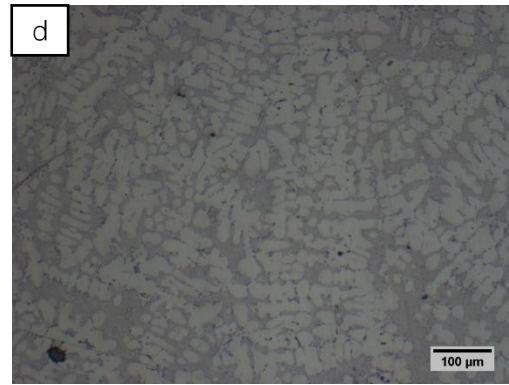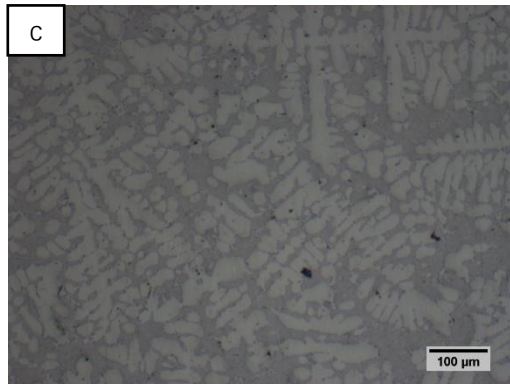*Figure 4.3 Microstructure-Optical microscopy observations (500x) - Foam 3 no etching*

• Foam 7
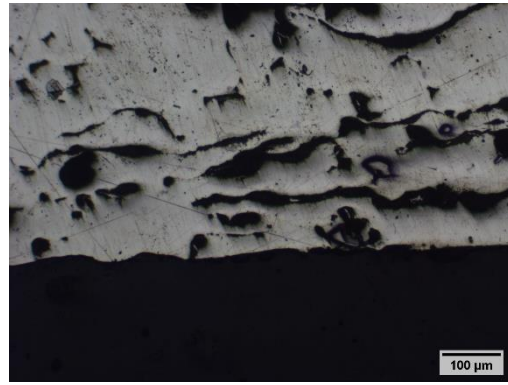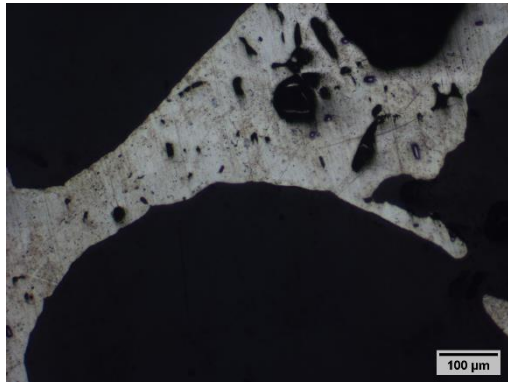
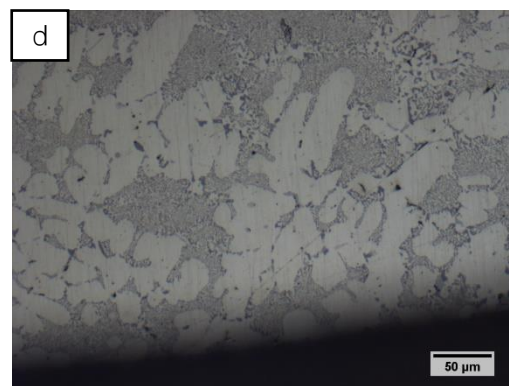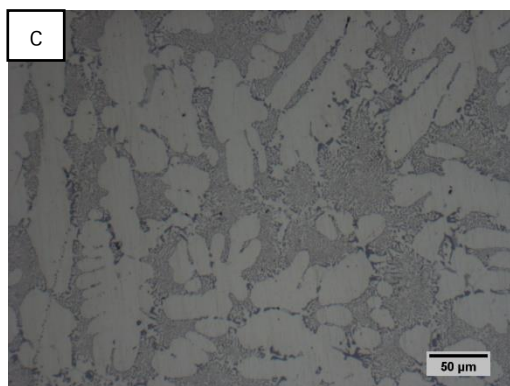*Figure 4.4 Microstructure-Optical microscopy observations (100x) - Foam 7 no etching*
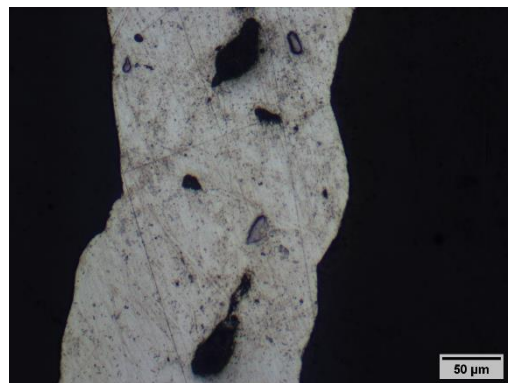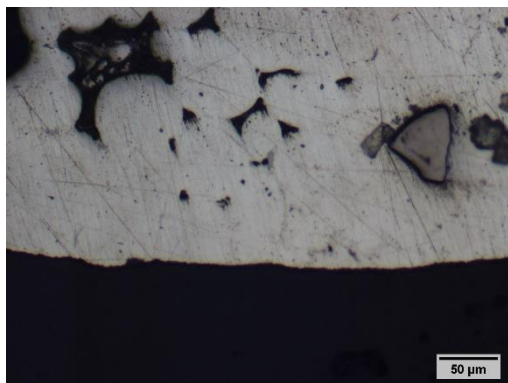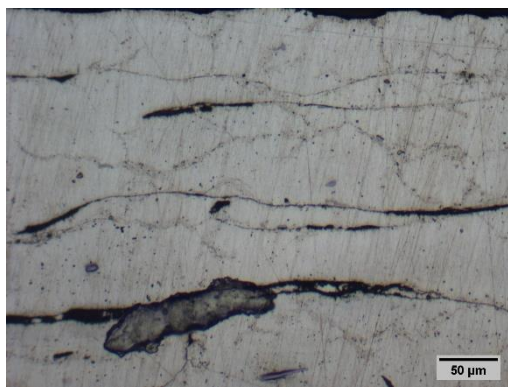
Figure 4.5 Microstructure-Optical microscopy observations (200x) - Foam 7   no etching
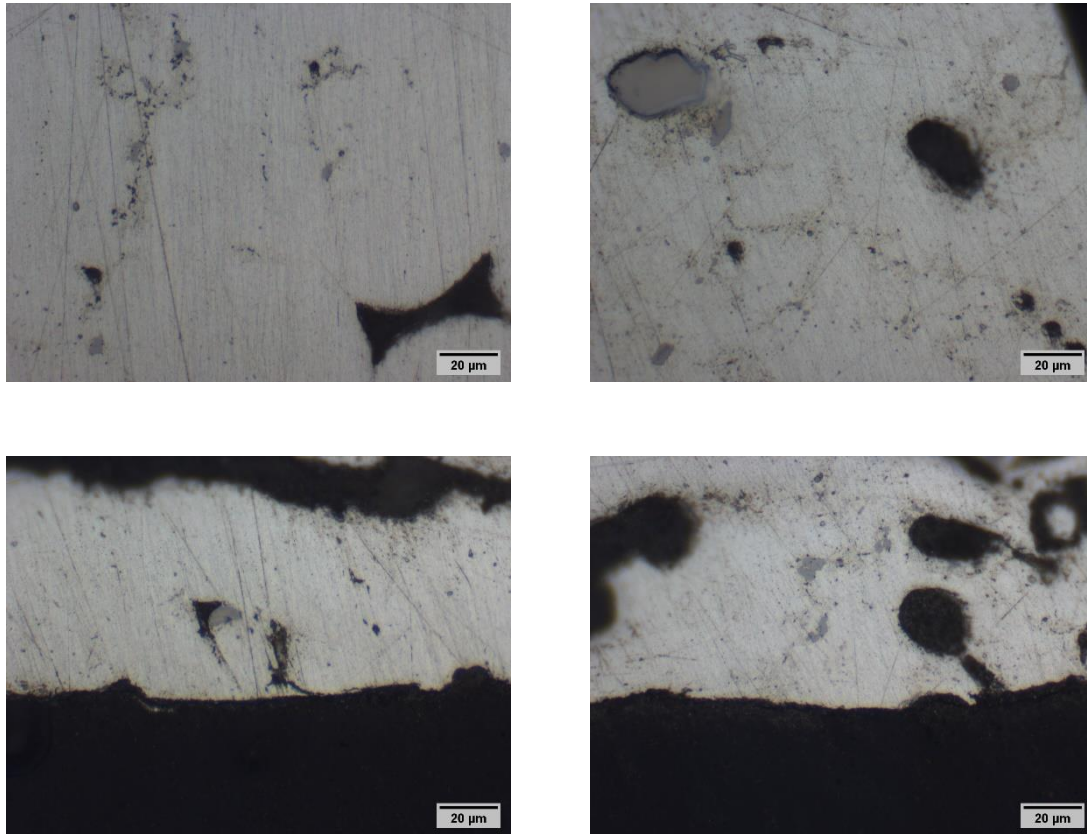
Figure 4.6 Microstructure-Optical microscopy observations (500x) - Foam 7 no etching

Optical images evidence the presence of numerous micro pores on the cell walls as well as on the dense outer skin. Moreover, some grey particles with polygonal shape can be observed. SEM-EDS analyses (section 4.5) will give more information on their composition.

a. Pore size

The results of pore dimension measurements are reported in Table 4.2 and Figure 4.7.

	Pore Sizes (µm)		
	Foam 3	Foam 7	Foam 11
Min	94.28	94.19	144.11
Max	2816.48	3934.38	3056.94
Mean	566.09	567.85	632.65
S.D.	510.34	542.23	456.06

Table 4.2 Statistical data of pore sizes of non-inserted foams
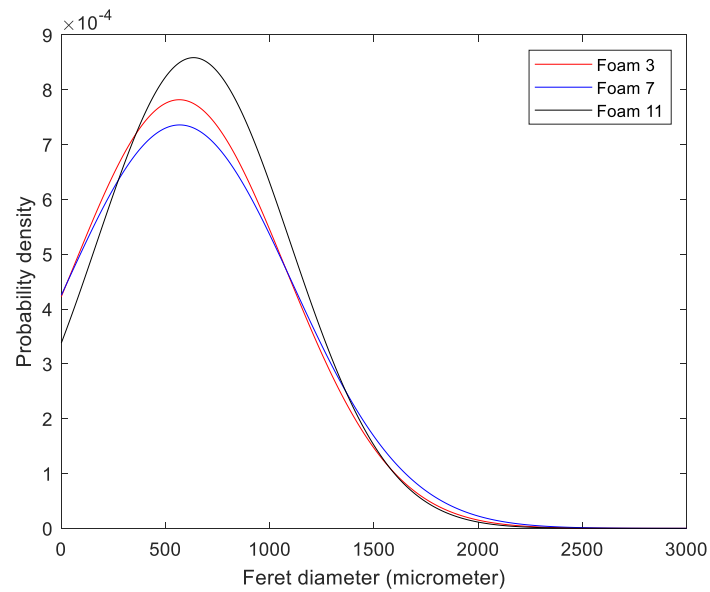
Figure 4.7 Gaussian distribution of pore sizes of non-inserted foams

* Results relative to 182 measurements for foam 3, 180 measurements for foam 7 and 682 measurements for foam 11.

The average pore sizes of three foams are very close to each other (around 570 µm), with a slightly different standard deviation.

b. Skin thickness

The results of skin thickness measurements are reported in Table 4.3 and Figure 4.8.

	Skin thickness (µm)		
	Foam 3	Foam 7	Foam 11
Min	35.43	33.99	52.43
Max	313.29	1273.35	1036.10
Mean	122.13	447.41	321.26
S.D.	63.09	346.00	236.53

Table 4.3 Statistical data of skin thicknesses of non-inserted foams
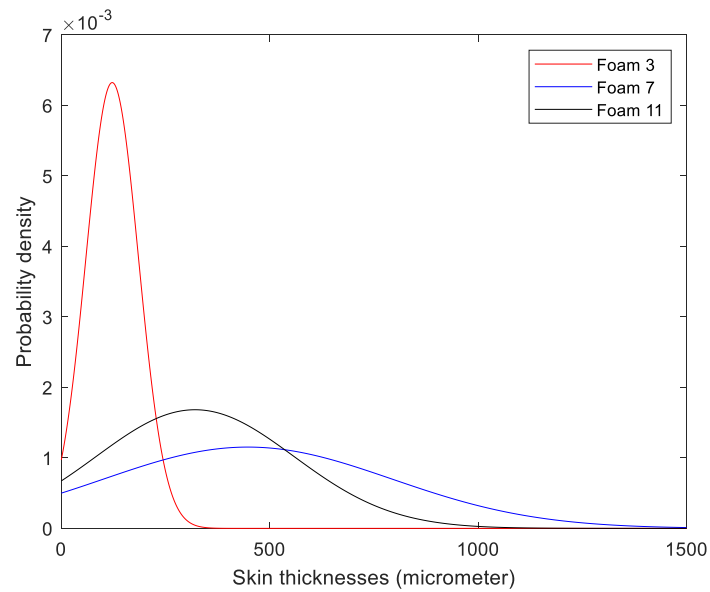
Figure 4.8 Gaussian distribution of skin thicknesses of non-inserted foams

* Results relative to 75 measurements for foam 3, 39 measurements for foam 7 and 136 measurements for foam 11.

For some edges of foam 7, there were almost no skin, so less measurements were obtained.

The skin thicknesses of three foams differ a lot from each other, which can also by recognized by macroscopic appearance. The two smaller edges of the foams have almost no skin. The average skin thickness and the standard deviation of foam 3 are much smaller than foam 7 and foam 11.

c. Wall thickness

The results of wall thickness measurements are reported in table 4.4 and figure 4.9.

	Wall thickness (μm)		
	Foam 3	Foam 7	Foam 11
Min	14.52	13.33	23.72
Max	162.21	394.76	399.11
Mean	58.72	76.99	111.26
S.D.	28.99	65.32	65.45

Table 4.4 Statistical data of wall thicknesses of non-inserted foams
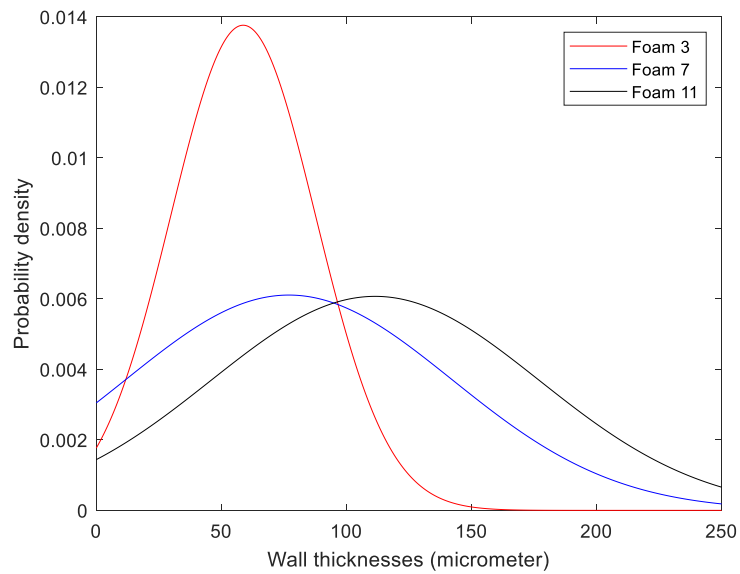
Figure 4.9 Gaussian distribution of wall thicknesses of non-inserted foams

* Results relative to 110 measurements for foam 3, 120 measurements for foam 7 and 407 measurements for foam 11.

The difference in wall thickness among the different foams is limited. However a moderate increase in the wall thickness can be noticed with the increase in the density.

4.2.2 Cast metal

In Figure 4.13-4.18, optical images of dense metal sample 1- step 1 and sample 1- step 2 at different magnifications are reported in figures 4.13-4.18.

• Sample 1-Step 1
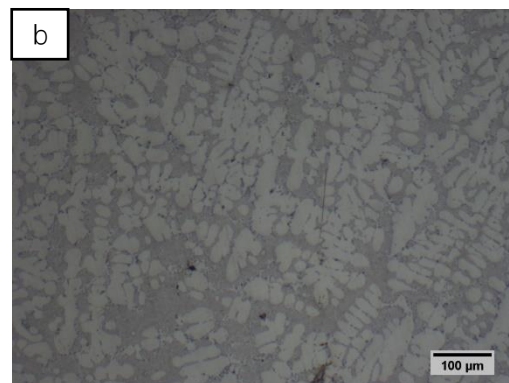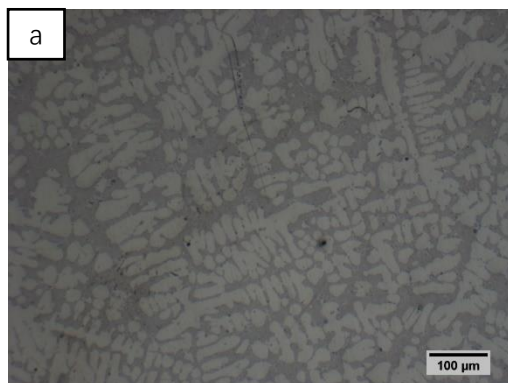
Figure 4.13 Microstructure-Optical microscopy observations (100x) – sample 1 step 1- no etching
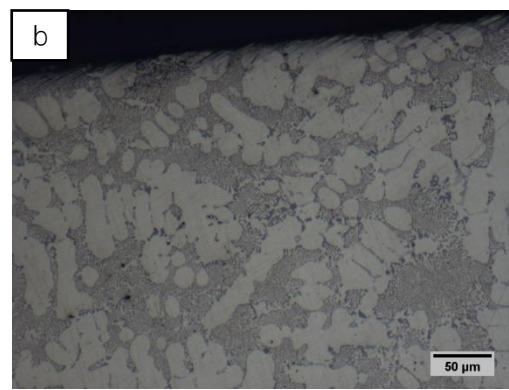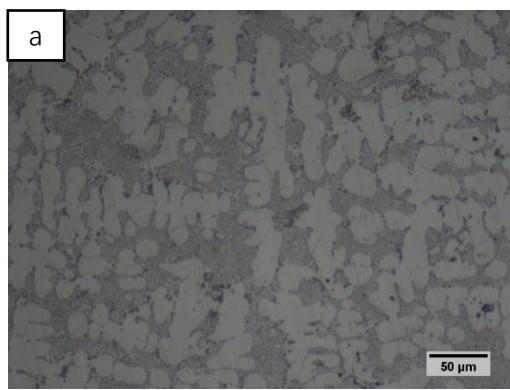
Figure 4.14 Microstructure-Optical microscopy observations (200x) - sample 1 step 1 no etching
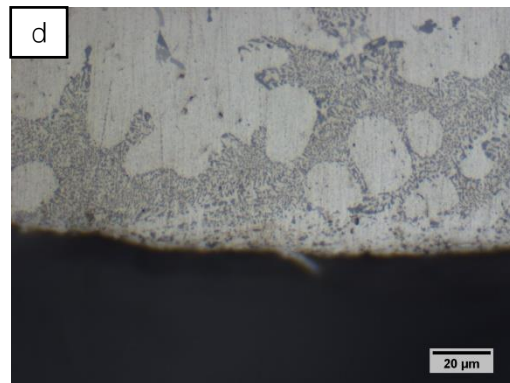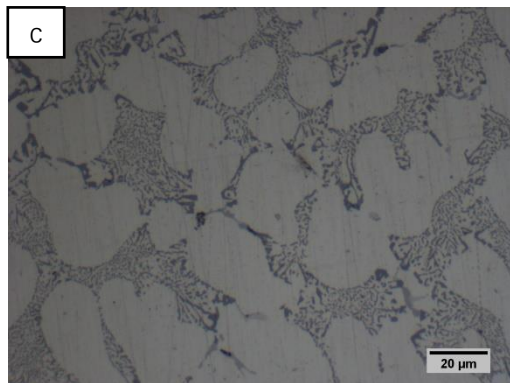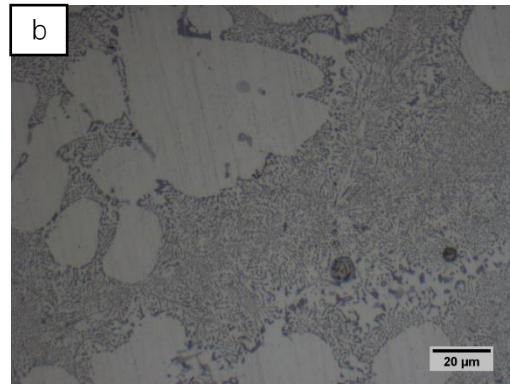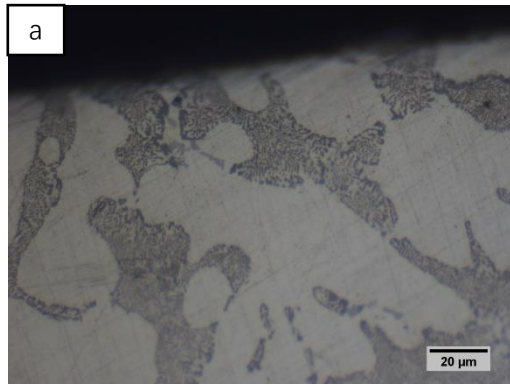
Figure 4.15 Microstructure-Optical microscopy observations (500x) - sample 1 step 1 no etching

• Sample 1-Step 2
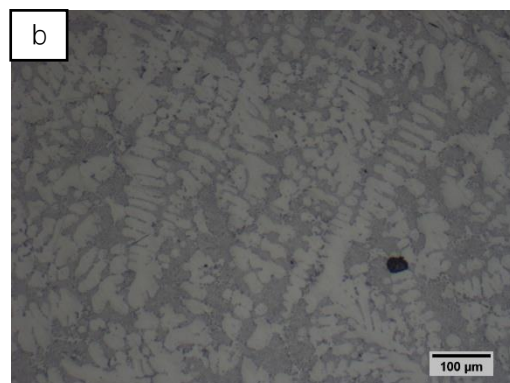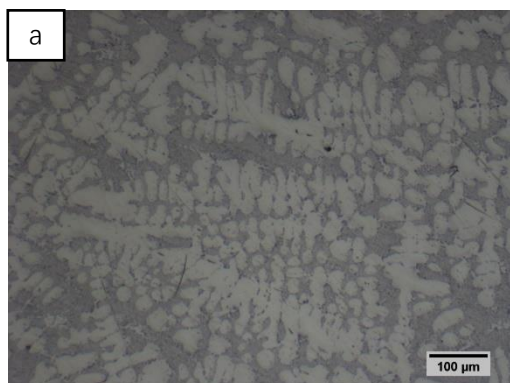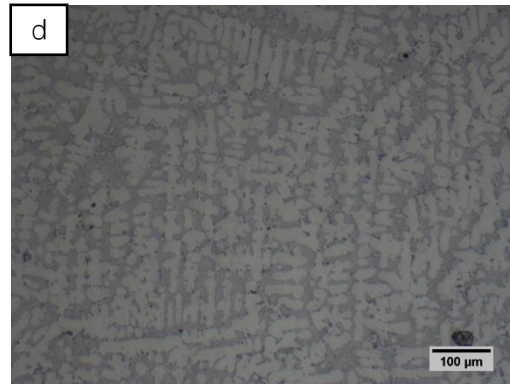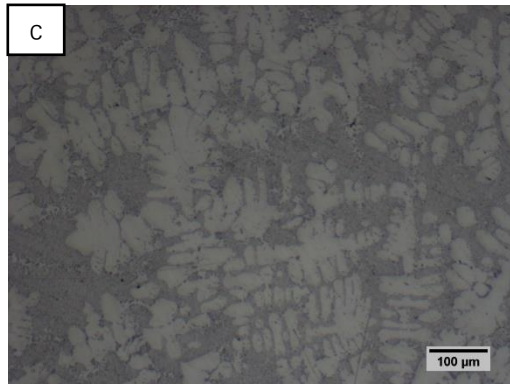
Figure 4.16 Microstructure-Optical microscopy observations (100x) - sample 1 step 2 no etching
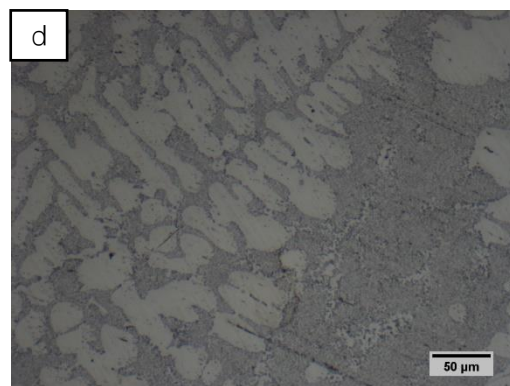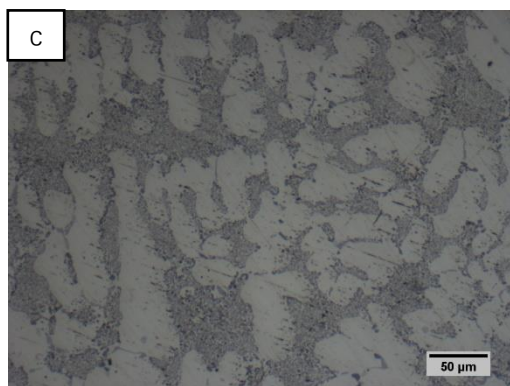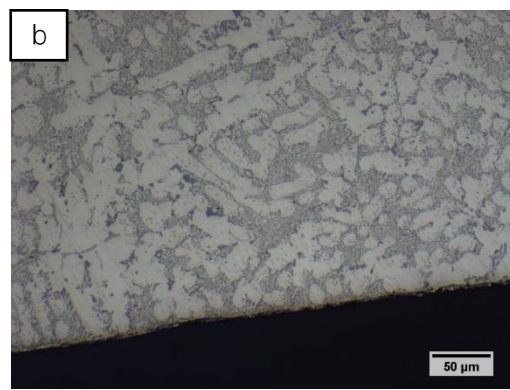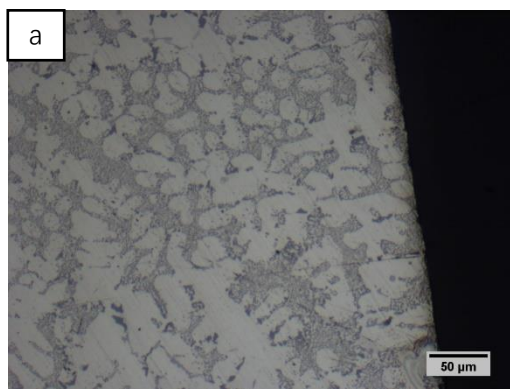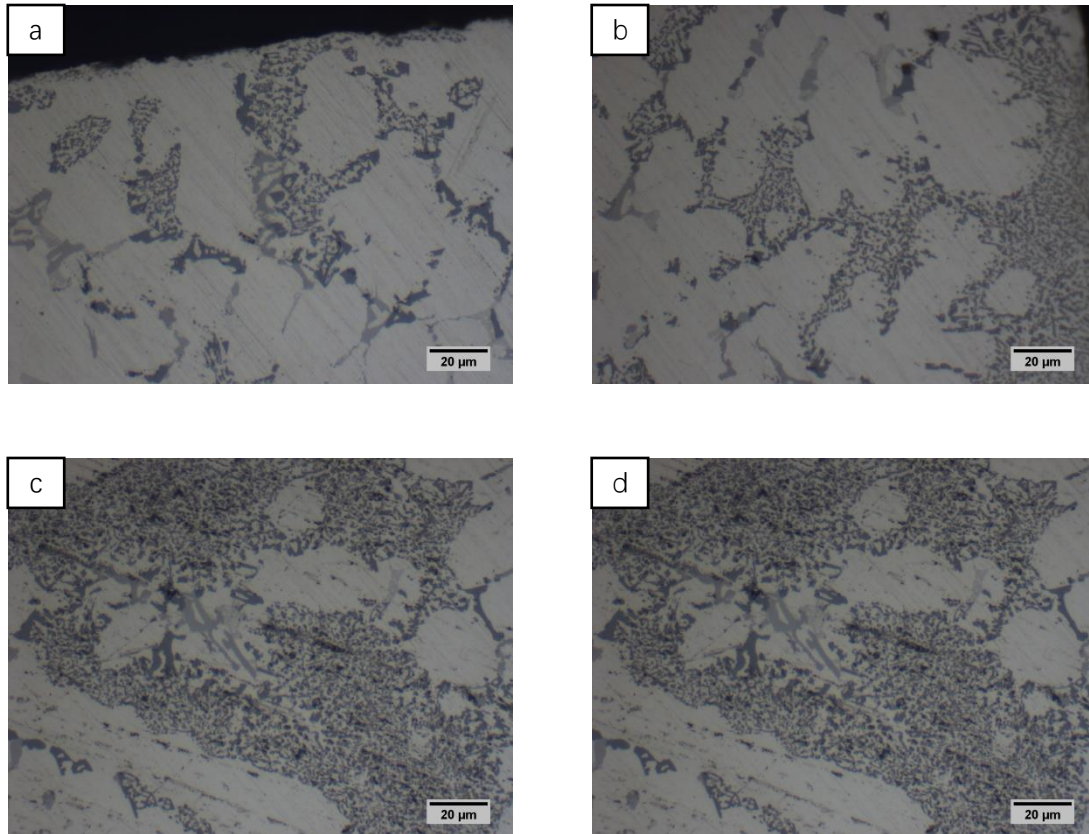

Figure 4.17 Microstructure-Optical microscopy observations (200x) - sample 1 step 2 no etching

Figure 4.18 Microstructure-Optical microscopy observations (500x) - sample 1 step 2 no etching

From Figure 4.13-4.18, it can be evidenced a dendritic structure (lighter color in optical images) which is typical of cast Al alloys and can be associated with the aluminum rich phase (α), the darker area can be related to the Al-Si eutectic microstructure. Moreover, some grey particles can be evidenced. SEM-EDS analyses (section 4.5) will clarify their composition.

The result of SDAS for dense metal are reported in Table 4.8 and the Gaussian distribution is shown in Figure 4.19:

	SDAS (µm)	
	1-1	1-2
Min	11.5	11.1
Max	26.3	34.9
Mean	17.7	20.2
S.D.	2.9	4.5

Table 4.8 SDAS measurements of 1-1 and 1-2

* Results relative to 80 measurements for Sample 1-Step 1 and 60 measurements for Sample 1-Step 2.
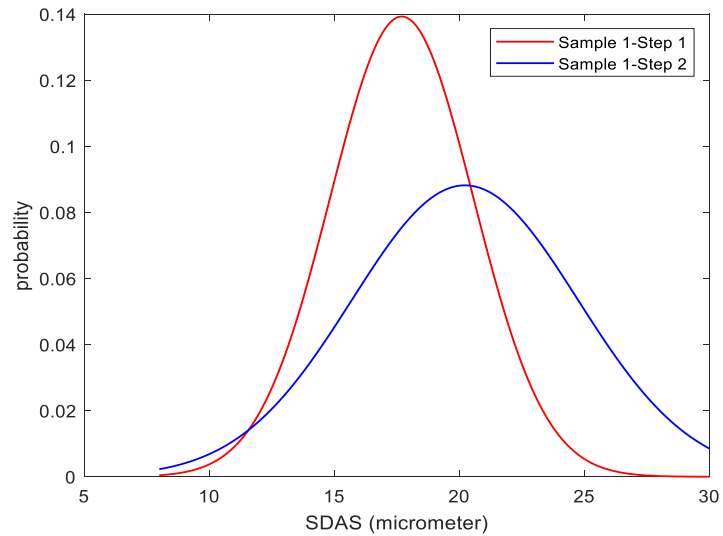
Figure 4.19 Gaussian distribution of SDAS of 1-1 and 1-2

From the diagram of SDAS distribution of the two samples (Figure 4.19), it can be observed that the average SDAS of sample 1-step 2 is higher than sample 1-step 1. Even if the difference is moderate, this result is consistent with the theory that higher cooling rate is associated with smaller SDAS. Step 1 is thinner than step 2, so it has higher percentage of material contacted with the mold, which results in higher cooling rate.

4.2.3 Inserted foams

The images of microstructures of sample 1 step 3 in different magnifications are shown in Figure 4.20-4.22:
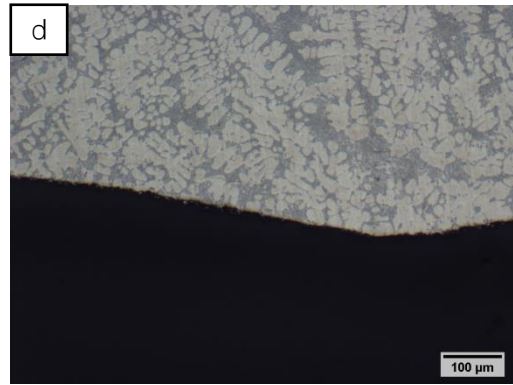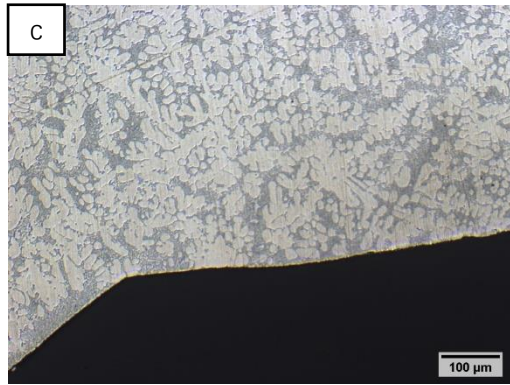
• Sample 1-3 (dense metal part)
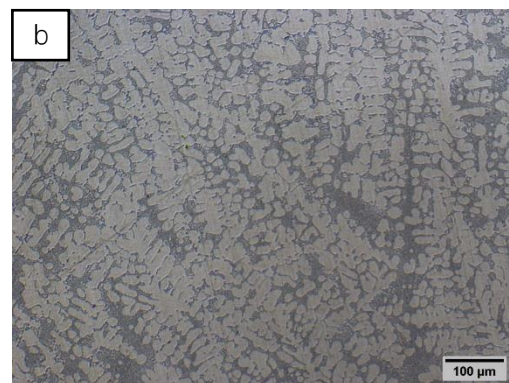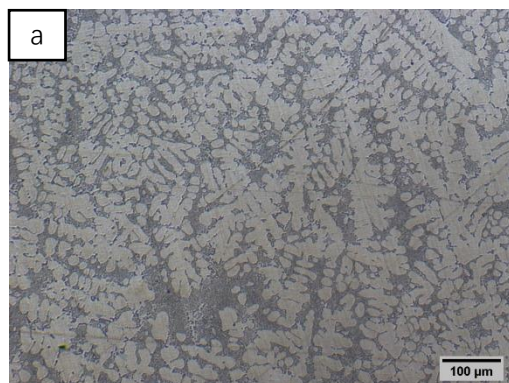
Figure 4.20 Microstructure-Optical microscopy observations (100x) - Sample 1-3 no etching
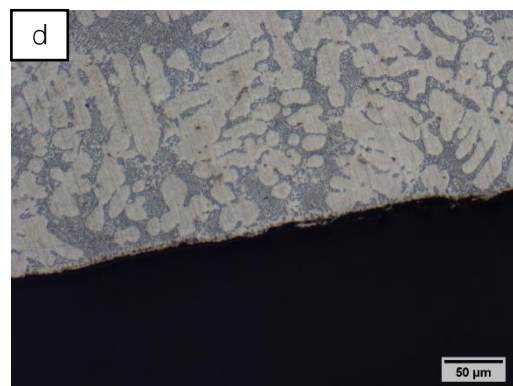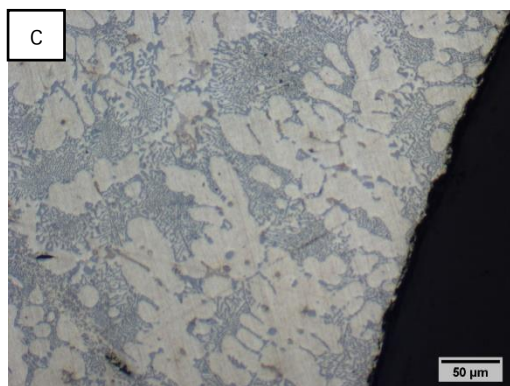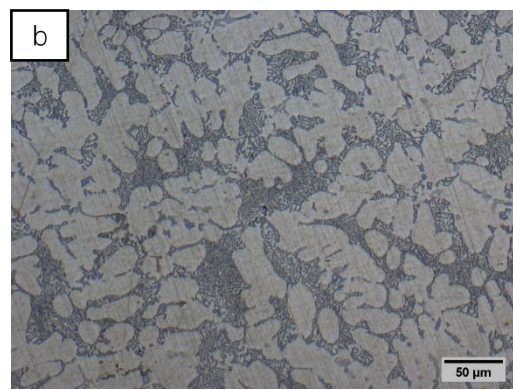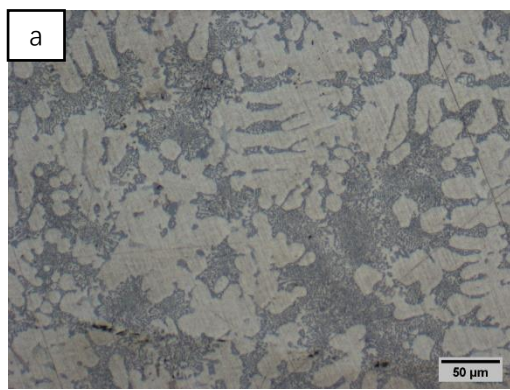

Figure 4.21 Microstructure-Optical microscopy observations (200x) - Sample 1-3 no etching
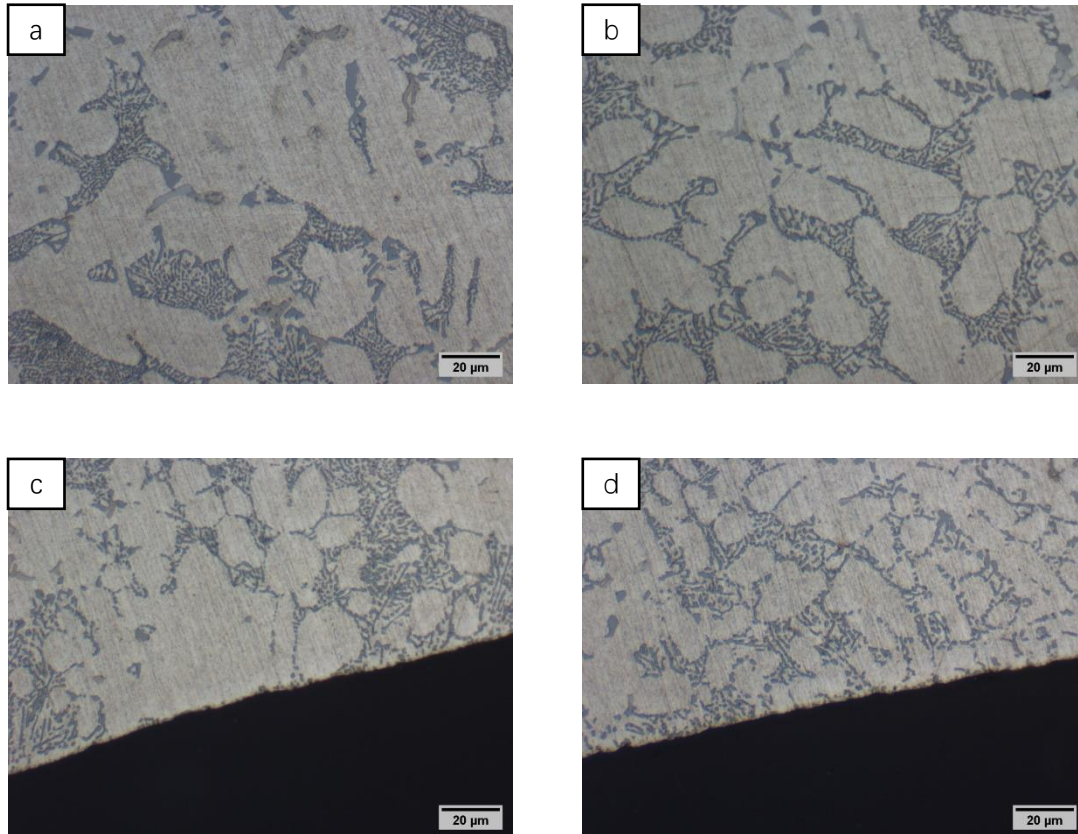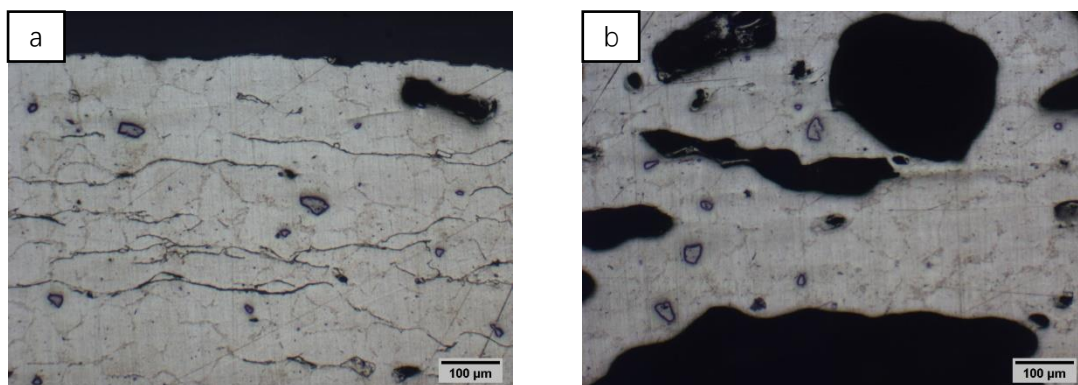
Figure 4.22 Microstructure-Optical microscopy observations (500x) - Sample 1-3 no etching

Optical images of the dense Al shell of sample 1 step 3 (Figures 4.20-4.22) evidence dendritic structure (lighter color in optical images) which is typical of cast Al alloys and can be associated with the aluminum rich phase (α), the darker area can be related to the Al-Si eutectic microstructure. This microstructure is analogous to the one of dense metal in steps 1 and 2 (described in paragraph 4.2.1).

Optical images of the foam insert are reported in Figures 4.23-4.31.

• Sample 1-3 (foam part)

Figure 4.23 Microstructure-Optical microscopy observations (100x) - Sample 1-3 no etching

Figure 4.24 Microstructure-Optical microscopy observations (200x) - Sample 1-3 no etching
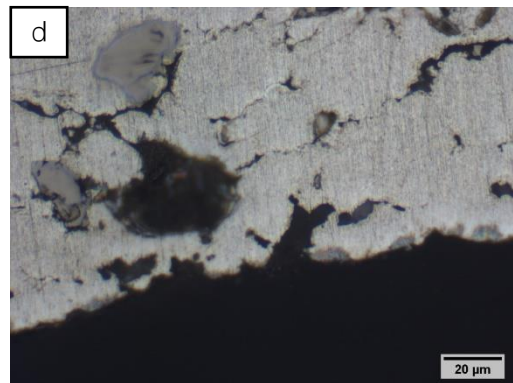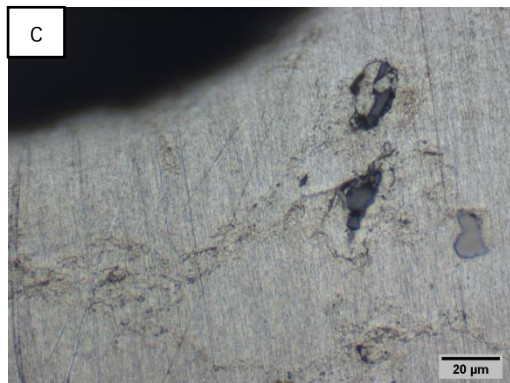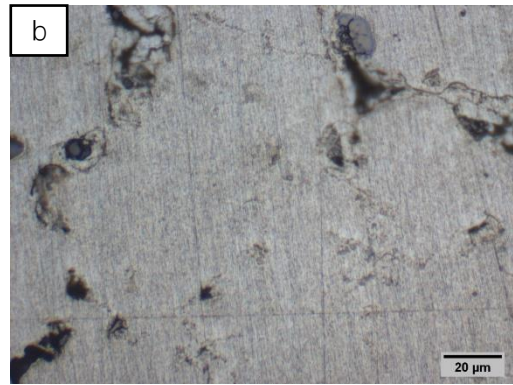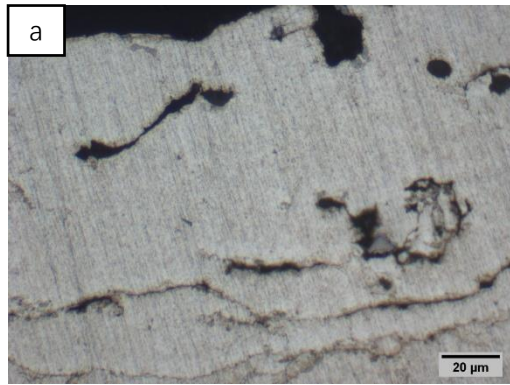
Figure 4.25 Microstructure-Optical microscopy observations (500x) - Sample 1-3 no etching

• Sample 1-3 El
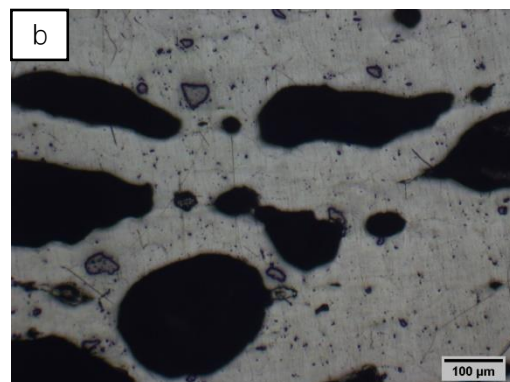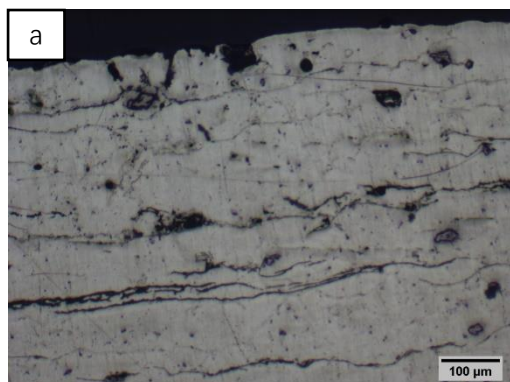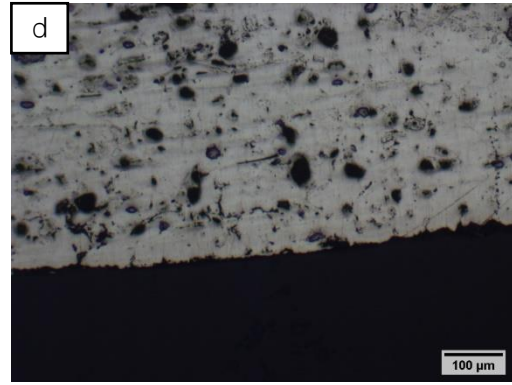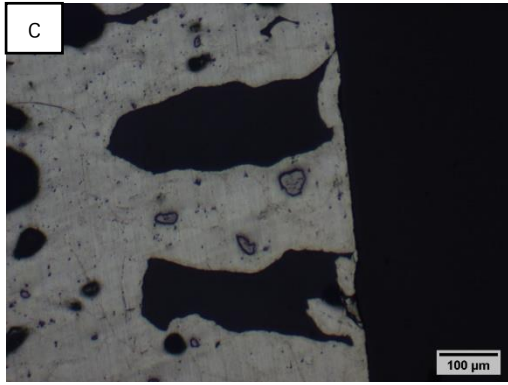
Figure 4.26 Microstructure-Optical microscopy observations (100x) - Sample 1-3 El no etching
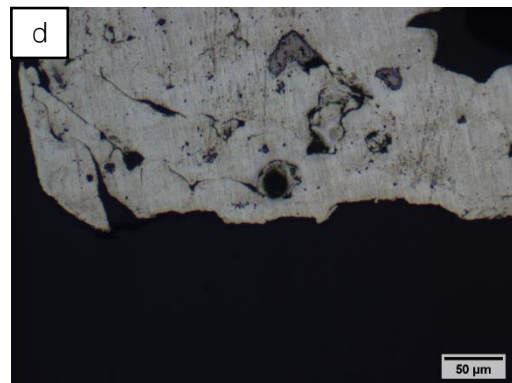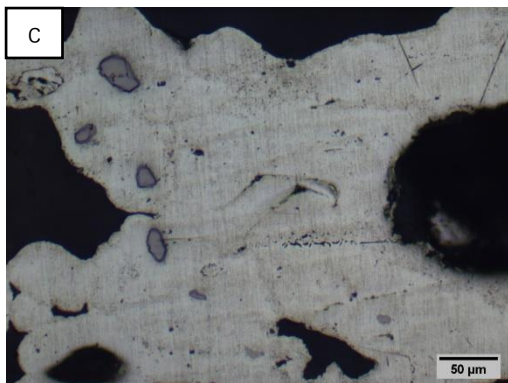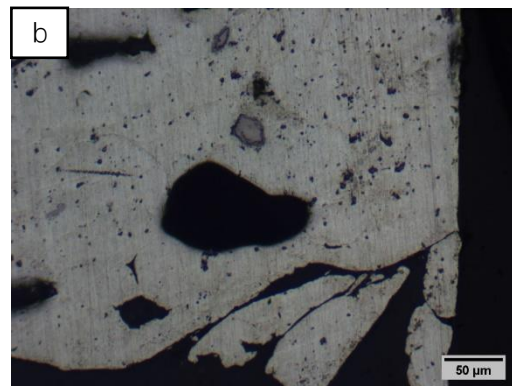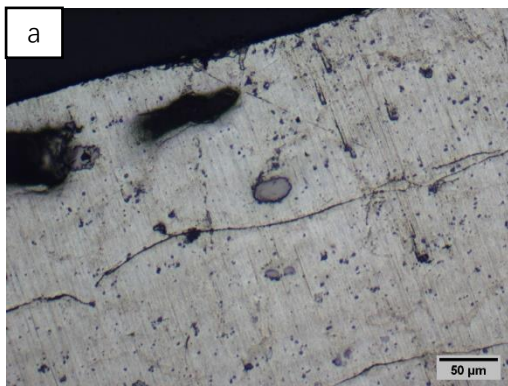
Figure 4.27 Microstructure-Optical microscopy observations (200x) - Sample 1-3 El no etching
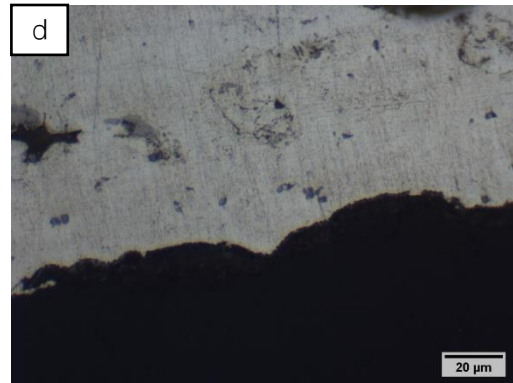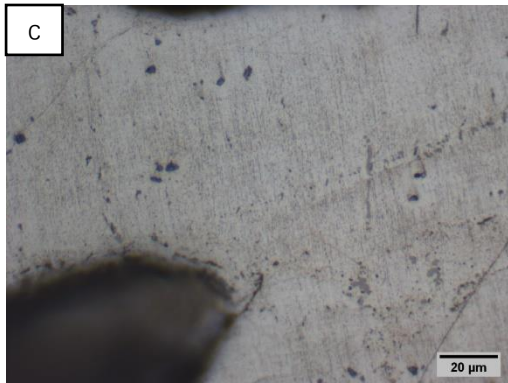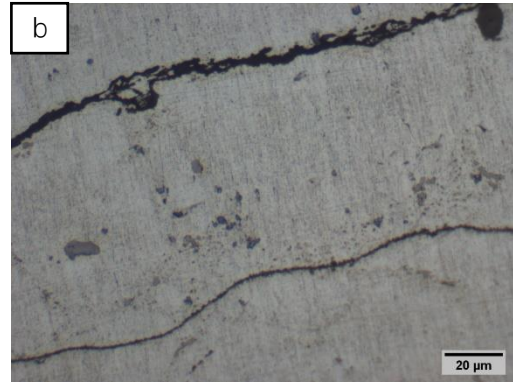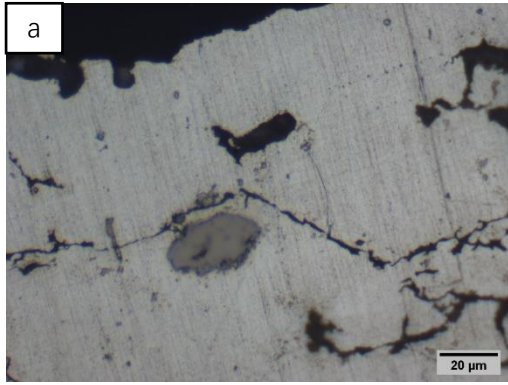
Figure 4.28 Microstructure-Optical microscopy observations (500x) - Sample 1-3 El no etching
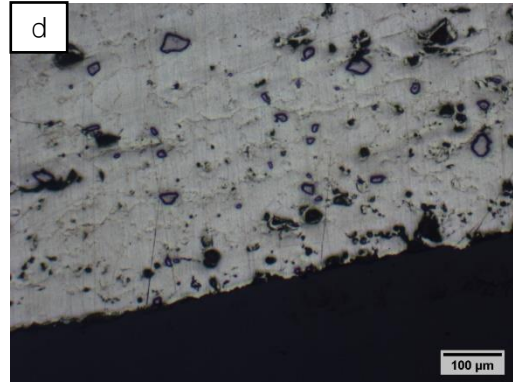
• Sample 1-3 Et
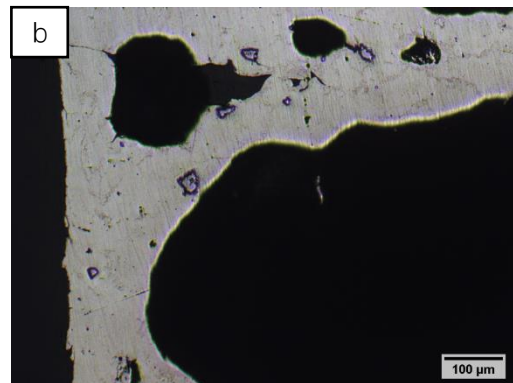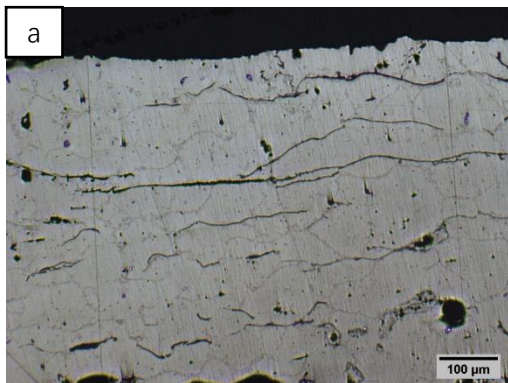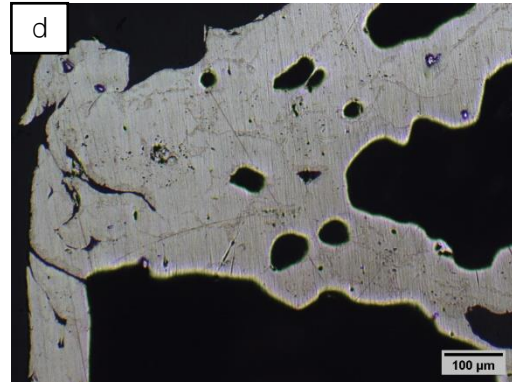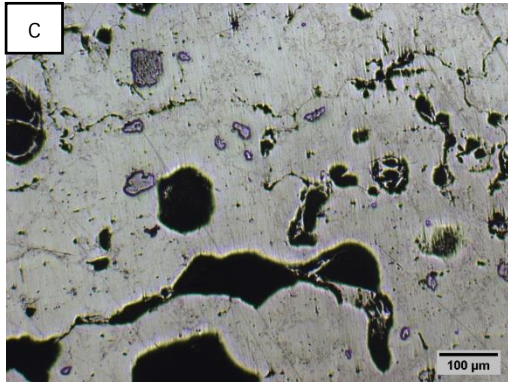
Figure 4.29 Microstructure-Optical microscopy observations (100x) - Sample 1-3 Et no etching
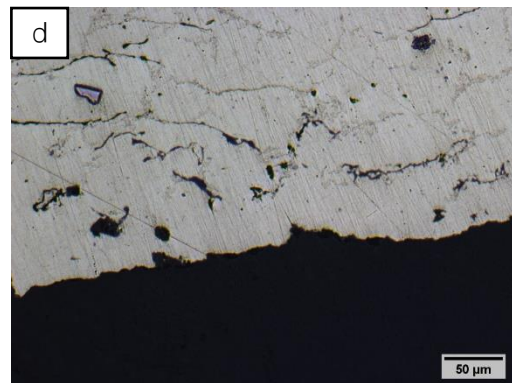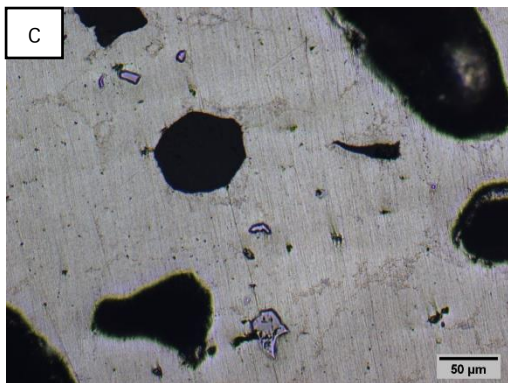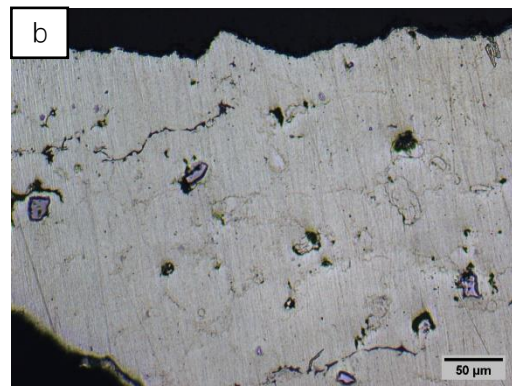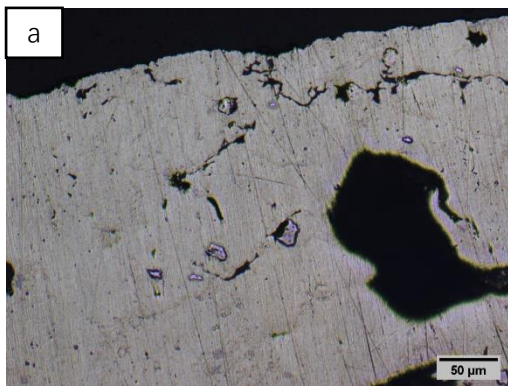
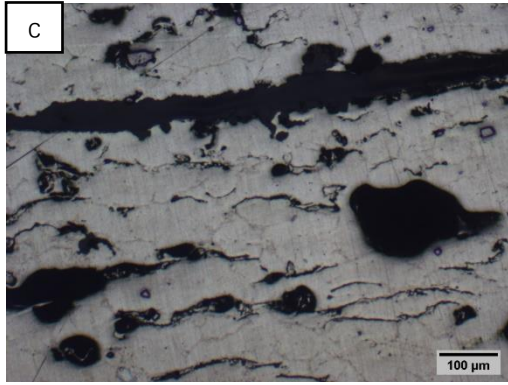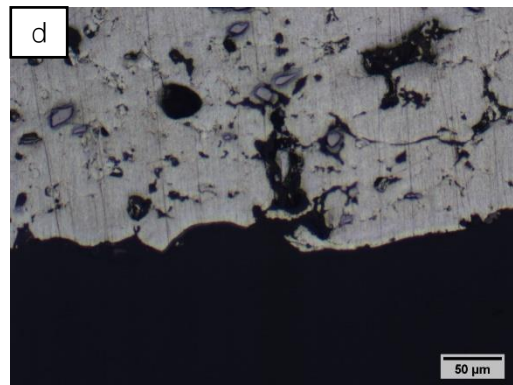*Figure 4.30 Microstructure-Optical microscopy observations (200x) - Sample 1-3 Et no etching*

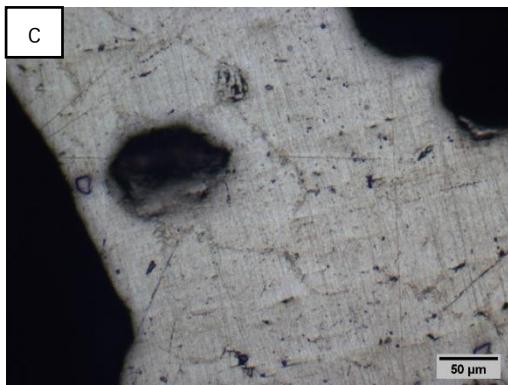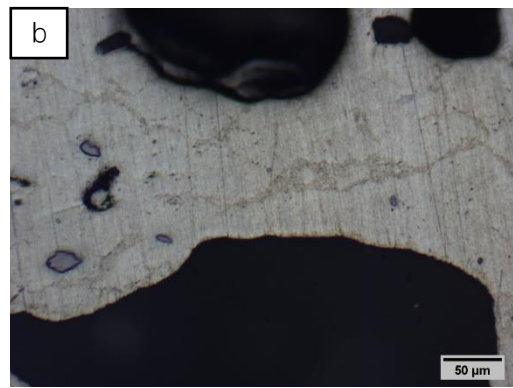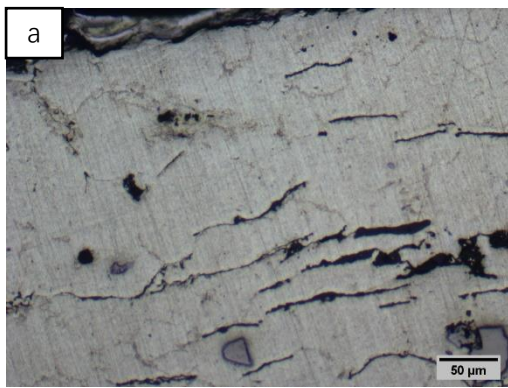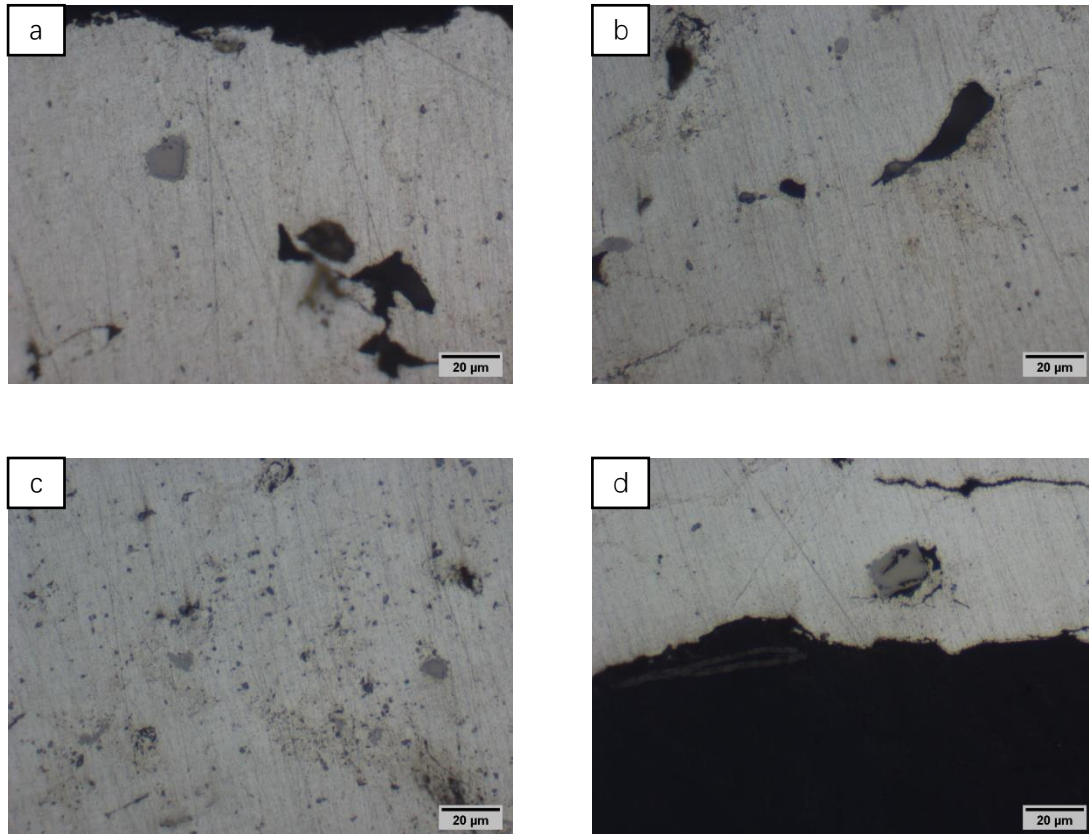*Figure 4.31 Microstructure-Optical microscopy observations (500x) - Sample 1-3 Et no etching*

Optical images of inserted foams (Figures 4.23-4.31) show the presence of numerous micro-pores and cracks, as well as of grey polygonal particles, already evidenced on not inserted foams (paragraph 4.2.2).

No alterations attributable to the contact with cast metal can be highlighted. The boundary between the foam core and the dense shell is always well defined and a micrometric gap is present between the two structures. Figure 4.32 shows the gap in optical microscope with x100 magnification.
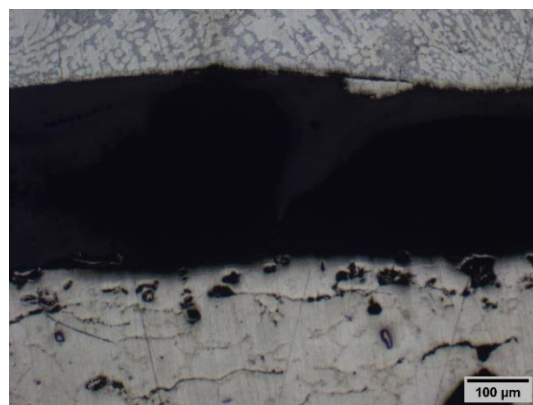
Figure 4.32 The gap between the dense shell and the foam core of sample 1-3 (x100)

Gaussian distribution method was adopted to show the results of pore sizes, skin thicknesses and wall thicknesses, in which the average value and the standard deviation can be easily compared among the three samples. The Gaussian distribution was shown in Figure 4.33-4.35. In addition, the minimum, maximum, mean value and standard deviation were calculated and summarized in Table 4.9-4.11.

a. pore sizes

	pore sizes (μm)		
	1-3	1-3 El	1-3 Et
Min	116.2	105.5	129.4
Max	2972.1	2421.3	2217.7
Mean	585.7	493.9	501.2
S.D.	399.6	393	361.9

Table 4.9 Statistical data of pore sizes of inserted foam 1-3
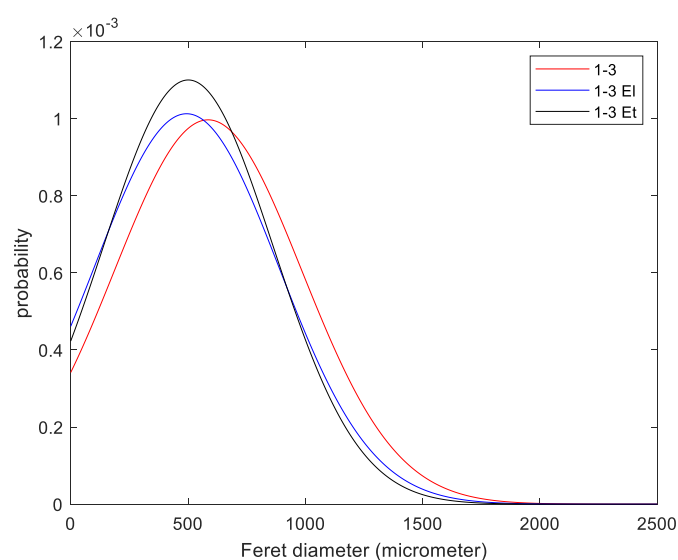
Figure 4.33 Gaussian distribution of pore sizes of inserted foam 1-3

* The results were obtained from 380 measurements for 1-3, 227 measurements for 1-3 El and 282 measurements for 1-3 Et.

The average values and standard deviations are very close to each other, especially sample 1-3 and 1-3El. The reason could be that they were all cut from the same inserted foam. The values are also close to the ones measured for not inserted foams, confirming the absence of alteration after insertion as cores.

b. skin thickness

	skin thickness (µm)		
	1-3	1-3 El	1-3 Et
Min	33.3	383.1	92.3
Max	1200.2	1204.1	1047.8
Mean	544.1	763.3	478.9
S.D.	275.82	173.9	264.6

Table 4.10 Statistical data of skin thicknesses of inserted foam 1-3
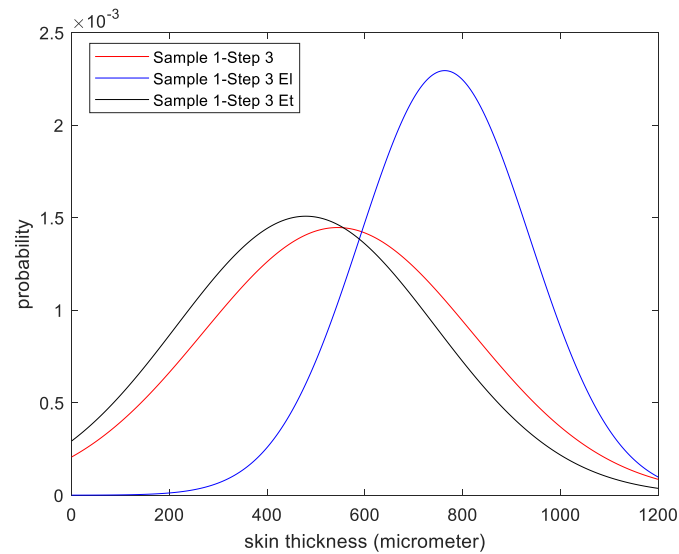
Figure 4.34 Gaussian distribution of skin thicknesses of inserted foam 1-3

* The results were obtained from 73 measurements for 1-3, 22 measurements for 1-3 El and 32 measurements for 1-3 Et.

The average skin thicknesses and standard deviations of 1-3 and 1-3 Et are very close to each other, while they differ a lot from 1-3 El. Some edges of 1-3 El could not be found a clear skin from the images, so they were neglected in calculation.   Values are not far from the ones measured on not inserted foams. No alteration or reaction of the foam skin with the melt metal can be evidenced.

c. wall thickness

	wall thickness (µm)		
	1-3	1-3 El	1-3 Et
Min	23.7	29.4	27.5
Max	231.1	197.4	268.7
Mean	90.8	96.0	112.0
S.D.	38.4	33.2	44.1

Table 4.11 Statistical data of wall thicknesses of inserted foam 1-3
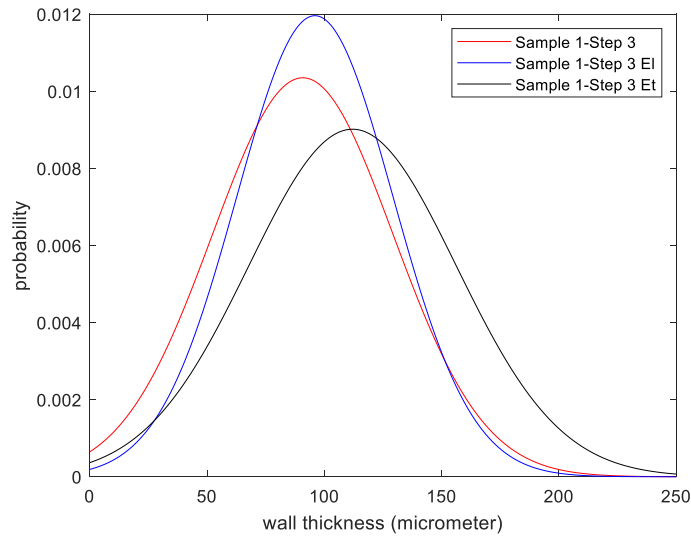
Figure 4.35 Gaussian distribution of wall thicknesses of inserted foam 1-3

* The results were obtained from 193 measurements for 1-3, 131 measurements for 1-3 El and 152 measurements for 1-3 Et.

The wall thickness values are analogous for the three analyzed samples and not far from the ones measured on not inserted foams, confirming that no alteration occurs after insertion in casting.

4.3 Porosity

Porosity was measured by the area fraction of pores with respect to the metal. Before it was measured, it was polished. In the preparation of samples, a black pigment was added into the resin which would be filled into the pores. In this way, a deep contrast between pores and metal was obtained. Porosity measurements were done on non-inserted foams, foam 3, foam 7 and foam 11.

The pores and metal can be distinguished by color, as shown in Figure 4.36 and 4.37, the dark color is associated with pores while the light color is associated with aluminum. However, since some pores were not filled with resin, binary could be difficult by ImageJ. So firstly, the pores which were in light color should be made black by a software GIMP.
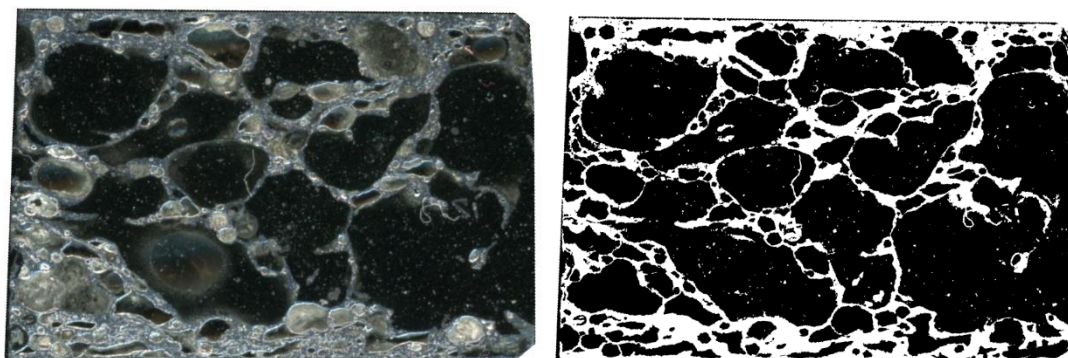
Figure 4.36 Scanning image of Foam 3 (left) and the image after binary by ImageJ (right)
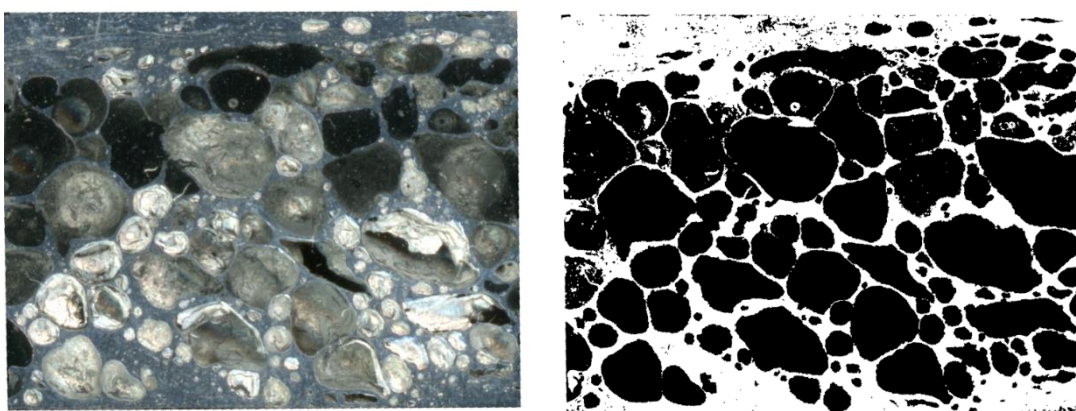
Figure 4.37 Scanning image of Foam 7 (left) and the image after binary by ImageJ (right)
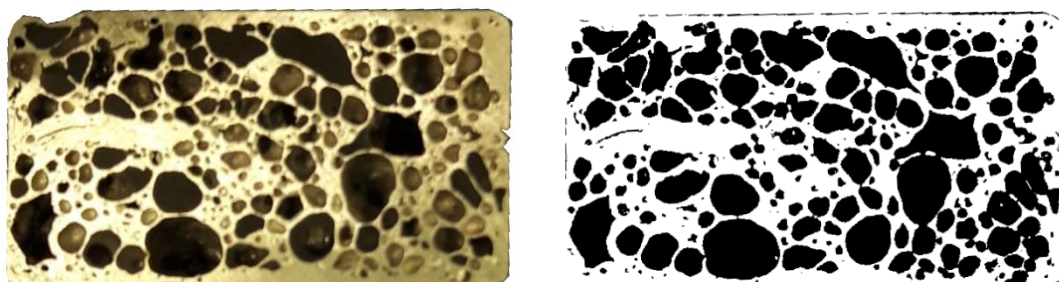
Figure 4.38 Scanning Image of foam 11 (left) and after binary by ImageJ (right)

There are two ways to measure the porosity:

• Porosity =1- Relative density

The densities and the relative densities were calculated by the same method used in chapter 3.2. The results are shown in Table 4.12:

	Density (g/m³)	Relative Density	Porosity
Foam 3	0.98	0.36	64%
Foam 7	1.25	0.46	54%
Foam 11	1.5	0.56	44%

Table 4.12 Porosities of non-inserted foams calculated by relative densities

- By measuring the area fraction of pores (from optical images)

The results are shown in Figure 4.13

	Porosity
Foam 3	74.55%
Foam 7	66.12%
Foam 11	51.42%

Table 4.13 Porosities of non-inserted foams calculated by area fraction of pores

Theoretically, the results obtained through these two ways should be coincident with each other, but since the porosity measurement in the second way was done based on only one cross section, considering the not complete homogeneity of foam samples, as previously discussed, there could be a deviation between these two results.

4.4 Dense metal-foam interface

Figure 4.40 and 4.41 shows the gap between the foam core and cast shell from macroscopic and microscopic point of view respectively.
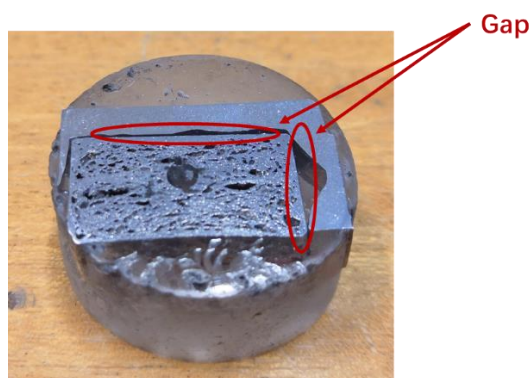
Figure 4.40 Macroscopic image of 1-3
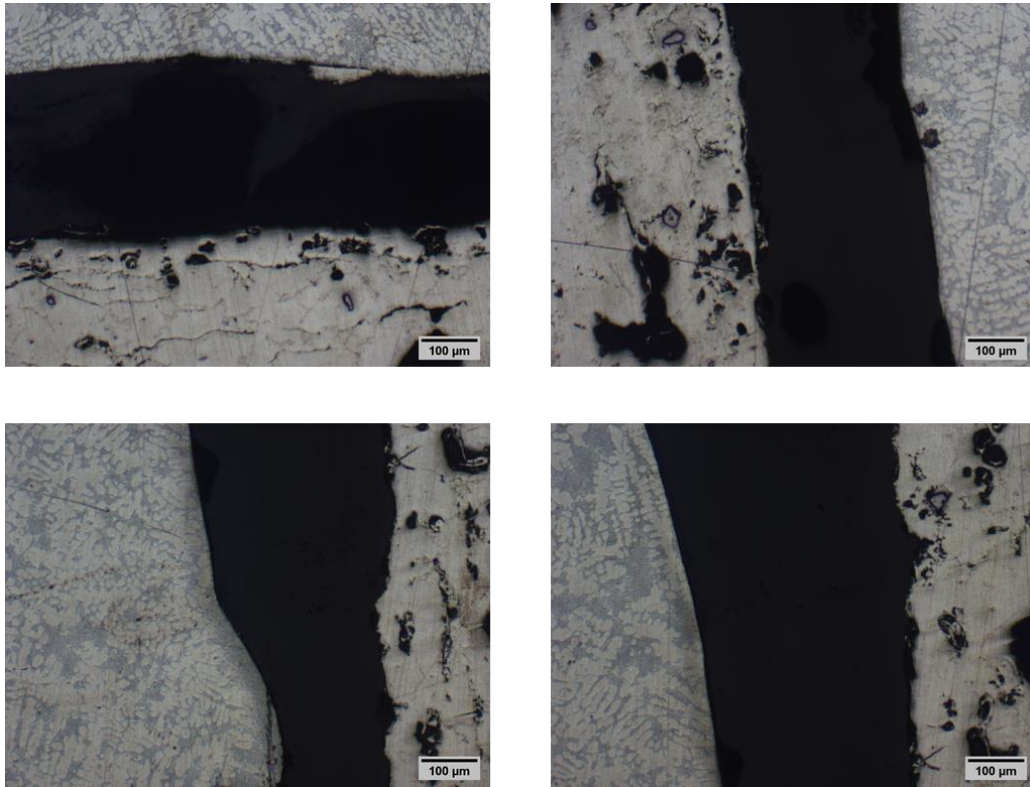
Figure 4.41 Microscopic image of 1-3 (x100)

A visible clearance can be evidenced both from the macroscopic and microscopic images, which means that no bonding exists between the dense metal and the foam core. This phenomenon can be explained by two reasons:

1. The oxide layer prevents the surface from reaction with the molten metal.

2. The temperature during casting process can reach a maximum value around 550℃, which is much lower than the melting point of the oxides (MgO: 2852℃; Al2O3: 2072℃) and of the foam skin.

4.5 Scanning Electron Microscopy (SEM) with Energy Dispersive Spectroscopy (EDS)-results

In order to better understand the behavior of foam cores in casting experiment morphological and compositional analyses, with SEM-EDS, were dome on not inserted and inserted foams. Three surface preparations were considered, in order to investigate the presence of surface contaminants, oxides, as well as the composition of the skin: foams as cut, washed foams and polished and washed foams.

Firstly, from an overall point of view, the average chemical composition was measured at low magnification. Since SEM allows to evaluate local chemical compositions by

selecting desirable regions, some second phases and particles can be analyzed also at higher magnifications.

4.5.1 Morphology and chemical compositions of non-inserted foams-skin

• Foam 3
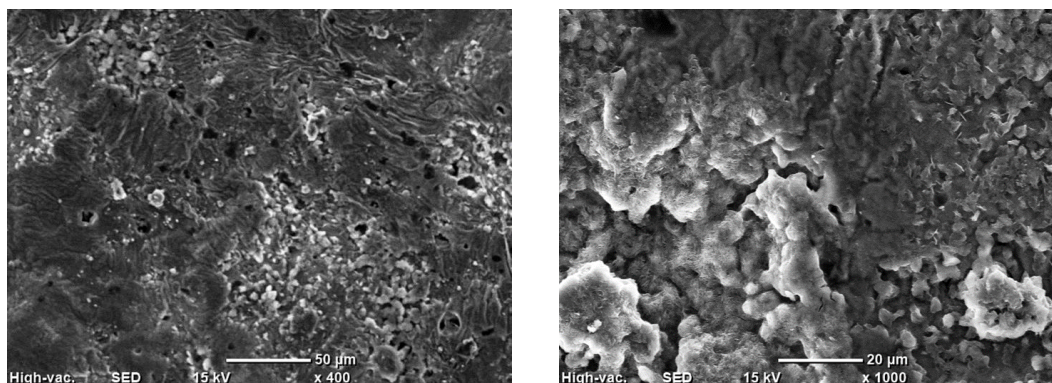
Figure 4.42 Morphology of non-inserted foam 3 as cut

The surface morphology of as cut Foam 3 is shown in Figure 4.42. The surface appears irregular, with a rough morphology and the presence of micro-pores and particles.

The average chemical composition (EDS analyses on 3 different areas) is reported in Table 4.15.

	foam 3 as cut			
	Mass %		Atom %	
Element	Mean	S.D.	Mean	S.D.
C	18.08	1.43	28.40	2.05
O	29.18	1.41	34.43	1.75
Mg	3.63	0.54	2.82	0.45
Al	49.07	0.68	34.33	0.69
P	0.04	0.04	0.02	0.03

Table 4.15 Average chemical compositions of foam 3 as cut

P only appeared in two measurements.

Some small amount elements that were found in some specific areas can be neglected.

Surface topography of Foam 3 after washing is reported in Figure 4.43. the morphology is still irregular (as expected) with the presence of micro-pores and particles.
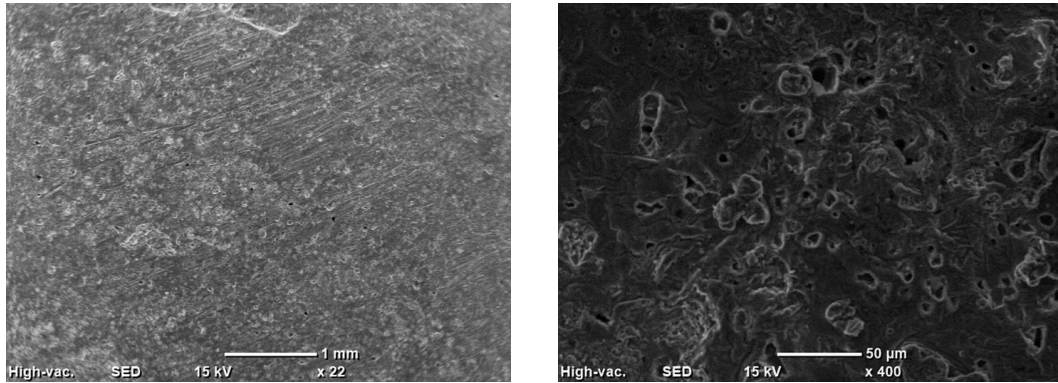
Figure 4.43 Morphology of non-inserted washed foam 3

The average chemical composition (EDS on 3 different areas) after washing is reported in Table 4.16.

	foam 3 wash			
	Mass %		Atom %	
Element	Mean	S.D.	Mean	S.D.
C	14.48	0.83	24.02	1.20
O	24.35	2.49	30.31	2.68
Mg	5.71	0.87	4.68	0.65
Al	55.46	3.55	41.00	3.29

Table 4.16 Average chemical composition of washed foam 3

The surface topography of Foam 3 after coarse polishing and washing is shown in Figure 4.44. The abrasive paper removes the first layer of the foam skin making the surface more regular, except of polishing tracks.
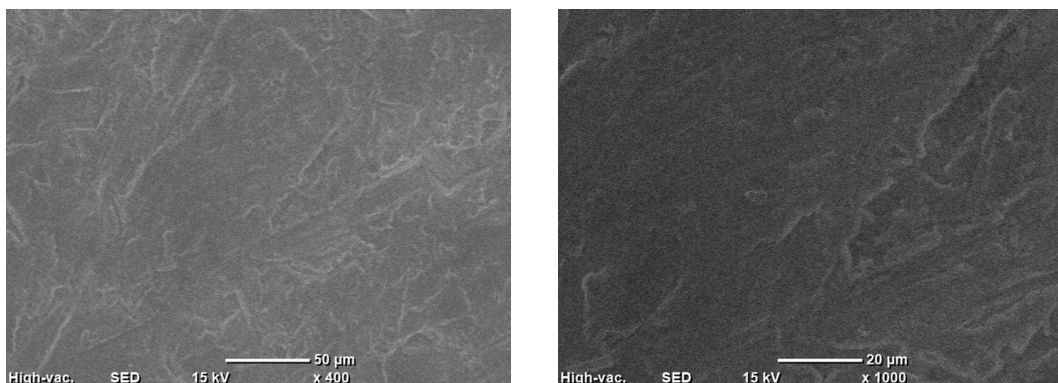
Figure 4.44 Morphology of non-inserted polished and washed foam 3

The average chemical composition (EDS on 3 different areas) after coarse polishing and washing is reported in Table 4.17:

	foam 3 pol wash			
	Mass %		**Atom %**	
Element	**Mean**	**S.D.**	**Mean**	**S.D.**
C	11.54	0.60	20.31	0.90
O	18.64	2.35	24.62	2.73
Mg	3.87	0.09	3.37	0.06
Al	65.62	2.97	51.47	3.08
P	0.33	0.34	0.22	0.23

Table 4.17 Average chemical composition of polished and washed foam 3

*P only appeared in two measurements.

The comparison of chemical analyses after different surface preparations is shown in Figure 4.45.
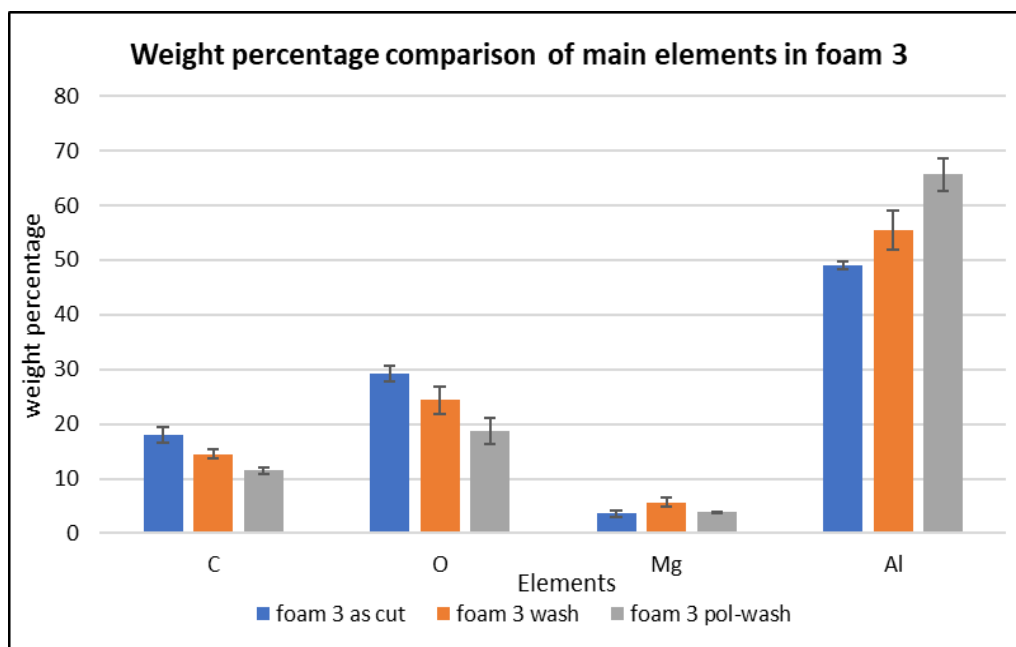
Figure 4.45 Comparison in average chemical compositions in three conditions of foam 3

The results show that aluminum is the main element in the foams since it accounts for the highest percentage in the foams. Magnesium, which is a common element in aluminum alloy, can be found in all the measurements. Since aluminum and magnesium are easily oxidized, there is also a large amount of oxygen.

Carbon accounts for a high percentage in the samples as cut, while it decreases a lot after washing and polishing. It can be introduced as contaminants during foams production and handling.   The carbon content is reduced after both washing and polishing.

As reported in Table 4.11-4.13 and Figure 4.45, after the samples are polished, also the

percentage of oxygen largely decreases. The reason for this could be that oxides can be partly removed by mechanical way (as observed by the removal of particles from SEM images). Moreover, a decrease of the Mg content can be also observed after polishing. This result suggest that Mg can be one of the main constituents of the surface oxide layer. The layer of MgO on the surface of foams will resist to the bonding between foams and melt metal and may also decreases the electrical conductivity. This could be explained by the lower wetting that normally occurs between MgO and the surrounding aluminum alloy [25] [26].

As illustrated before, optical microscope can not recognize the second phases of the samples, while SEM has the capability to measure the local chemical composition by selecting a specific area. The selected areas and the corresponding results of EDS analyses are reported in Figure 4.46-4.49 and Table 4.18-4.21 respectively.
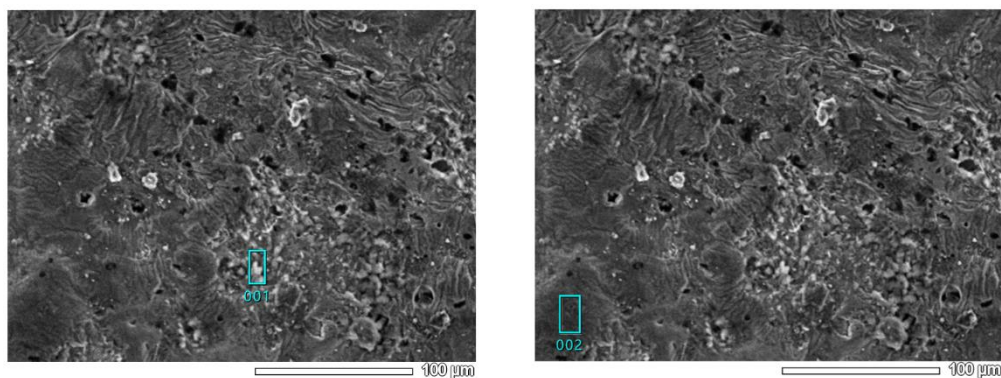
Figure 4.46 Selected area for local chemical composition measurement of foam 3 as cut

	foam 3 as cut 001					
Element	C	O	Mg	Al	Si	P
Mass %	19.04	39.66	6.93	33.45	0.20	0.72
Atom %	28.21	44.11	5.07	22.06	0.13	0.42
	foam 3 as cut 002					
Element	C	O	Mg	Al	Si	P
Mass %	15.76	40.58	5.37	37.88	0.18	0.22
Atom %	23.92	46.22	4.02	25.59	0.12	0.13

Table 4.18 Local chemical composition of foam 3 as cut
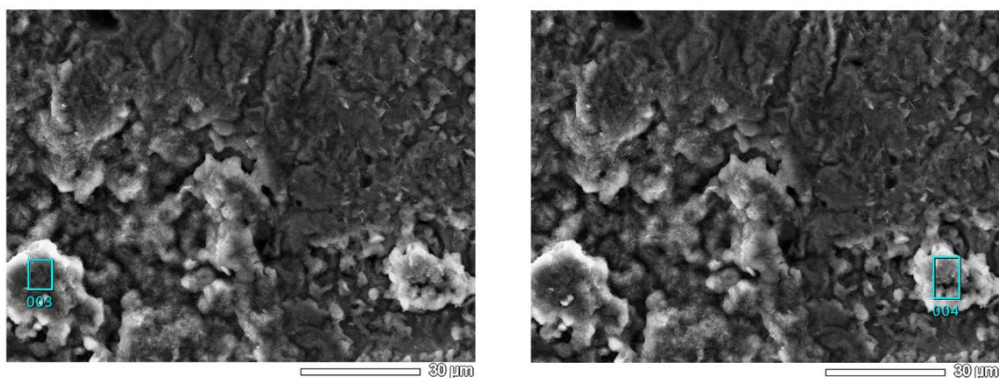
Figure 4.47 Selected area for local chemical composition measurement of foam 3 as cut

Element	C	O	Mg	Al	Si	P	
			foam 3 as cut 003				
Element	C	O	Mg	Al	Si	P	
Mass %	12.52	66.66	18.20	1.98	0.07	0.58	
Atom %	17.23	68.84	12.37	1.21	0.04	0.31	
			foam 3 as cut 004				
Element	C	O	Mg	Al	Si	P	Ca
Mass %	24.76	55.98	11.67	4.94	0.61	1.43	0.60
Atom %	32.69	55.48	7.61	2.90	0.35	0.73	0.24

Table 4.19 Local chemical composition of foam 3 as cut

A high percentage of oxygen indicates large amount of oxides. Particles 003 and 004 are rich in oxygen and magnesium, even more than aluminum, suggesting, as reported before, the presence of magnesium oxides on the surface.
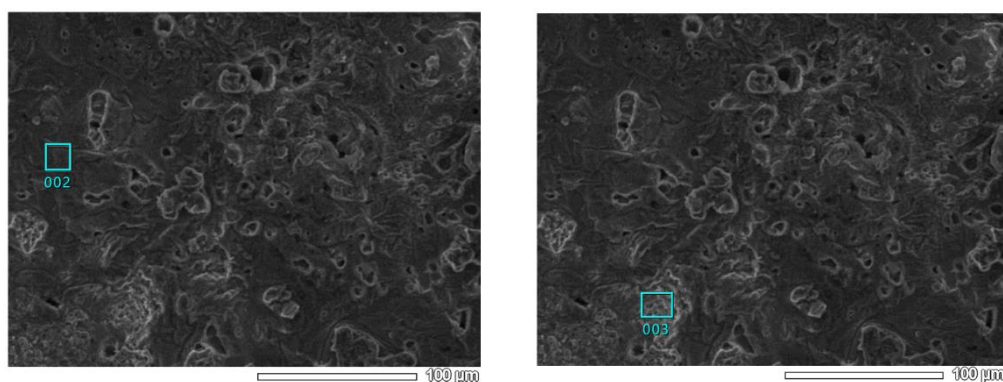
Figure 4.48 Selected area for local chemical composition measurement of washed foam 3

	foam 3 wash 002			
Element	C	O	Mg	Al
Mass %	14.28	31.75	9.27	44.70
Atom %	22.81	38.08	7.32	31.79
	foam 3 wash 003			
Element	C	O	Mg	Al
Mass %	12.97	19.80	3.27	63.95
Atom %	22.40	25.66	2.79	49.15

Table 4.20 Local chemical composition of foam 3 as cut
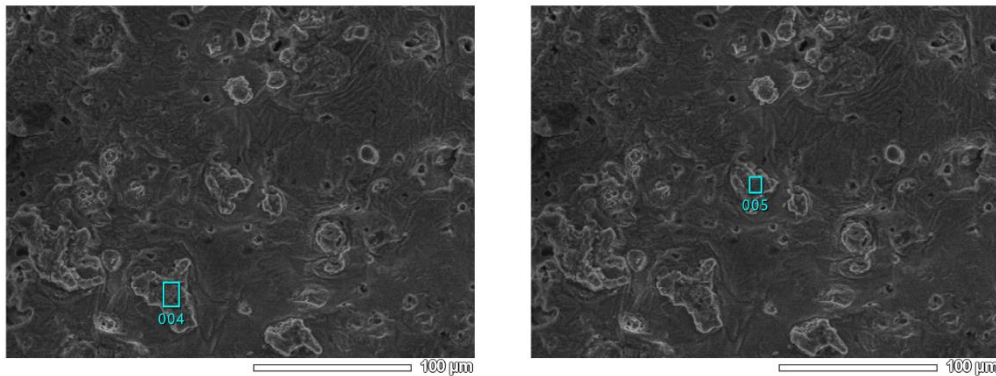
Figure 4.49 Selected area for local chemical composition measurement of washed foam 3

	foam 3 wash 004				
Element	C	O	Mg	Al	P
Mass %	20.67	45.97	24.74	6.35	2.26
Atom %	29.07	48.53	17.19	3.98	1.23
	foam 3 wash 005				
Element	C	O	Mg	Al	P
Mass %	21.75	44.24	25.80	6.88	1.34
Atom %	30.51	46.59	17.88	4.29	0.73

Table 4.21 Local chemical composition of washed foam 3

Particles 004 and 005 are rich in oxygen and magnesium, even more than aluminum.

• Foam 7

The procedures were the same as the ones for foam 3. Figures 4.50-4.52 show the morphology of foam 7 in three conditions (as cut, washed and coarse polished and washed) and the corresponding average chemical compositions are reported in Table 4.22-4.24.
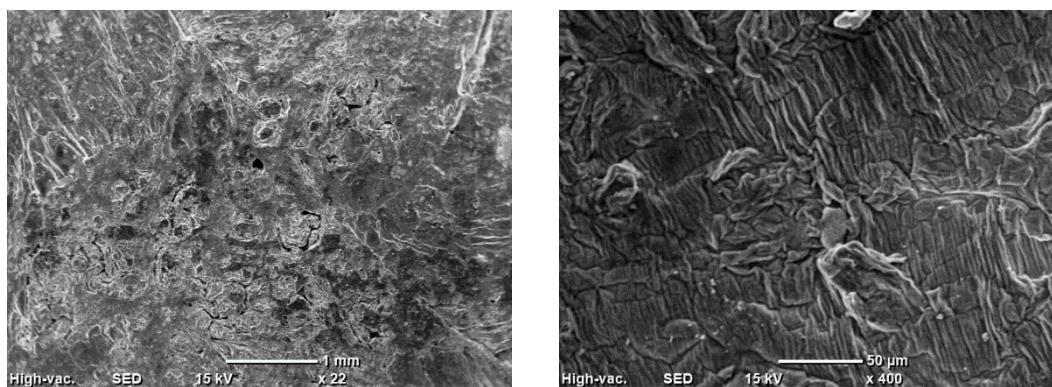
Figure 4.50 Morphology of foam 7 as cut

	foam 7 as cut			
	Mass %		Atom %	
Element	Mean	S.D.	Mean	S.D.
C	29.20	0.21	40.29	0.48
O	37.17	1.82	38.49	1.63
Mg	9.21	1.37	6.27	0.91
Al	23.65	2.64	14.54	1.72
Si	0.36	0.11	0.21	0.07
P	0.31	0.24	0.16	0.13
Ca	0.11	0.08	0.05	0.03

Table 4.22 Average chemical composition of foam 7 as cut
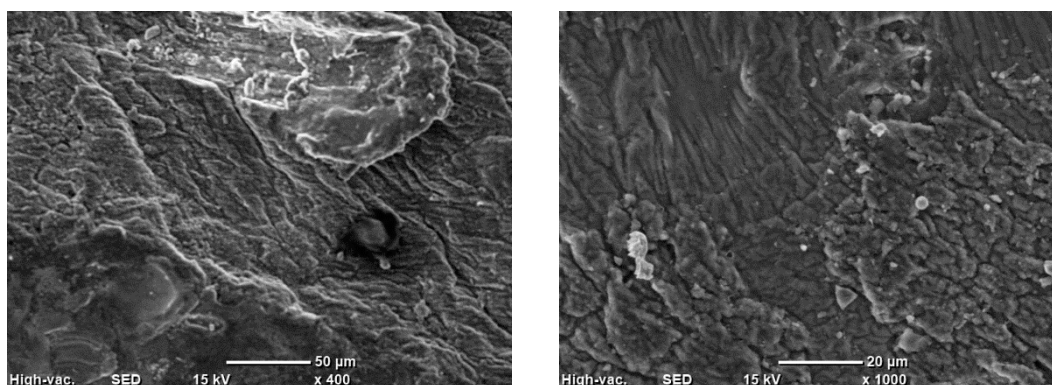
Figure 4.51 Morphology of washed foam 7

	foam 7 wash			
	Mass %		Atom %	
Element	Mean	S.D.	Mean	S.D.
C	15.22	1.36	24.68	2.46
O	27.50	5.15	33.39	5.63
Mg	7.90	2.92	6.30	2.20
Al	48.18	7.21	34.83	5.77
Si	0.68	0.17	0.47	0.12
P	0.45	0.32	0.29	0.19
Ca	0.07	0.10	0.03	0.05

Table 4.23 Average chemical composition of washed foam 7

Ca only appeared in two measurements.
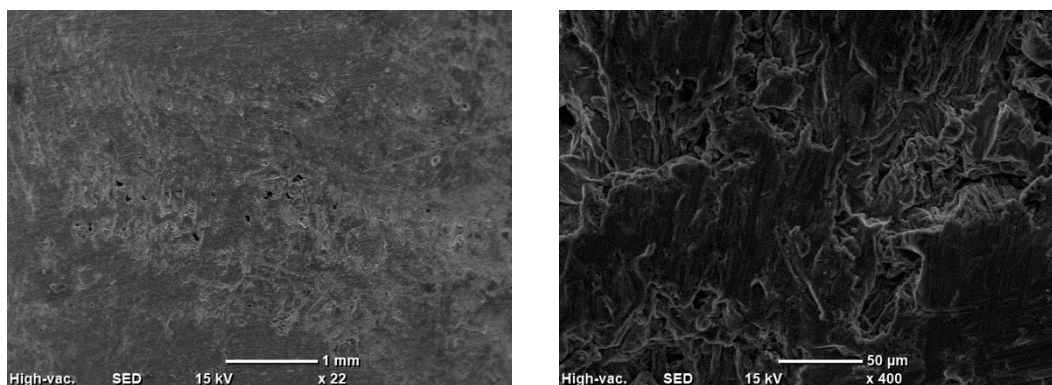
Figure4.52 Morphology of polished and washed foam 7

	foam 7 pol wash			
	Mass %		Atom %	
Element	Mean	S.D.	Mean	S.D.
C	12.41	2.38	20.87	3.61
O	24.86	0.90	31.48	1.38
Mg	7.71	1.16	6.43	1.05
Al	53.61	2.10	40.27	2.25
Si	0.79	0.02	0.57	0.02
P	0.45	0.21	0.30	0.15
Ca	0.16	0.16	0.08	0.08

Table 4.24 Average chemical composition of polished and washed foam 7

Ca only appeared in two measurements.
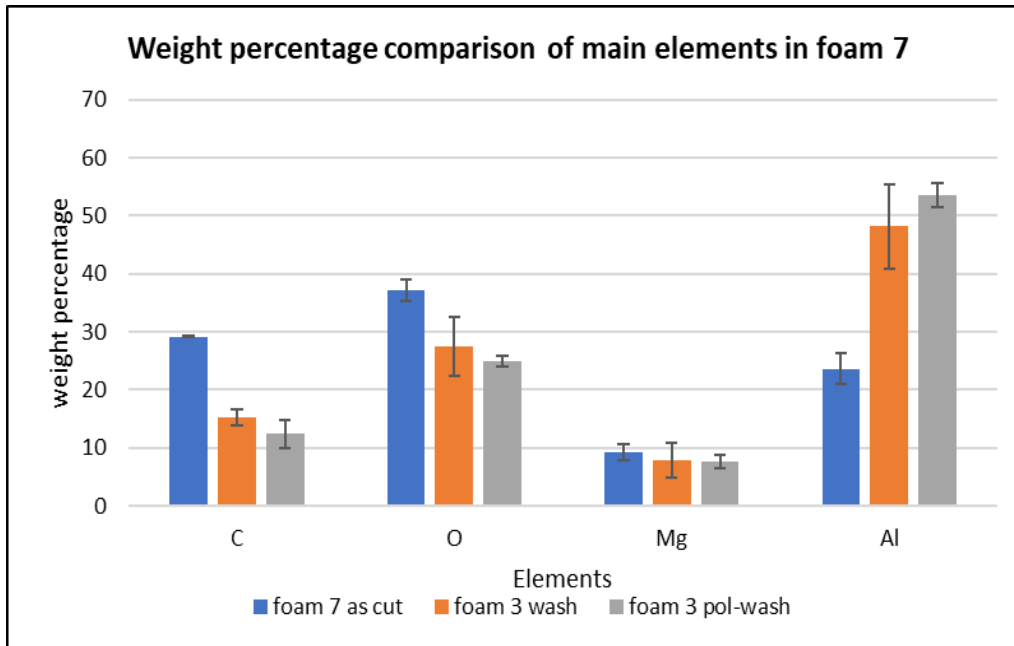
Figure 4.53 Comparison in average chemical compositions in three conditions of foam 7

From Figure 4.53 and Table 4.22-4.24 it can be observed that the main features of Foam 7 are analogous to the ones of the previously described Foam 3. Washing mainly reduces the carbon content (as possible reduction of contaminants). After the samples are polished, the percentage of carbon, oxygen and magnesium largely decreases while there is an increase in aluminum. Suggesting the removal of surface oxides (mainly Mg-containing oxides), as previously discussed.

Then, local chemical composition can also be measured by selecting some specific areas. The selected areas and the corresponding results are reported in Figure 4.54-4.56 and Table 4.25-4.27 respectively.
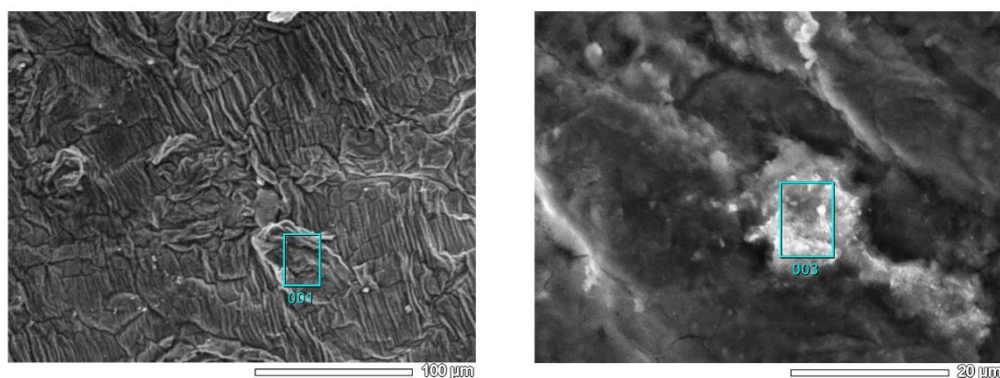
Figure 4.54 Selected area for local chemical composition measurement of foam 7 as cut

foam 7 as cut 001						
Element	**C**	**O**	**Mg**	**Al**	**Si**	**P**	**Ca**
Mass %	40.42	17.93	3.84	36.98	0.59	0.19	0.05
Atom %	55.69	18.55	2.61	22.68	0.35	0.10	0.02
foam 7 as cut 003						
Element	**C**	**O**	**Mg**	**Al**	**Si**	**P**	**Ca**
Mass %	37.15	46.75	6.78	7.71	1.23	0.33	0.06
Atom %	46.61	44.04	4.20	4.31	0.66	0.16	0.02

Table 4.25 Local chemical composition of foam 7 as cut

A high percentage of oxygen indicates large amount of oxides and carbon contamination, as proved by large signal of C.
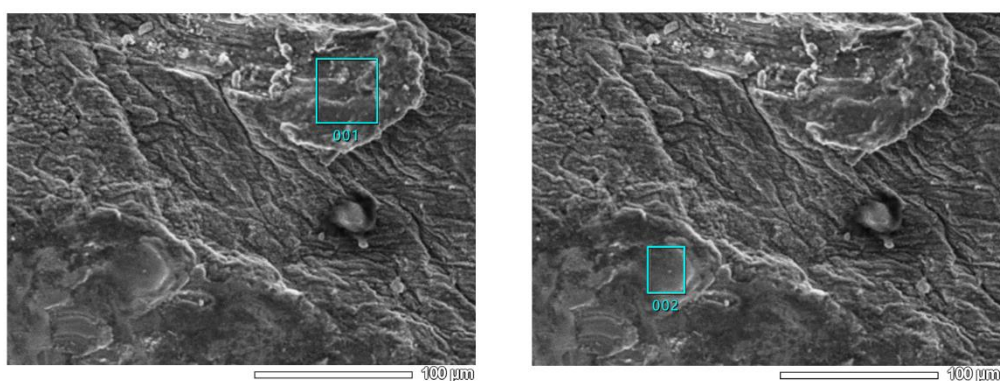
Figure 4.55 Selected area for local chemical composition measurement of washed foam 7

foam 7 wash 001							
Element	**C**	**O**	**Mg**	**Al**	**Si**	**P**	**K**	**Ca**
Mass %	10.36	54.01	2.64	31.25	0.14	0.37	1.03	0.20
Atom %	15.53	60.79	1.96	20.86	0.09	0.21	0.47	0.09
foam 7 wash 002							
Element	**C**	**O**	**Mg**	**Al**	**Si**	**P**		
Mass %	16.97	23.41	5.05	54.06	0.18	0.32		
Atom %	27.68	28.67	4.07	39.25	0.13	0.20		

Table 4.26 Local chemical composition of washed foam 7
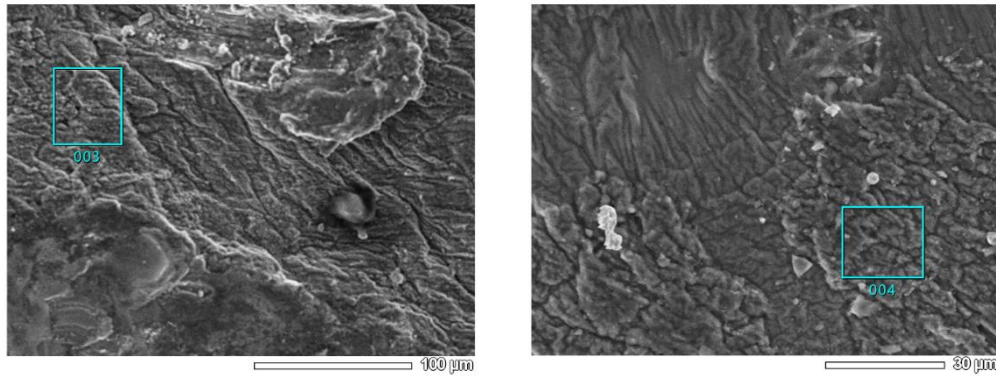
Figure 4.56 Selected area for local chemical composition measurement of washed foam 7

		foam 7 wash 003						
Element	**C**	**O**	**Mg**	**Al**	**Si**	**P**	**K**	**Ca**
Mass %	9.69	49.01	25.14	14.57	0.23	1.13	0.14	0.10
Atom %	14.68	55.75	18.82	9.83	0.15	0.66	0.07	0.05
		foam 7 wash 004						
Element	**C**	**O**	**Mg**	**Al**	**Si**	**P**	**K**	**Ca**
Mass %	13.26	40.80	16.92	27.85	0.33	0.78	0.03	0.04
Atom %	20.37	47.05	12.84	19.04	0.21	0.47	0.01	0.02

Table 4.27 Local chemical composition of washed foam 7

These two particles are rich in oxygen and magnesium, even more than aluminum, suggesting the presence of Mg-rich oxides.

4.5.2 Morphology and chemical composition of inserted foams-skin

The same procedures were followed, as in section 4.5.1, for the characterization of inserted foams. Foam samples were obtained from the edges of the cast objects. Firstly, the average chemical composition was measured under low magnification. Then, local chemical composition measurement can be done based on some selected areas.

• Foam 2-Step 3

Figures 4.57-4.59 show the morphology of foam 2-3 in three conditions (as cut, washed and coarse polished and washed) and the corresponding average chemical compositions are reported in Table 4.28-4.30.
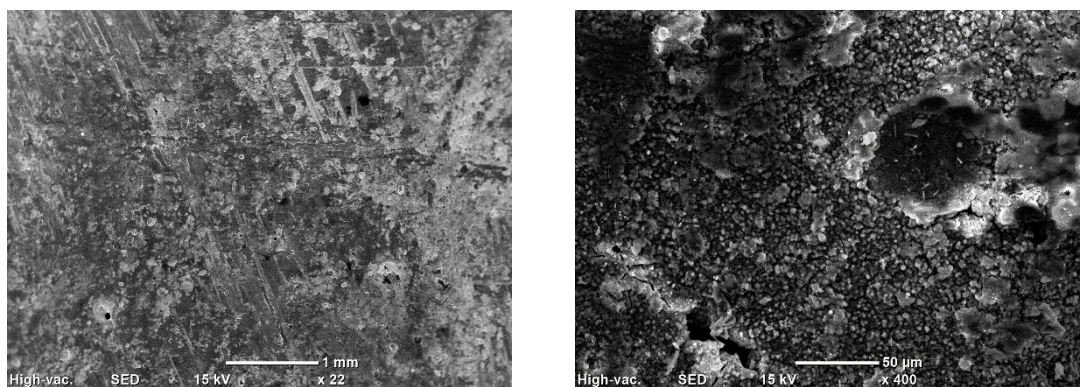
Figure 4.57 Morphology of foam 2-3 as cut

	2-3 as cut			
	Mass %		**Atom %**	
Element	**Mean**	**S.D.**	**Mean**	**S.D.**
C	13.54	1.57	23.57	2.30
O	17.51	2.11	22.90	2.70
Na	0.85	0.20	0.77	0.18
Mg	7.52	1.15	6.48	0.98
Al	58.15	4.46	45.15	3.94
Si	0.18	0.35	0.13	0.25
Cl	0.17	0.34	0.10	0.20
K	1.30	0.39	0.70	0.20
As	0.79	1.58	0.22	0.45

Table 4.28 Average chemical composition of foam 2-3 as cut

*Si, Cl and As appeared in one measurement.
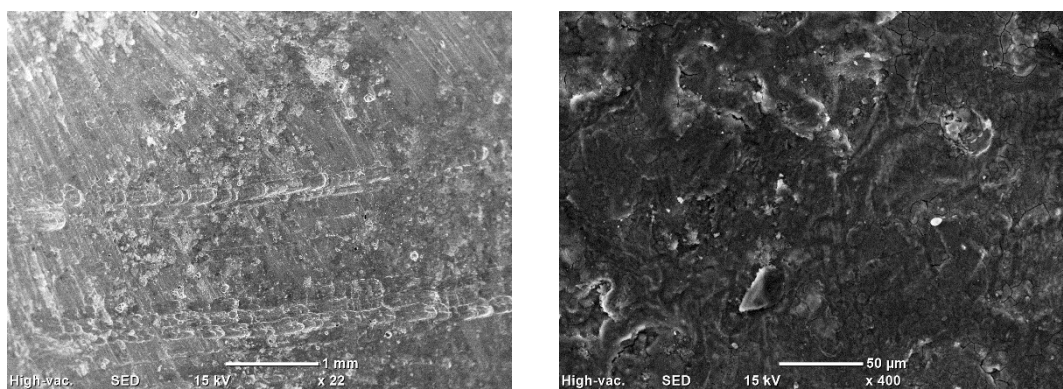
Figure 4.58 Morphology of washed foam 2-3

	2-3 wash			
	Mass %		Atom %	
Element	Mean	S.D.	Mean	S.D.
C	7.33	1.22	13.58	1.95
O	16.24	2.29	22.59	2.64
Na	0.68	0.35	0.66	0.32
Mg	8.31	1.74	7.61	1.43
Al	65.72	5.90	54.46	6.32
Si	0.57	0.04	0.45	0.02
K	1.16	0.72	0.66	0.40

Table 4.29 Average chemical composition of washed foam 2-3
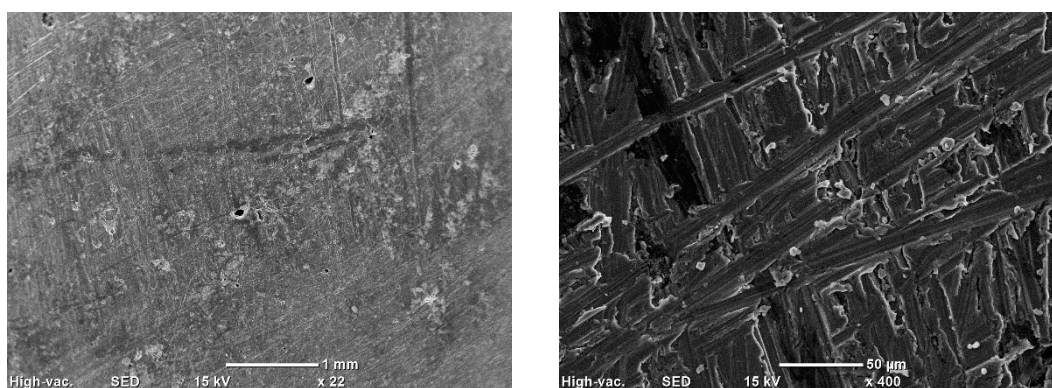
Figure 4.59 Morphology of polished and washed foam 2-3

	2-3 pol-wash			
	Mass %		Atom %	
Element	Mean	S.D.	Mean	S.D.
C	1.18	1.36	2.50	2.89
O	3.96	1.82	6.44	3.04
Mg	2.54	0.66	2.72	0.73
Al	90.10	5.51	86.88	5.45
Si	0.54	0.09	0.50	0.09
Ti	1.73	3.47	0.96	1.92

Table 4.30 Average chemical composition of polished and washed foam 2-3

Ti appeared in one measurement.
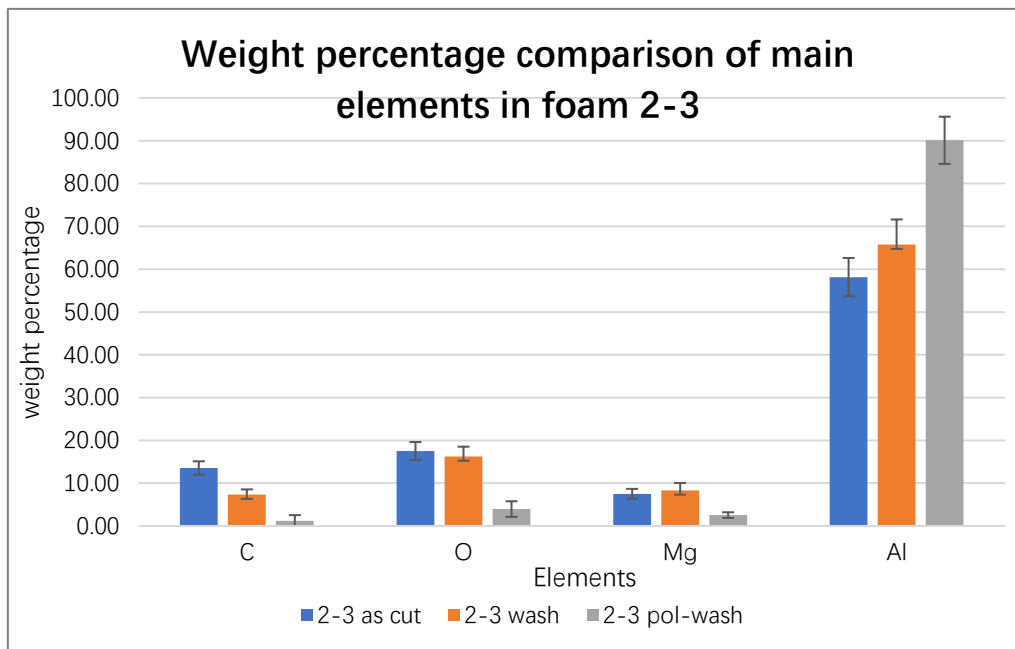
Figure 4.60 Comparison in average chemical compositions in three conditions of foam 2-3

From Figure 4.60, the same conclusion as the non-inserted foams can be drawn since the changes in the weight percentage of the main elements show a same trend (illustrated in section 4.5.1).

The carbon content progressively decreases after washing and polishing, suggesting the removal of contaminants and potential detaching agents. Oxygen is almost constant after washing but significantly decreases after polishing, in accordance with the possible removal of oxides by the action of abrasive papers. A similar trend can be evidenced for magnesium, suggesting the mechanical removal of Mg-rich oxides. On the other hand, an increase in the aluminum content can be evidenced after the various treatments indicating the progressive exposure of the AL-based metallic matrix.

Figures 4.61-4.62 show the selected areas for local chemical composition analysis and Table 4.26-27 report the corresponding results.
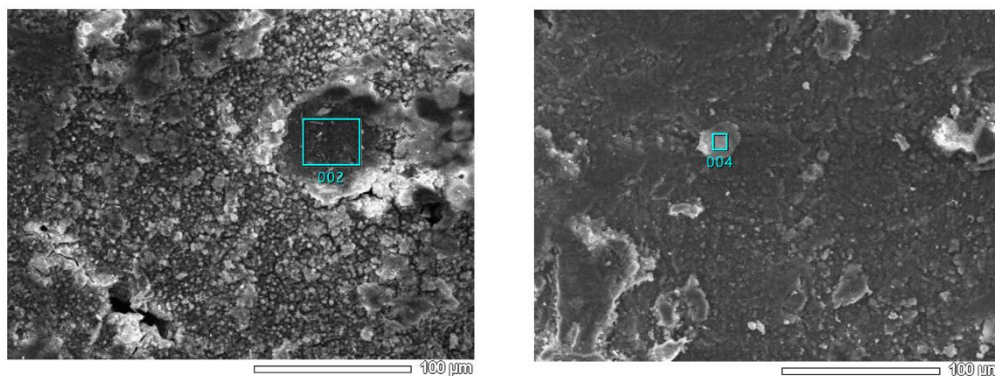
Figure 4.61 Selected area for local chemical composition measurement of foam 2-3 as cut

			2-3 as cut 002					
Element	C	O	Na	Mg	Al	Cl	K	S
Mass %	10.68	25.70	1.29	10.79	49.25	1.21	1.07	0.00
Atom %	18.21	32.90	1.15	9.10	37.38	0.70	0.56	0.00
			2-3 as cut 004					
Mass %	68.11	13.16	2.20	3.00	6.74	2.65	2.86	1.28
Atom %	79.31	11.51	1.34	1.72	3.49	1.04	1.02	0.56

Table 4.31 Local chemical composition of foam 2-3 as cut

Carbon contamination, as proved by large signal of C. Presence of Na and K in this area, along with other elements; maybe the mold walls were coated with sodium and potassium carbonates, as possible detaching agents. These elements were not detected in non-inserted foams. Detaching agents in casting process can be used to facilitate the removal of the cast sample from the die. Detaching agent may be present in the form of powders which can also prevent bonding between foams and melt metal.
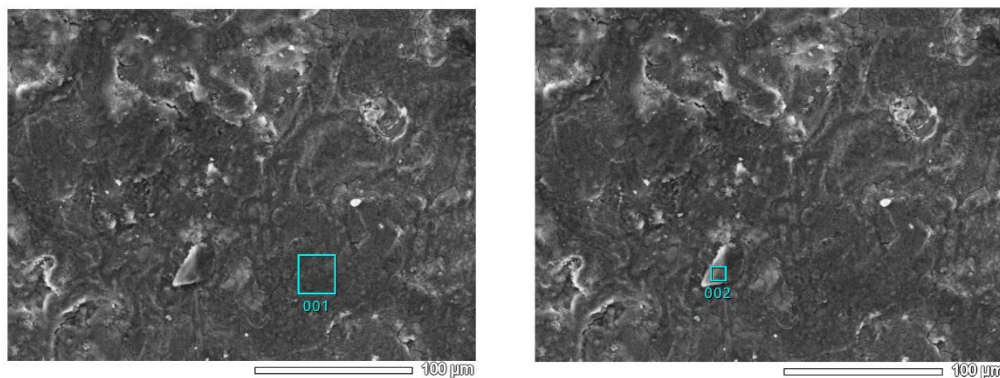
Figure 4.62 Selected area for local chemical composition measurement of washed foam 2-3

			2-3 wash 001				
Element	C	O	Na	Mg	Al	Si	K
Mass %	9.61	22.12	0.62	15.28	49.15	0.83	2.39
Atom %	16.84	29.11	0.57	13.23	38.34	0.62	1.29
			2-3 wash 002				
Element	C	N	O	Na	Mg	Al	Cl	K
Mass %	66.60	4.36	12.69	0.94	5.35	5.11	0.88	4.06
Atom %	76.70	4.30	10.98	0.57	3.04	2.62	0.35	1.44

Table 4.32 Local chemical composition of washed foam 2-3

Carbon contamination, as proved by large signal of C.

• Foam 6-3

Figures 4.63-4.65 show the morphology of foam 6-3 in three conditions (as cut, washed and coarse polished and washed) and the corresponding average chemical compositions are reported in Table 4.33-4.35.
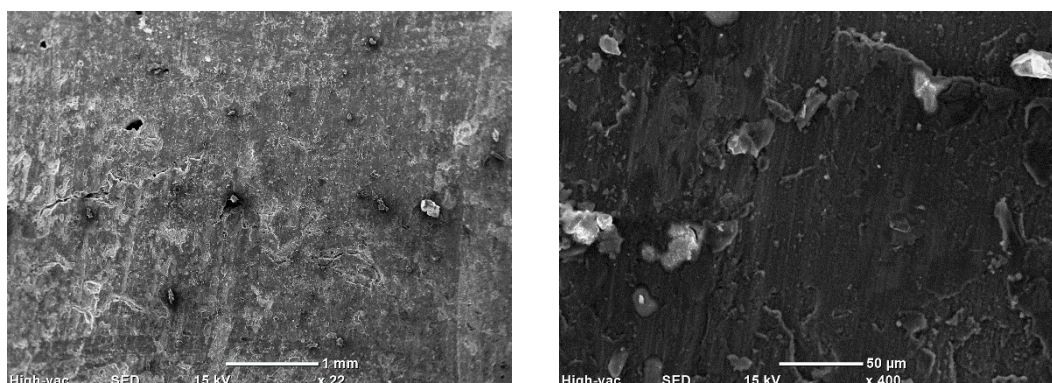
Figure 4.63 Morphology of foam 6-3 as cut

	6-3 as cut			
	Mass %		**Atom %**	
Element	**Mean**	**S.D.**	**Mean**	**S.D.**
C	16.35	1.67	28.84	2.07
O	9.54	2.45	12.59	2.87
Na	0.57	0.13	0.53	0.11
Mg	4.70	2.59	4.06	2.13
Al	66.66	7.43	52.59	7.45
Si	0.88	0.38	0.66	0.27
Cl	0.68	0.25	0.41	0.13
K	0.63	0.28	0.34	0.15

Table 4.33 Average chemical composition of foam 6-3 as cut
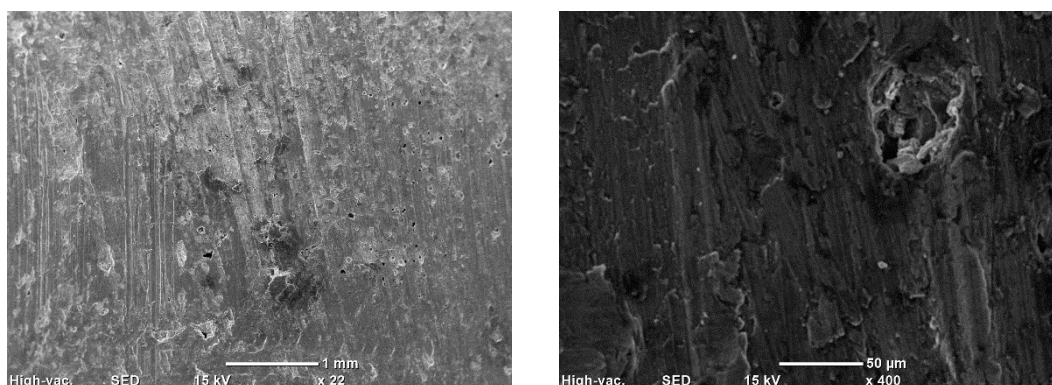
Figure 4.64 Morphology of washed foam 6-3

	6-3 wash			
	Mass %		Atom %	
Element	Mean	S.D.	Mean	S.D.
C	6.41	0.76	12.81	1.35
O	5.76	1.24	8.64	1.73
Na	0.14	0.17	0.15	0.18
Mg	3.67	0.71	3.62	0.66
Al	83.11	2.88	74.08	3.63
Si	0.56	0.15	0.48	0.12
Cl	0.15	0.12	0.10	0.08
K	0.20	0.14	0.12	0.08

Table 4.34 Average chemical composition of washed foam 6-3
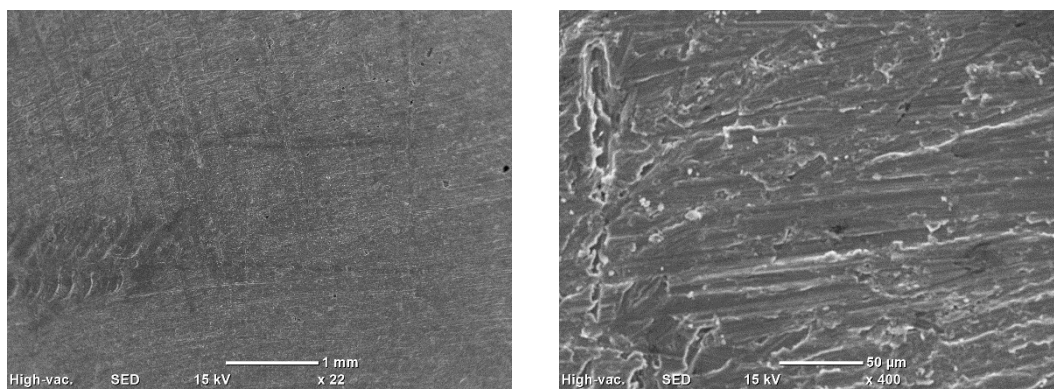
Figure 4.65 Morphology of polished and washed foam 6-3

	6-3 pol-wash			
	Mass %		Atom %	
Element	Mean	S.D.	Mean	S.D.
C	1.68	0.14	3.64	0.29
O	2.29	1.30	3.73	2.09
Na	0.08	0.09	0.09	0.10
Mg	2.10	0.59	2.24	0.62
Al	92.65	3.01	89.49	3.53
Si	0.29	0.28	0.27	0.26
K	0.25	0.10	0.17	0.07
Ti	0.62	0.81	0.33	0.43

Table 4.35 Average chemical composition of polished and washed foam 6-3

*Ti appeared in three measurements.

Figure 4.66 Comparison in average chemical compositions in three conditions of foam 6-3

From Figure 4.66, the same conclusion as the non-inserted foams can be drawn since the changes in the weight percentage of the main elements show a same trend (illustrated in section 4.5.1). The carbon content progressively decreases after washing and polishing, suggesting the removal of contaminants and potential detaching agents. Oxygen is almost constant after washing but significantly decreases after polishing, in accordance with the possible removal of oxides by the action of ab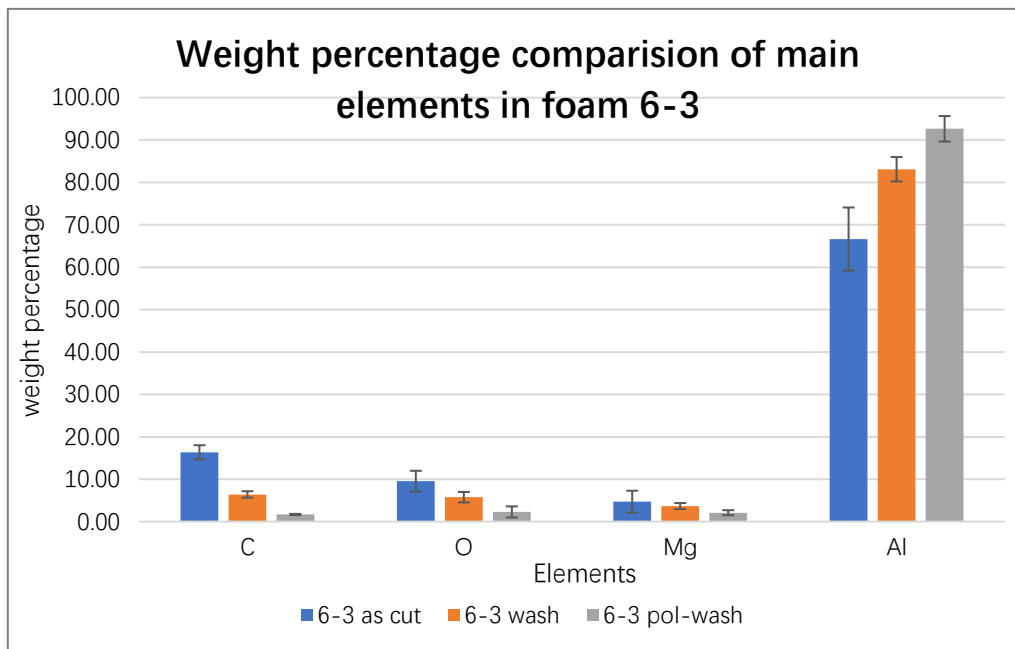rasive papers. A similar trend can be evidenced for magnesium, suggesting the mechanical removal of Mg-rich oxides. On the other hand, an increase in the aluminum content can be evidenced after the various treatments indicating the progressive exposure of the AL-based metallic matrix.

Figure 4.67-4.69 show the selected areas for local chemical composition analysis and Table 4.36-4.38 report the corresponding results.
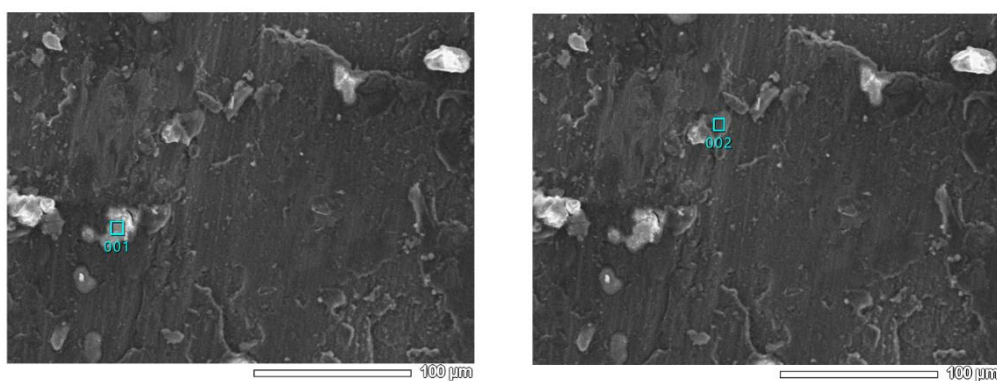

Figure 4.67 Selected area for local chemical composition measurement of foam 6-3 as cut

			6-3 as cut 001					
Element	C	O	Na	Mg	Al	Si	Cl	K
Mass %	31.09	23.57	1.48	4.21	35.56	1.09	1.36	1.64
Atom %	45.12	25.69	1.12	3.02	22.97	0.68	0.67	0.73
			6-3 as cut 002					
Element	C	O	Na	Mg	Al	Si	Cl	K
Mass %	44.90	11.82	1.24	1.58	39.03	0.11	0.82	0.49
Atom %	61.46	12.15	0.89	1.07	23.78	0.06	0.38	0.21

Table 4.36 Local chemical composition of foam 6-3 as cut

Carbon contamination, as proved by large signal of C.
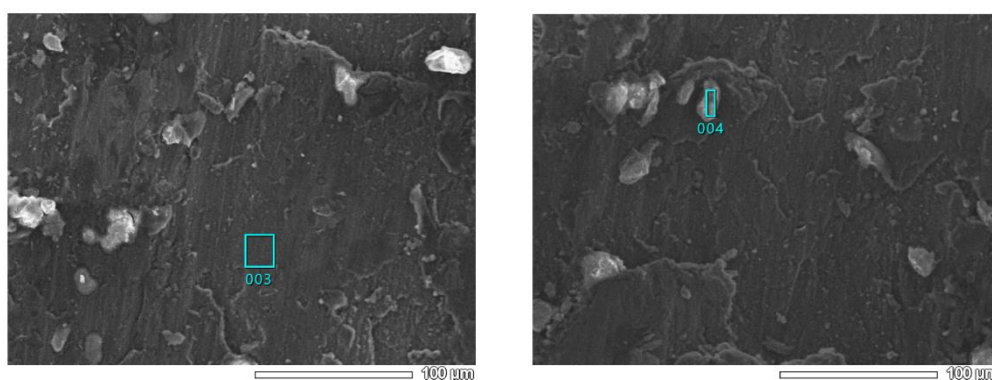
Figure 4.68 Selected area for local chemical composition measurement of foam 6-3 as cut

			6-3 as cut 003				
Element	C	O	Na	Mg	Al	Si	Cl
Mass %	6.87	5.12	0.12	1.11	86.14	47.41	0.19
Atom %	13.76	7.70	0.12	1.10	76.80	0.38	0.13
			6-3 as cut 004				
Element	C	O	Na	Mg	Al	Si	Cl	K
Mass %	24.38	22.51	0.99	1.43	20.26	26.92	2.28	1.22
Atom %	37.99	26.33	0.81	1.10	14.05	17.94	1.21	0.58

Table 4.37 Local chemical composition of foam 6-3 as cut

These two parts are also rich in Si, which could be the composition of aluminum alloy.
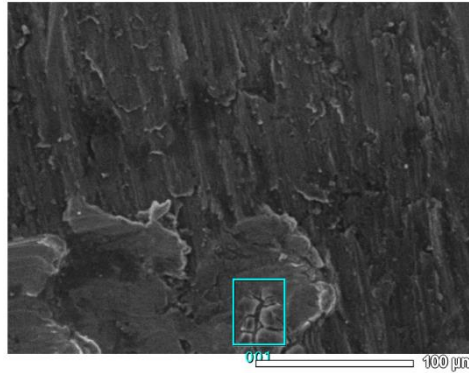
Figure 4.69 Selected area for local chemical composition measurement of washed foam 6-3

Element	C	O	Na	Mg	Al	Si	Cl	K
			6-3 wash 001					
Mass %	4.55	8.47	0.03	1.19	82.69	0.18	2.71	0.18
Atom %	9.22	12.87	0.03	1.20	74.55	0.15	1.86	0.11

Table4.38 Local chemical composition of washed foam 6-3

By comparing all the results of all the foams, it is clear that some oxides and contaminations can be removed by washing and polishing, so the weight percentage of aluminum increases after washing and polishing while other elements, such as Mg, O and C decreases.

The conclusion is valid for both non-inserted foams and inserted foams. The only difference between them is that some elements, such as Na and K, which are not presented in non-inserted foams, maybe introduced by the casting mold.

4.5.3 Morphology and chemical composition of foams-cross section

In this section, the morphologies and average chemical compositions of cross sections of both non-inserted foams and inserted foams are analyzed. All the foams were embedded in resin and mirror polished. Since the resin was not electrically conductive, it had to be metalized by a chromium layer.

• Non-inserted foam 3

Figure 4.70 shows the morphology of non-inserted foam 3 cross section after mirror polishing and the average chemical composition (Table 4.39) is measured by selecting the base area.

Figure 4.70 Morphology of non-inserted mirror polished foam 3

		foam 3		
	Mass %		Atom %	
Element	Mean	S.D.	Mean	S.D.
C	2.97	5.93	5.51	11.02
O	10.38	1.75	15.89	3.12
Mg	0.99	0.47	1.01	0.50
Al	85.14	4.56	77.24	8.43
Si	0.23	0.27	0.21	0.24
Ti	0.29	0.33	0.16	0.18

Table 4.39 Average chemical composition of mirror polished foam 3

Chromium was measured in the mirror polished foam which might be introduced by metallization, so it was neglected in the table.

• Non-inserted foam 7

Figure 4.71 shows the morphology of non-inserted foam 7 cross section after mirror polishing and the average chemical composition (Table 4.40) is measured by selecting the base area.
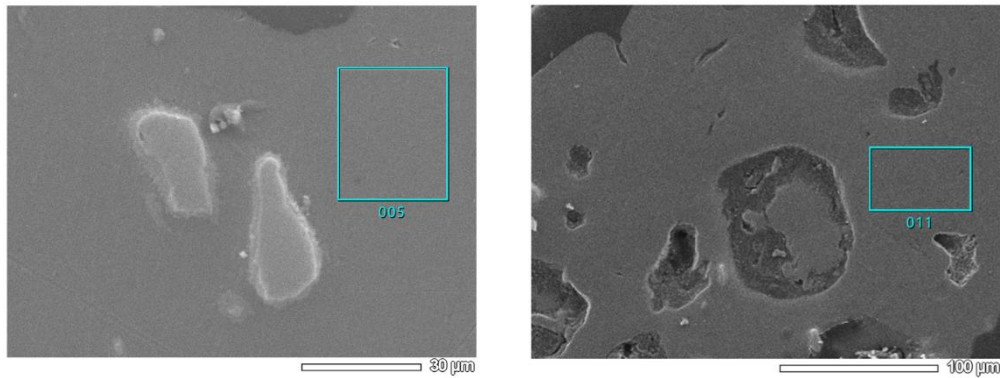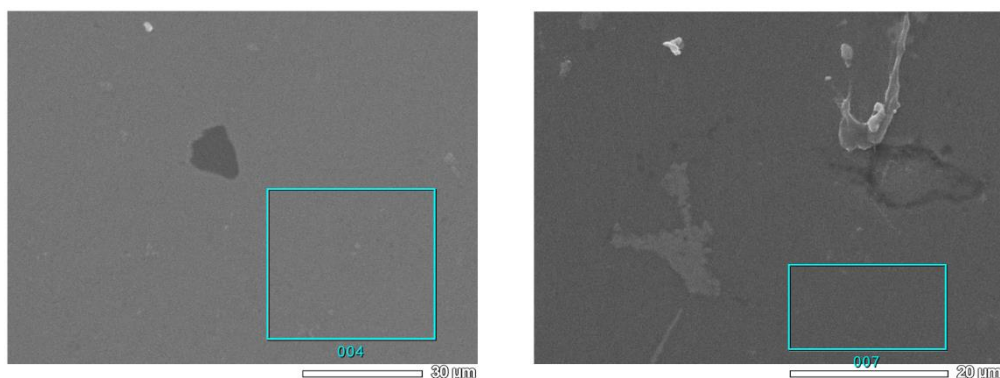

Figure 4.71 Morphology of non-inserted mirror polished foam 3

		foam 7			
	Mass %		Atom %		
Element	Mean	S.D.	Mean	S.D.
C	5.17	7.30	9.75	13.79
O	8.10	0.98	12.16	0.41
Mg	0.95	0.16	0.94	0.07
Al	85.36	7.83	76.76	13.72
Si	0.43	0.61	0.39	0.55

Table 4.40 Average chemical composition of mirror polished foam 3

• Inserted foam 1-3 (dense metal)

Figure 4.72 shows the morphology of dense metal of 1-3 after mirror polishing and the average chemical composition (Table 4.41) is measured by selecting the base area.
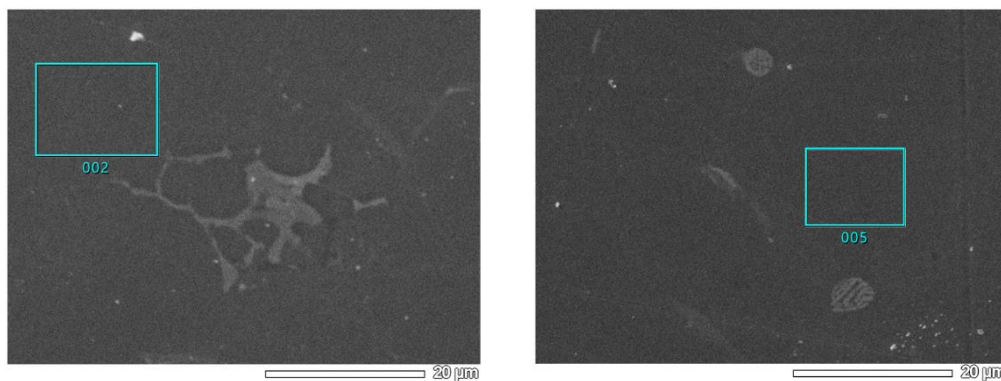

Figure 4.72 Morphology of mirror polished dense metal of 1-3

		1-3 dense metal			
	Mass %		Atom %		
Element	Mean	S.D.	Mean	S.D.
O	6.77	0.65	11.15	0.78
Mg	0.06	0.11	0.07	0.12
Al	82.13	7.56	80.35	8.10
Si	6.83	10.03	6.29	9.22
Cr	3.66	6.33	1.92	3.32
Cu	0.55	0.96	0.23	0.39

Table 4.41 Average chemical compositions of mirror polished dense metal of 1-3

• Inserted foam 1-3 (foam)

Figure 4.73 shows the morphology of inserted foam 1-3 cross section after mirror polishing and the average chemical composition (Table 4.42) is measured by selecting the base area.
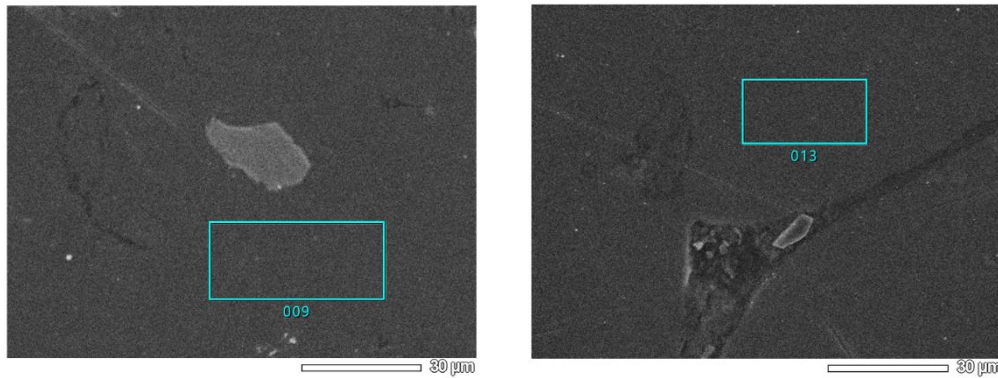
Figure 4.73 Morphology of mirror polished foam 1-3

	1-3 foam			
	Mass %		**Atom %**	
Element	**Mean**	**S.D.**	**Mean**	**S.D.**
O	6.08	5.34	9.65	8.46
Mg	0.64	0.18	0.68	0.20
Al	93.19	5.34	89.60	8.42
Si	0.08	0.14	0.07	0.13

Table 4.42 Average chemical compositions of mirror polished foam 1-3

4.5.4 Second phases

Since optical microscope is not able to determine the chemical compositions of second phases, the particles observed under optical microscope cannot be recognized. In this section, the particles are recognized by comparing the appearances under optical microscope and SEM.

The second phases analysis is done on three types of materials: non-inserted foams, dense metal of 1-3 and inserted foam 1-3.

• Non inserted foams

Figure 4.74-4.83 shows the second phases of non-inserted foams observed in optical microscope and their corresponding chemical compositions measured by SEM
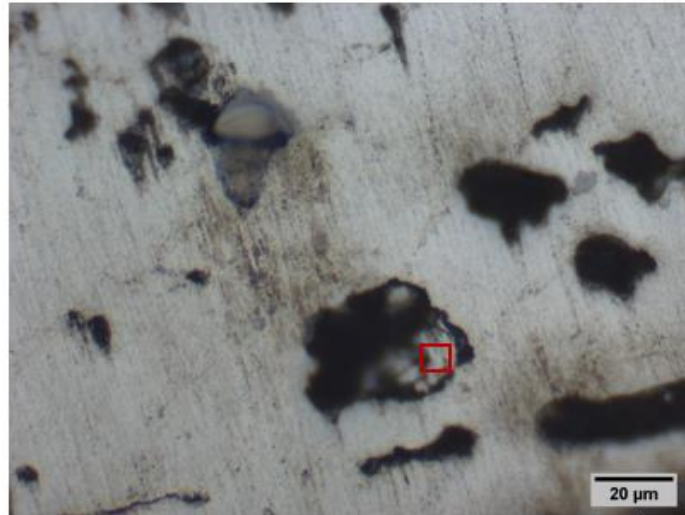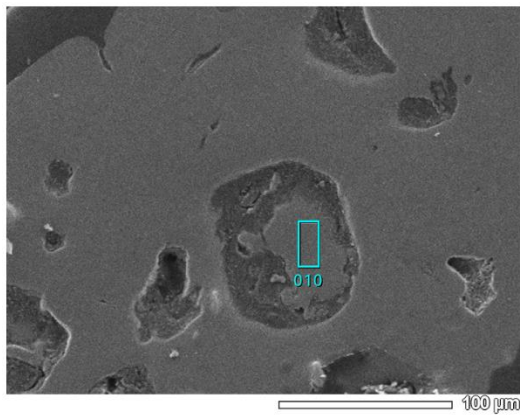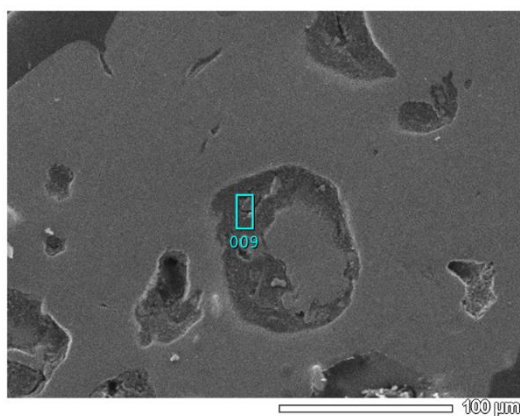
Figure 4.74 Particles of foam 3 in optical microscope

non-inserted foam-3		
Element	Mass %	Atom %
O	10.47	16.98
Mg	1.42	1.52
Al	80.77	77.70
Si	0.30	0.28
Cr	7.04	3.51

non-inserted foam-3		
Element	Mass %	Atom %
O	45.67	54.82
Mg	44.33	39.94
Al	5.11	2.73
Si	4.89	2.51

Figure 4.75 Particles of foam 3 in SEM and corresponding chemical compositions

Cr could be introduced in metallization process while Mg can be aluminum alloy element. In zone 009, there is a large amount of oxygen, which can be presented as metal oxides.
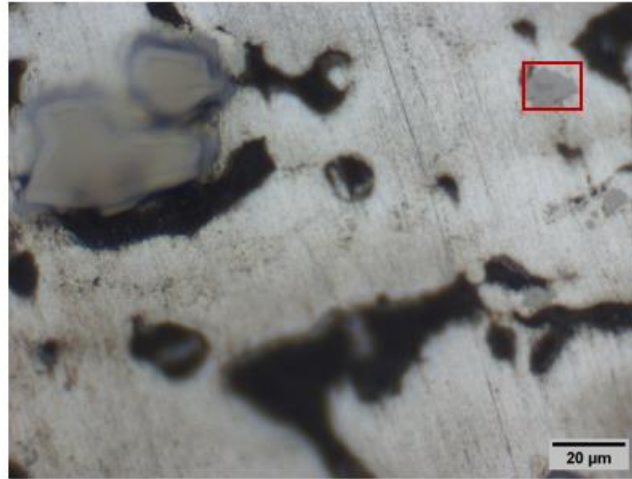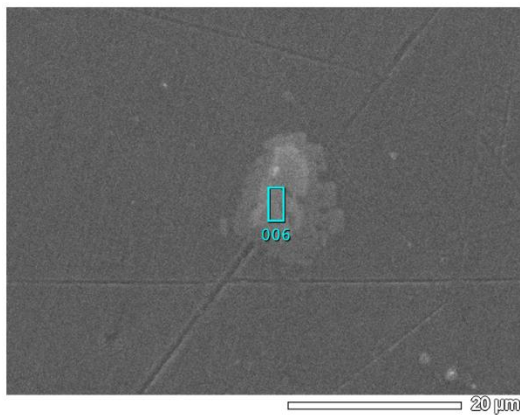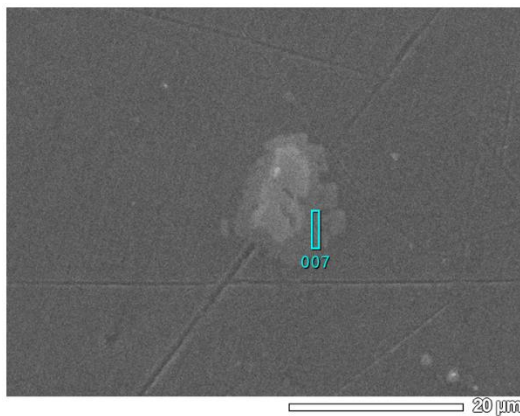
Figure 4.76 Particles of foam 3 in optical microscope

non-inserted foam-3		
Element	Mass %	Atom %
O	24.55	47.59
Mg	0.07	0.09
Al	6.66	7.65
Si	0.37	0.41
Ti	68.35	44.26

non-inserted foam-3		
Element	Mass %	Atom %
O	13.35	23.03
Mg	0.71	0.81
Al	55.55	56.82
Si	4.52	4.44
Ti	25.87	14.90

Figure 4.77 Particles of foam 3 in SEM and corresponding chemical compositions

These light grey particles in foams contain a high percentage of Titanium, which can come from the decomposition of the foaming agent (TiH_2) use in the production of the foam cores.

Figure 4.78 Particles of foam 3 in optical microscope
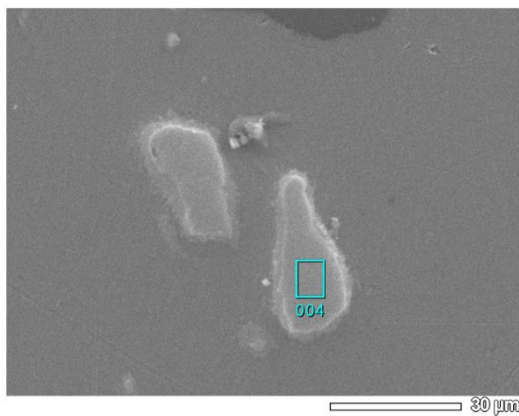
non-inserted foam-3		
Element	Mass %	Atom %
O	27.19	52.11
Al	2.61	2.96
Ti	70.20	44.93

Figure 4.79 Particles of foam 3 in SEM and corresponding chemical compositions

Similarly, Titanium could be introduced as foaming agent in foam manufacturing process.
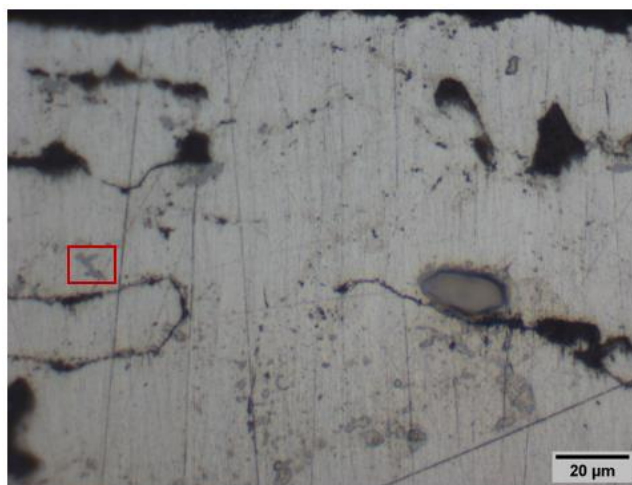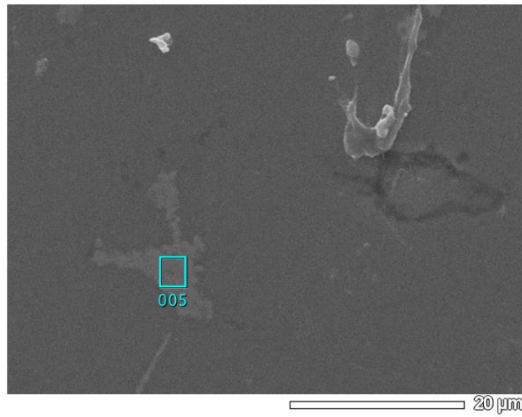

Figure 4.80 Particles of foam 7 in optical microscope

non-inserted foam-7		
Element	Mass %	Atom %
O	7.93	14.58
Mg	1.70	2.06
Al	57.17	62.34
Si	6.76	7.08
Fe	26.44	13.93

Figure 4.81 Particles of foam 7 in SEM and corresponding chemical compositions

A large amount of Fe was found, which could be aluminum alloy element.

Figure 4.82 Particles of foam 7 in optical microscope
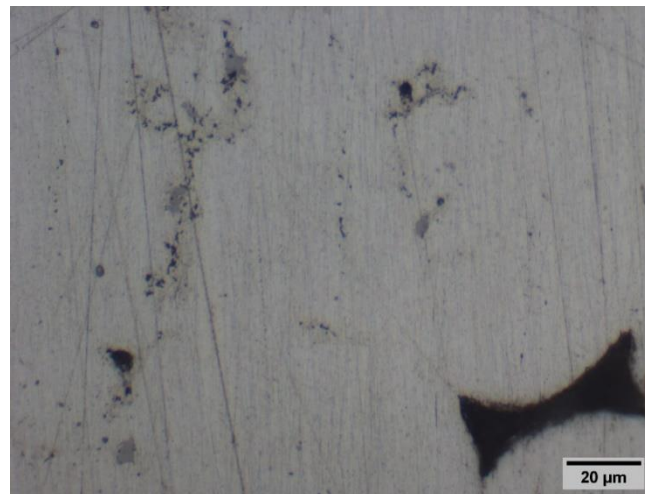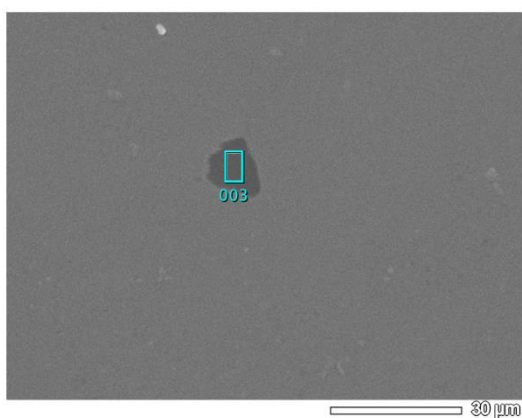

non-inserted foam-7		
Element	Mass %	Atom %
C	63.87	72.25
O	27.64	23.47
Al	8.49	4.27

Figure 4.83 Particles of foam 7 in SEM and corresponding chemical compositions

A high percentage of C in the particle can be contamination.

• Dense metal of 1-3

Figure 4.74-4.83 shows the second phases of dense metal of sample 1 step 3 observed in optical microscope and their corresponding chemical compositions measured by SEM.
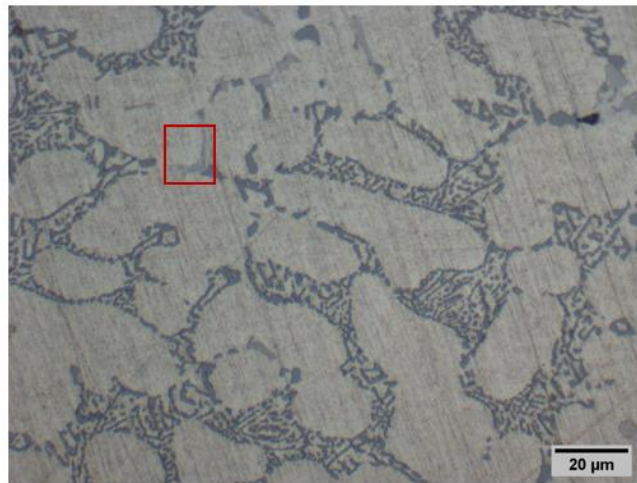
Figure 4.84 Particles in dense metal of 1-3 in optical microscope
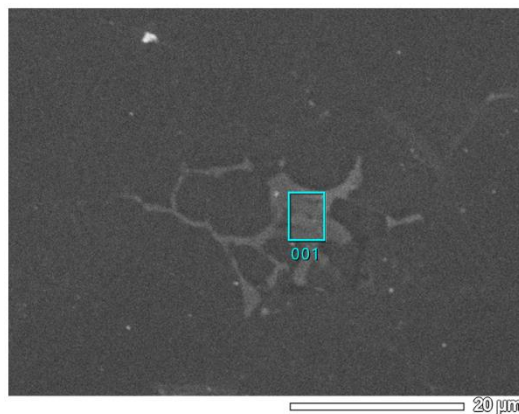
dense metal		
Element	Mass %	Atom %
O	4.54	9.11
Al	54.29	64.59
Si	6.92	7.90
Mn	2.21	1.29
Fe	13.25	7.61
Cu	18.79	9.49

Figure 4.85 Particles in dense metal of 1-3 in SEM and corresponding chemical compositions

This particle contains elements Mn, Fe and Cu, which could be introduced as aluminum alloy composition.
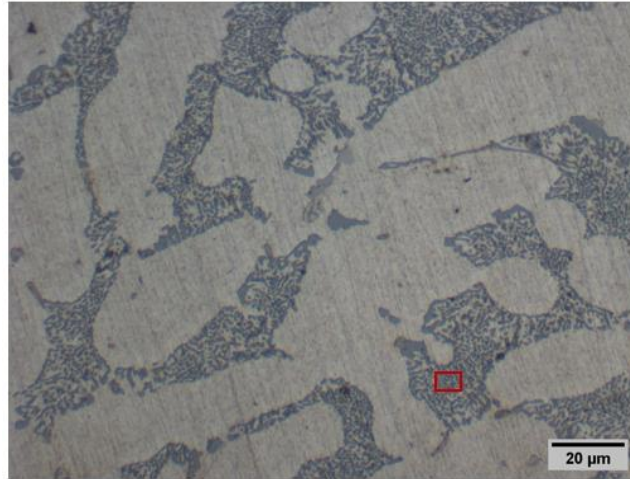
Figure 4.86 Particles in dense metal of 1-3 in optical microscope
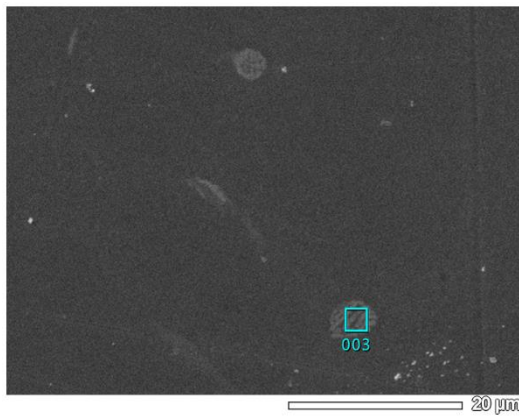
dense metal		
Element	**Mass %**	**Atom %**
O	6.21	12.28
Mg	1.01	1.31
Al	53.50	62.70
Si	6.62	7.46
Cu	32.66	16.25

Figure 4.83 Particles in dense metal of 1-3 in SEM and corresponding chemical compositions

There are many grey dot-like particles in dense aluminum microstructure, which is similar to the morphology observed in SEM. This particle contains a large amount of Cu which could be the alloy element.

• Inserted foam 1-3

Figure 4.74-4.83 shows the second phases of inserted foam sample 1 step 3 observed in optical microscope and their corresponding chemical compositions measured by SEM.
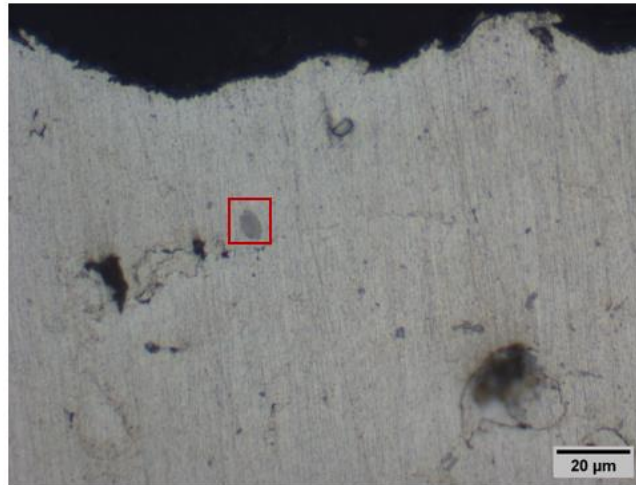
Figure 4.87 Particles of inserted foam 1-3 in optical microscope
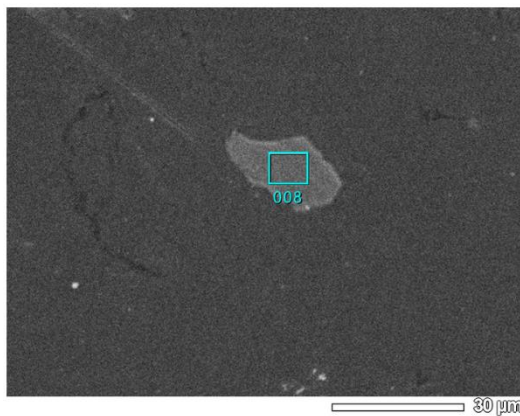
inserted foam 1-3		
Element	Mass %	Atom %
Al	11.14	18.21
Ti	88.86	81.79

Figure 4.88 Particles of inserted foam 1-3 in SEM and corresponding chemical compositions

These light grey particles in foams contain a high percentage of Titanium, which could be introduced as foaming agent in foam manufacturing process.
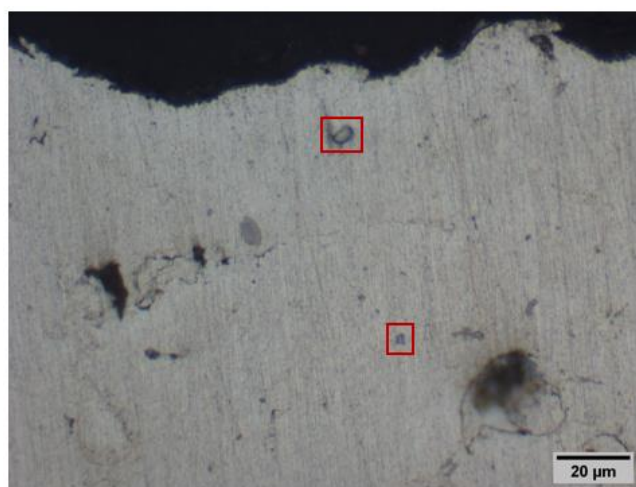
Figure 4.89 Particles of inserted foam 1-3 in optical microscope
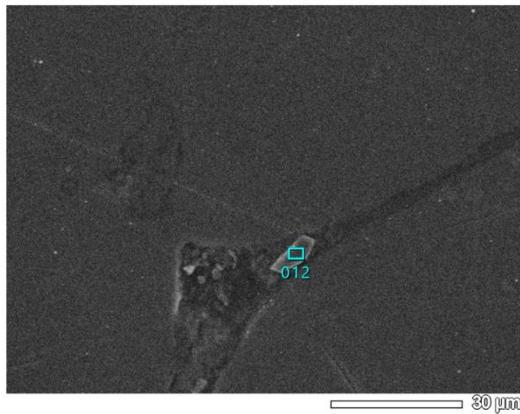
inserted foam 1-3		
Element	Mass %	Atom %
Al	20.55	21.22
Si	79.45	78.78

Figure 4.90 Particles of inserted foam 1-3 in SEM and corresponding chemical compositions

Si could be aluminum alloy element.
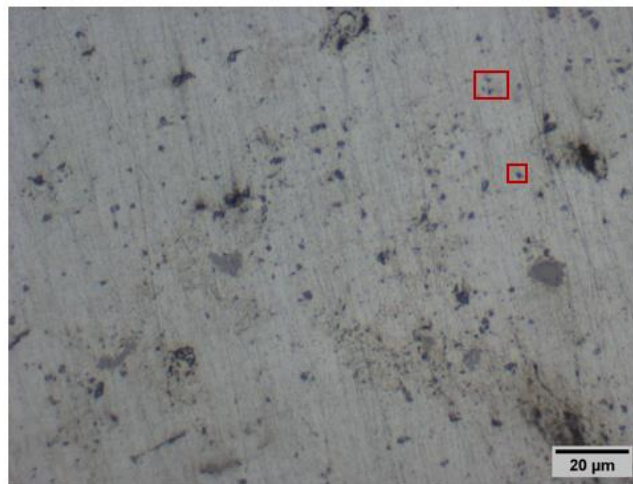
Figure 4.91 Particles of inserted foam 1-3 in optical microscope
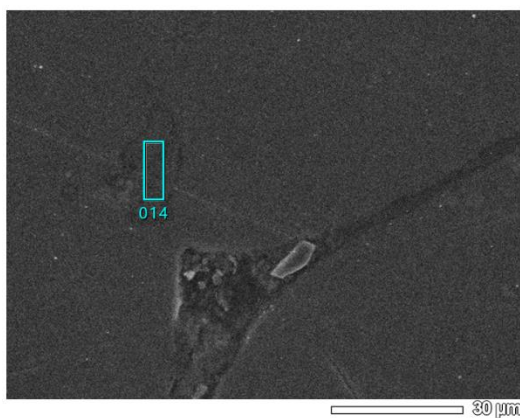
inserted foam 1-3		
Element	Mass %	Atom %
O	24.82	35.72
Mg	1.84	1.74
Al	72.11	61.53
Si	1.23	1.01

Figure 4.92 Particles of inserted foam 1-3 in SEM and corresponding chemical compositions

This particle contains a small amount of Mg and Si, and relatively a large amount of oxygen which can be oxides.

4.6 Thermal conductivity measurements-results

Table 4.43 lists the relative densities and the results of measured thermal conductivities of the two samples.

	Relative density	Mean (W/mK)	Standard Deiviation
Q1	0.12	8.80	0.22
Q2	0.14	8.71	0.26

Table 4.43 Results of thermal conductivity measurement

The thermal conductivity of Aluminum and its alloys ranges between 88 and 251W/mK [27], which is significantly higher than the values of foam Q1 and Q2.

The values obtained for foam samples are in line with the values reported in literature for closed cells aluminum foam with a dense skin [1].

Normally, thermal conductivity increases with foam density [24]. Since the difference in density between samples Q1 and Q2 is limited it is reasonable that no significant differences in the thermal conductivity was recorded in measurements.

Conclusions

Aluminum foams with a dense outer skin and different densities (1-1.5 g/cm^3) were studied in the present thesis. Foams were characterized as received and used as inserts in gravity casting experiments. This research investigated the characteristics of non-inserted foams, dense metal of cast aluminum and inserted foams in casting. Non-inserted foams were characterized by pore sizes, skin thicknesses and wall thicknesses, as well as for their microstructure and chemical composition. As expected a certain variability in pore size, wall and skin thickness was recorded due to foams intrinsic inhomogeneities. On the other hand, chemical composition and microstructure were highly reproducible. SEM-EDS analyses suggest the presence of a significant amount of Mg-rich oxides on the foams surfaces. The microstructure of dense metal showed typical dendrites of Al-alloy. SDAS obtained from tens of measurements proved that higher cooling rate associated with lower SDAS. No infiltration of the foam after insertion in casting was observed, indicating that the external skin effectively protected the foam core from collapse and melt metal infiltration. Moreover, no bonding between the cast metal shell and the foam core was observed. This behavior can be associated with the presence of abundant oxides on the foams outer skin. The absence of a metallurgical bonding between the dense shell and the porous core can be advantageous for dumping effects, however it can reduce the final mechanical properties of the object, so surface treatments of the foam skins can be considered in future works for the improvement of core-shell bonding.

References

[1] H. -P. Degischer and B. Kriszt, Handbook of Cellular Metals: Production, Processing, Applications, Wiley-VCH Verlag GmbH & Co. KGaA, 2002.

[2] "Google," [Online].

[3] "EXXENTIS," [Online]. Available: www.exxentis.co.uk.

[4] "metal foam," wikipedia, [Online]. Available: https://en.wikipedia.org/wiki/Metal_foam.

[5] M. F. Ashby, A. G. Evans, N. A. Fleck, L. J. Gibson, J. W. Hutchinson and H. N. Wadley, Metal Foams: A Design Guide, Butterworth-Heinemann, 2000.

[6] "Fraunhofer IFAM," [Online]. Available: www.ifam-dd.fraunhofer.de.

[7] B. Brauer, S. Kralj and M. Busic, "Production and application of metal foams in casting technology," *Tehnički vjesnik,* pp. 1095-1102, 2013.

[8] J. T. Wood, "Production and Application of Continuously Cast, Foamed Aluminum," in *Proc. Fraunhofer USA Metal Foam Symposium*, Stanton, Delaware, October 1997.

[9] T. Miyoshi, M. Itoh, S. Akiyama and A. Kitahara, "Aluminum Foam, Alporas: The Production Process, Properties and Applications," *Metal Foams and Porous Metal Structures,* p. 125, 1999.

[10] H. P. Degischer and H. Worz.DE patent Patent 4206303, 1992.

[11] D. Stauffer and A. Aharony, Introduction to Per-colation Theory, London: Taylor&Francis, 1992.

[12] T. J. Lu, A. Hess and M. F. Ashby, "Sound absorption in metallic foams," *Journal of Applied Physics,* pp. 7528-7539, 1999.

[13] T. Hopler, F. Schorghuber and F. Simancik, "Foamed aluminium cores for aluminium casting".

[14] A. Bhatt, M. Khanna and B. S. Pimoli, "Metal Foaming of Aluminium Alloys," *Journal of Mechanical and Civil Engineering,* pp. 40-44, 2015.

[15] J. Banhart, "Metal foams-From fundamental research to applications," in *Frontiers in the Design of Materials*, Universities Press (India) Limited, 2007, pp. 279-289.

[16] Z. Odanovic, M. Durdevic, J. Krstic Pavlvic, M. Arsic and B. Katavic, "Some Applications of the Image Analysis in the Metal Material Science," *ACTA PHYSICA POLONICA A,* pp. 111-113, 2012.

[17] L. Y. Zhang, Y. H. Jiang, Z. Ma, S. F. Shan, Y. Z. Jia, C. Z. Fan and W. K. Wang, "Effect of cooling rate on solidified microstructure and mechanical properties of aluminium-A356 Alloy," *JOURNAL OF MATERIAL PROCESSING TECHNOLOGY,* pp. 107-111, 7 2 2008.

[18] Z. R. Khayat and T. A. Palmer, "Impact of Iron composition on the properties of an additively manufactured solid solution strengthened nickle base alloy," *Materials Science & Engineering A,* pp. 123-134, 18 7 2018.

[19] "Feret diameter," Wikipedia, [Online]. Available: https://en.wikipedia.org/wiki/Feret_diameter.

[20] "Scanning Electron Microscope," Encyclopedia Britannica, [Online]. Available: https://www.britannica.com/technology/scanning-electron-microscope.

[21] "Scanning Electron Microscope," Wikipedia, [Online]. Available: https://en.wikipedia.org/wiki/Scanning_electron_microscope#Scanning_process_and_image_formation.

[22] "Scanning Electron Microscopy," Nanoscience, [Online]. Available: https://www.nanoscience.com/techniques/scanning-electron-microscopy/.

[23] Hot Disk Thermal Constants Analyser Instruction Manual, 2013.

[24] M. A. Rodriguez-Perez, J. A. Reglero, D. Lehmhus, M. Wichmann, J. A. de Saja and A. Ferandez, "The Transient Plane Source Technique (TPS) to measure thermal conductivity and its potential as a tool to detect in-homogeneities in metal foams," in *ADVANCED METALLIC MATERIALS*, Smolenice, 2003.

[25] B. Xiao, D. Wang, F. Cheng and Y. Wang, "Oxide film on 5052 aluminum alloy: Its structure and removal mechanism by activated CsF-AlF3 flux in brazing," *Applied Surface Science,* pp. 208-215, 2015.

[26] Z. Zhu, Y. Chen, A. A. Luo and L. Liu, "First conductive atomic force microscopy investigation on the oxide-film removal mechanism by chloride fluxes in aluminum brazing," *Scripta Materialia,* pp. 12-16, 2017.

[27] J. G. Kaufman, "Properties and Characteristics of Aluminum and Aluminum Alloys," in *Fire Resistance of Aluminum and Aluminum Alloys and Measuring the Effects of Fire Exposure on the Properties of Aluminum Alloys*, 2016, pp. 1-9.

[28] L. -P. Lefebvre, J. Banhart and C. D. David, "Porous Metals and Metallic Foams: Current Status and Recent Developments," *Advanced Engineering Materials,* pp. 775-787, 9 10 2008.